

UNIVERSITY OF CALGARY

Structural studies of proteins regulating plant carbon and nitrogen metabolism

by

Yutaka Mizuno

A THESIS

SUBMITTED TO THE FACULTY OF GRADUATE STUDIES
IN PARTIAL FULFILMENT OF THE REQUIREMENTS FOR THE
DEGREE OF MASTER OF SCIENCE

DEPARTMENT OF BIOLOGICAL SCIENCES

CALGARY, ALBERTA

SEPTEMBER, 2007

© Yutaka Mizuno 2007



Library and
Archives Canada

Bibliothèque et
Archives Canada

Published Heritage
Branch

Direction du
Patrimoine de l'édition

395 Wellington Street
Ottawa ON K1A 0N4
Canada

395, rue Wellington
Ottawa ON K1A 0N4
Canada

Your file *Votre référence*

ISBN: 978-0-494-34238-1

Our file *Notre référence*

ISBN: 978-0-494-34238-1

NOTICE:

The author has granted a non-exclusive license allowing Library and Archives Canada to reproduce, publish, archive, preserve, conserve, communicate to the public by telecommunication or on the Internet, loan, distribute and sell theses worldwide, for commercial or non-commercial purposes, in microform, paper, electronic and/or any other formats.

The author retains copyright ownership and moral rights in this thesis. Neither the thesis nor substantial extracts from it may be printed or otherwise reproduced without the author's permission.

AVIS:

L'auteur a accordé une licence non exclusive permettant à la Bibliothèque et Archives Canada de reproduire, publier, archiver, sauvegarder, conserver, transmettre au public par télécommunication ou par l'Internet, prêter, distribuer et vendre des thèses partout dans le monde, à des fins commerciales ou autres, sur support microforme, papier, électronique et/ou autres formats.

L'auteur conserve la propriété du droit d'auteur et des droits moraux qui protègent cette thèse. Ni la thèse ni des extraits substantiels de celle-ci ne doivent être imprimés ou autrement reproduits sans son autorisation.

In compliance with the Canadian Privacy Act some supporting forms may have been removed from this thesis.

Conformément à la loi canadienne sur la protection de la vie privée, quelques formulaires secondaires ont été enlevés de cette thèse.

While these forms may be included in the document page count, their removal does not represent any loss of content from the thesis.

Bien que ces formulaires aient inclus dans la pagination, il n'y aura aucun contenu manquant.


Canada

Abstract

PII is a plant carbon and nitrogen sensing protein and known as one of the most ancient and conserved signaling proteins. The 1.9Å resolution crystal structure of PII from *Arabidopsis thaliana* reveals the first molecular structure of PII from a eukaryote. The structure of PII provides a framework for understanding the arrangement of highly conserved residues shared with PII proteins from bacteria, archaea, and red algae as well as residues conserved only in plants PII. Recently, N-acetyl glutamate kinase (NAGK) was found as the primary binding protein of PII in plants. The 2.5Å resolution crystal structure of the PII: NAGK complex was determined in the presence of NAG, ADP, ATP, Mg²⁺, and arginine. This is the first three-dimensional structure of a complex formed between PII and a target enzyme. The structure of the PII: NAGK complex reveals for the first time the molecular mechanism by which PII relieves the inhibition of NAGK by arginine. Two NAGK structures without bound PII were also determined and compared with the PII: NAGK structure.

Acknowledgements

First of all, I would like to thank my supervisor, Dr. Ken Ng. Dr. Ng has helped me a lot for my research project and gave me a great opportunity to obtain a lot of knowledge and experiences in the lab for the last three years since I joined his lab as an undergraduate project student.

I would also like to thank people in the lab, Dr. Isabelle Barrette-Ng, Gurkirti Brar, Tony Greco, Dr. Jason Ho, Christine Holko, Keith Huber, Vivian Hung, Mike Jones, Dr. Tomohiko Murase, Harinder Rai, Ryan Vu, Dr. Robert Wheatley, Matthew Workentine, and Dr. Dmitry Zamyatkin for their help and advice.

Dr. Greg Moorhead gave me a lot of advice, insight and knowledge for my understanding of plant nitrogen metabolism. I would also like to recognize the generous support from Yan Ming Chen, Tony Ferrar and Mhairi Nimick in Dr. Moorhead lab.

Some X-ray diffraction data were collected at beamline 8.3.1 of the Advanced Light Source (ALS) at Lawrence Berkeley Lab, under an agreement with the Alberta Synchrotron Institute (ASI). The ALS is operated by the Department of Energy and supported by the National Institute of Health. Beamline 8.3.1 was funded by the National Science Foundation, the University of California and Henry Wheeler. The ASI synchrotron access program is supported by grants from the Alberta Science and Research Authority (ASRA) and the Alberta Heritage Foundation for Medical Research (AHFMR).

X-ray diffraction data were also collected at beamline CMCF-1 of the Canadian Light Source (CLS). Alan Duffy and Pawel Grochulski gave generous support and instructions for data collection.

I would like to thank NSERC and AICCS for funding. I would also like to recognize the generous support from AHFMR, CFI, CIHR for lab setup and funding.

Finally, I would like to thank my family and friends for their help and support to accomplish my goal.

Table of Contents

Approval Page.....	ii
Abstract.....	ii
Acknowledgements.....	iii
Table of Contents.....	v
List of Tables.....	vii
List of Figures and Illustrations.....	viii
List of Symbols, Abbreviations and Nomenclature.....	x
Epigraph.....	xii
Chapter One: Introduction.....	1
1.1. Bacterial Nitrogen Metabolism.....	1
1.1.1 Glutamine Synthetase and PII.....	1
1.1.2 Transmembrane Ammonia Channels and PII.....	2
1.2 Cyanobacterial PII.....	4
1.3 Plant PII.....	5
1.4 Solved PII Structures.....	7
1.5 N-Acetyl Glutamate Kinase (NAGK).....	8
1.5.1 NAGK in Cyanobacteria.....	8
1.5.2 NAGK in Plants.....	10
1.6 Solved Structures of NAGK.....	11
1.7 Objective of this Study.....	12
Chapter Two: Materials and Methods.....	20
2.1 Expression of PII.....	20
2.2 Purification of PII.....	20
2.3 Crystallization of PII.....	22
2.3.1 Crystal Growth Screening.....	22
2.3.2 Crystal Optimization.....	22
2.3.3 Post-Crystallization Treatments.....	23
2.3.4 X-ray Analysis of PII Crystals.....	24
2.4 Digestion of His-tagged NAGK.....	25
2.5 Cloning of NAGK.....	26
2.6 Expression and Purification of NAGK.....	27
2.7 Crystallization of NAGK.....	28
2.7.1 Crystal Growth Screening.....	28
2.7.2 Crystallization of the PII: NAGK Complex.....	29
2.7.3 X-ray Analysis of NAGK and the PII: NAGK Complex Crystals.....	30
Chapter Three: Results 1: Structures of PII.....	34
3.1 Purification of PII.....	34
3.2 Crystallization and X-ray Diffraction Analysis of PII.....	34
3.3 Interactions with Citrate and Malonate.....	35
3.4 Crystal Structures of PII.....	35

3.4.1 Overall Structure of PII.....	35
3.4.2 N-terminal Region of PII	36
3.4.3 C-terminal Region of PII	37
3.4.4 Other Conserved Residues.....	38
Chapter Four: Result 2: Structures of the PII: NAGK complex and NAGK.....	48
4.1 Digestion of His-tagged NAGK.....	48
4.2 Cloning, Expression and Purification of NAGK	48
4.3 Crystallization and X-ray Diffraction Analysis of the PII: NAGK Complex.....	49
4.4 Crystal Structure of the PII: NAGK Complex.....	51
4.4.1 Complex Formation between PII and NAGK.....	51
4.4.2 Overall Structure of <i>A. thaliana</i> NAGK.	52
4.4.3 Structural Differences between NAGK protomers in the PII: NAGK Complex.	53
4.4.4 Arginine Binding Site of the PII: NAGK Complex.....	55
4.4.5 Structure of PII in the PII: NAGK Complex	57
4.4.6 Function of ATP Binding on PII.....	59
4.4.7 Comparison of Structural Data with the Experimental Data.	61
4.4.8 Activity Change by 2-ketoglutarate (2KG) Binding to PII.....	62
4.5 Crystallization and X-ray Diffraction Analysis of NAGK.....	63
4.6 Crystal Structures of NAGK.....	65
Chapter Five: Discussion	98
5.1 Structure of PII from <i>A. thaliana</i>	98
5.2 Structure of the PII: NAGK Complex from <i>A. thaliana</i>	99
5.2.1 PII Binding on NAGK	100
5.2.2 Structure of PII.....	101
5.2.3 Function of 2KG for PII.....	102
5.3 Research in the future	104
References.....	106

List of Tables

Table 2.1. Sequences of primers used for NAGK cloning	33
Table 3.1. X-ray diffraction and refinement statistics for <i>A. thaliana</i> PII crystal	41
Table 4.1. X-ray diffraction and refinement statistics for <i>A. thaliana</i> PII: NAGK complex crystal.....	68
Table 4.2. X-ray diffraction and refinement statistics for <i>A. thaliana</i> NAGK crystals	95

List of Figures and Illustrations

Figure 1.1. Model for the role of PII in <i>E. coli</i> (Moorhead and Smith 2003).....	13
Figure 1.2. PII structures.....	15
Figure 1.3. Generalized arginine biosynthesis route from glutamate (Ramon-Maiques et al. 2006).	16
Figure 1.4. Effect of PII on the kinetic profile of NAGK under arginine inhibition (Chen et al. 2006).	17
Figure 1.5. Structures of bacterial NAGK.	19
Figure 3.1. SDS-PAGE analysis of purified PII.	39
Figure 3.2. PII crystals grown in citrate.....	40
Figure 3.3. Conformational differences between <i>A. thaliana</i> PII structure and <i>E. coli</i> PII structure with ATP.....	43
Figure 3.4. ATP binding sites of PII protein.....	44
Figure 3.5. Sequence alignments of PII.	46
Figure 3.6. View of the N-terminal region of <i>A. thaliana</i> PII.	47
Figure 4.1. SDS-PAGE analysis of purified NAGK.....	66
Figure 4.2. Crystals of the PII: NAGK complex.	67
Figure 4.3. Ramachandran plot of the PII: NAGK crystal structure.	70
Figure 4.4. Structures of <i>A. thaliana</i> PII: NAGK complex.	72
Figure 4.5. PII binding site of the PII: NAGK complex.....	73
Figure 4.6. Sequence alignments of NAGK.	75
Figure 4.7. Interaction of NAGK protomers.....	76
Figure 4.8. Conformational differences between two NAGK protomers in the PII: NAGK complex.....	77

Figure 4.9. NAG binding sites of NAGK in the PII: NAGK complex.....	78
Figure 4.10. ADP binding sites of NAGK in the PII: NAGK complex.....	79
Figure 4.11. Conformational differences between two NAGK protomers in the PII: NAGK complex and bacterial <i>T. maritima</i> NAGK bound to arginine molecule. ...	80
Figure 4.12. Arginine binding site of the closed NAGK protomer in the PII: NAGK complex.....	81
Figure 4.13. Conformational differences between <i>A. thaliana</i> PII without NAGK and <i>A.</i> <i>thaliana</i> PII complexed with NAGK.	82
Figure 4.14. Interactions around the edge of the T-loop.....	83
Figure 4.15. Conformational differences around ATP binding site between <i>A. thaliana</i> PII complexed and non-complexed with NAGK.....	85
Figure 4.16. Difference electron density map at the ATP binding site in <i>A. thaliana</i> PII.	86
Figure 4.17. ATP binding sites of PII.....	88
Figure 4.18. Structural differences of the T-loops.....	89
Figure 4.19. Superposition of the possible 2KG binding sites on the T-loops of the <i>M.</i> <i>jannaschii</i> PII and the PII: NAGK complex.....	91
Figure 4.20. Superposition of the possible 2KG binding sites of the GlnK: AmtB complex and the PII: NAGK complexes.	92
Figure 4.21. Crystals grown in the PEG3350 conditions with different substrates.	93
Figure 4.22. Crystals of NAGK.	94
Figure 4.23. Structures of <i>A. thaliana</i> NAGK hexamers.....	97

List of Symbols, Abbreviations and Nomenclature

<i>A. thaliana</i>	<i>Arabidopsis thaliana</i>
ATP	adenosine triphosphate
ADP	adenosine diphosphate
AMP-PNP	Adenosine 5'-(β,γ -imido)triphosphate
Atase	adenylyltransferase
BSA	bovine serum albumin
CHAPS	3-[(3-Cholamidopropyl)dimethylammonio]-1-propanesulfonate
DTT	dithiothreitol
<i>E. coli</i>	<i>Escherichia coli</i>
EDTA	ethylenediaminetetraacetic acid
GS	glutamine synthetase
HEPES	N-(2-Hydroxyethyl)piperazine-N'-2-ethane sulfonic acid
IPTG	isopropyl-beta-D-thiogalactopyranoside
ITC	isothermal titration calorimetry
LB	Luria-Bertani
<i>M. jannaschii</i>	<i>Methanococcus jannaschii</i>
NAG	N-acetyl glutamate
NAGK	N-acetyl glutamate kinase
NRI	Nitrogen regulatory protein I
NRII	Nitrogen regulatory protein II
NRT	nitrate/nitrite transporter

OD	optical density
PCR	polymerase chain reaction
<i>P. aeruginosa</i>	<i>Pseudomonas aeruginosa</i>
PDB	protein data bank
PEG	polyethylene glycol
PMSF	phenylmethyl sulphonyl fluoride
2KG	2-ketoglutarate
SDS-PAGE	sodium dodecyl sulfate-polyacrylamide gel electrophoresis
TMAO	trimethylamine oxide
<i>T. maritima</i>	<i>Thermotoga maritima</i>
<i>T. thermophilus</i>	<i>Thermus thermophilus</i>
UR/Utase	uridylyltransferase/ uridylyl removing bifunctional complex

Epigraph

Every failure is a stepping stone to success.

Chapter One: Introduction

1.1. Bacterial Nitrogen Metabolism

For plants and most microorganisms, it is important to store nitrogen from their environment by converting inorganic nitrogen to organic forms, which are used to synthesize the amino acids glutamate and glutamine. In plants, these amino acids are synthesized primarily in the chloroplast and can be used to build proteins, but also they deliver nitrogen atoms to enzymes that can build nitrogen-rich molecules, such as DNA bases and other amino acids (Moorhead and Smith 2003). Therefore, the regulation of nitrogen, carbon and energy metabolism in the cell has to be controlled precisely for plants to live in constantly changing growth conditions and nutrient availability.

1.1.1 Glutamine Synthetase and PII

Many classical studies on the regulation of nitrogen metabolism have been done with *E. coli* glutamine synthetase (GS) (Stadtman 2001). GS was found to be a key enzyme for the uptake of nitrogen and usage inside cells, and feedback inhibited by downstream products. In many bacteria, it was found that there is a complex cascade activating GS, and that the PII protein has a crucial function for activation (Arcondeguy et al. 2001). Nitrogen metabolism in archaea and bacteria is regulated by the soluble PII proteins, which are among the most ancient, ubiquitous and versatile signaling proteins (Ninfa and Jiang 2005). The PII proteins form homotrimers and each monomer has a long flexible T-loop, which is important for interacting with other proteins. In *E. coli*, GS is regulated at both the transcriptional and posttranslational level by controlling adenylyltransferase (Atase) and the nitrogen regulatory protein II (NRII) (Figure 1.1). When the cellular

nitrogen level is low, cells need to store more nitrogen in the form of glutamine (Magasanik 1993). Under these conditions, the uridylylation of the PII protein on a conserved tyrosine residue in the T-loop by uridylyltransferase/ uridylyl removing bifunctional complex (UR/Utase) is greatly enhanced, and UMP is covalently bound to PII (Son and Rhee 1987). This only occurs in the presence of ATP and α -ketoglutarate when energy and carbon levels are high (Kamberov et al. 1994). Uridylylated PII protein dissociates from Atase, which leads to its deactivation. Without PII, Atase can not adenylylate GS, which leads to its activation. Also, in parallel with this process, NRII can phosphorylate the nitrogen regulatory protein I (NRI) in the absence of PII to increase transcription of *glnA*, which is the structural gene for GS. However, if the nitrogen concentration is high in the cell, cells do not need to store any more glutamine. Under these conditions, the uridylyl removing function is activated by glutamine. As a result, PII becomes unmodified and forms the PII-Atase complex. Once GS is adenylylated, it becomes deactivated (Kamberov et al. 1994). Finally, unmodified PII binds to NRII and activates the dephosphorylation of NRI, thus reducing the transcription of *glnA*. This binding is enhanced in the presence of ATP and 2KG (Kamberov et al. 1995). In these ways, PII controls the rate of nitrogen assimilation (Edwards et al. 1996; Smith et al. 2002).

1.1.2 Transmembrane Ammonia Channels and PII

In addition to GS, PII is important for regulating nitrogen metabolism by controlling transmembrane ammonia channels. Ammonia conductance has been found to be highly

regulated in response to the intracellular nitrogen status, and PII homologue GlnK in *E. coli* is the final regulator of transmembrane ammonia conductance by the ammonia channel AmtB in *E. coli* (Durand and Merrick 2006; Merrick et al. 2006). AmtB is a stable homotrimer in the cytoplasmic membrane. Because ammonia is the preferred source of nitrogen for most microorganisms, ammonia transportation across biological membrane is a key physiological process. After ammonia is transported into the cell, ammonia is used by GS to synthesize glutamine, maintaining an inward gradient of the substrate ammonia (Eisenberg et al. 2000). Amt genes are induced in response to nitrogen limitation in cells, but GlnK also serves to tightly regulate nitrogen assimilation. In most bacteria, the gene for AmtB is linked to *glnK*, which is a gene for PII homologue GlnK in *E. coli* (Thomas et al. 2000). The GlnK trimer binds to the AmtB trimer and blocks ammonia conduction directly (Durand and Merrick 2006; Merrick et al. 2006). GlnK with no binding molecules binds and inhibits AmtB more tightly, while the uridylylated form of GlnK has less binding affinity for AmtB (Javelle et al. 2004; Durand and Merrick 2006).

Furthermore, the PII-binding metabolite, 2-ketoglutarate (2KG), has an important function for AmtB regulation. 2KG concentration in cells rises as the cell becomes more nitrogen limited. Thus, 2KG binding to GlnK causes dissociation of the GlnK: AmtB complex in the presence of ATP and Mg^{2+} , and increases the ammonia levels in cells by opening the channel. Gel filtration chromatography and co-precipitation experiments showed that the complex is stable in the absence of Mg^{2+} -ATP, but Mg^{2+} -ATP inhibits complex formation, and, together with 2KG, prevents it completely (Yildiz et al. 2007).

Also, it was mentioned that GS is not activated in the absence of 2KG, and the absence of 2KG inhibits the ability to use assimilated ammonia by GS in cells (Figure 1.1). However, GS can be activated when the concentration of 2KG is increased under nitrogen limitation, and more glutamine is produced to store nitrogen. After the nitrogen levels become sufficient again, the levels of 2KG decrease, and GS is inhibited to avoid overproduction of glutamine (Ehlers et al. 2005). In this way, 2KG and PII separately regulate the AmtB and GS depending on the nitrogen levels in the cell.

1.2 Cyanobacterial PII

Cyanobacteria are prokaryotes performing oxygenic photosynthesis, and their ability to fix carbon is important in the global carbon cycle (Li 1994). PII protein in cyanobacteria was first identified in *Synechococcus* sp. PCC 6301. Similar to the *E. coli* PII, *Synechococcus* PII forms a homotrimer, and each monomer binds ATP and 2KG. 2KG binds PII only if ATP binds PII (Forchhammer and Hedler 1997). In cyanobacteria, 2KG is almost solely used for nitrogen assimilation, and nitrogen depletion results in intracellular accumulation of 2KG. Thus, 2KG is a signaling metabolite for the cellular nitrogen status (Muro-Pastor et al. 2001).

The PII protein of cyanobacteria can be phosphorylated at a conserved serine residue in the T-loop, and it is different from the uridylylation of a tyrosine residue in the *E. coli* T-loop. Cyanobacterial PII is phosphorylated under nitrogen-depleted condition, and dephosphorylated under nitrogen-replete conditions (Forchhammer and Tandeau de Marsac 1994). In addition to the nitrogen status, the carbon status also alters PII

phosphorylation. When more carbon is fixed, the degree of phosphorylation increases (Lee et al. 1998). In this way, cyanobacterial PII phosphorylation is modulated by the nitrogen and carbon status.

One example of PII function in cyanobacteria is that PII affects the nitrate/nitrite transporter (NRT) activity. NRT is active in a PII-deficient mutant, but inactivated in the presence of ammonium in the wild-type cyanobacterium. Substitution of the serine residue, which can be phosphorylated, to alanine inhibited nitrate uptake, because it mimics non-phosphorylated PII (Lee et al. 1998).

PII is also important for the bicarbonate transporter as well. The PII-deficient mutant was unable to deactivate the bicarbonate transporter in the presence of high inorganic carbon concentrations. However, the transporter is deactivated under this condition in the wild-type cyanobacterium (Hisbergues et al. 1999). In these ways, cyanobacterial PII regulates the transporters for nitrogen and carbon sources according to the nutrient availability.

1.3 Plant PII

Recently, a PII-like protein was discovered in the higher plant *Arabidopsis thaliana* (*A. thaliana*), and the *A. thaliana* PII gene encodes a 196 amino acid protein with a predicted chloroplast transit peptide (Hsieh et al. 1998; Smith et al. 2002). It is found that *A. thaliana* PII also allosterically binds to ATP and 2KG, and 2KG binds PII only if ATP binds PII first (Smith et al. 2003). There are other significant similarities between

bacterial PII and plant PII. First, the *Arabidopsis* PII protein is 50% identical to the *E. coli* PII and 55% identical to cyanobacterial PII at the amino acid level. In addition, all PII proteins form homotrimers. Also, ATP-binding residues are highly conserved, which suggests that the binding to ATP is also very important for plant PII to function. Furthermore, the amino acid residues that make salt bridges for trimer formation are highly conserved (Moorhead and Smith 2003).

Most non-plant PII proteins are uridylylated on a conserved tyrosine residue in the T-loop, and some cyanobacterial PII are phosphorylated on a conserved serine residue in the T-loop. The tyrosine residue, which is uridylylated to transmit the nitrogen status signal of the cell in bacterial PII, is not conserved at all in plant PII. Though the serine residue is conserved in all plant PII sequences, no covalent modification was detected in any plant PII including *A. thaliana* PII under any conditions tested (Smith et al. 2004).

It is expected that the PII protein in all plants is crucial for survival, since PII is highly conserved among plants and bacteria. *A. thaliana* PII knock-out mutants showed a higher sensitivity to nitrite and a decrease in total amino acids, primarily glutamine, compared to the wild-type plants (Ferrario-Mery et al. 2005). Also, their mutants displayed a decreased ammonium and a slightly increased level of carbohydrates, such as starch and sugars. These experiments were performed with ammonium re-supply after nitrogen starvation.

1.4 Solved PII Structures

PII structures from several prokaryotes have been solved so far (Cheah et al. 1994; Carr et al. 1996; Xu et al. 1998; Xu et al. 2001; Machado Benelli et al. 2002; Xu et al. 2003; Schwarzenbacher et al. 2004; Sakai et al. 2005; Nichols et al. 2006; Yildiz et al. 2007). At the start of my project, no three-dimensional structure of PII had been determined from eukaryotes. All known prokaryotic PII are homotrimers, and the structures are highly conserved (Figure 1.2). At the central part of the homotrimer, three copies of a protomer containing a highly conserved double β - α - β fold are arranged to form a cylinder. Also, each protomer has a long loop of ~ 20 residues (T-loop), which connects the $\beta 2$ and $\beta 3$ strands and projects from a common face of the cylindrical trimer. The covalent modification of highly conserved tyrosine and serine residues near the centre of this loop by uridylylation and phosphorylation in different species affects interactions between PII and target enzymes (Forchhammer 2004).

Recently, crystal structures of *E. coli* PII homologue GlnK bound to the AmtB transmembrane ammonia channel were determined (Conroy et al. 2007; Gruswitz et al. 2007) (Figure 1.2). However, complexed PII structures with other proteins including enzymes have not yet been solved. In the GlnK: AmtB complex structure, a highly conserved arginine residue on the T-loop works as a plug stopping the flow of ammonia.

Also, *Methanococcus jannaschii* (*M. jannaschii*) crystal structures of PII with effector molecules, Mg^{2+} -ATP and 2KG, have been determined, and binding of Mg^{2+} -ATP and 2KG has an important function for the complex formation of PII and ammonia

transporter (Yildiz et al. 2007). From these structures, the T-loop has two distinct conformations. One of the conformations is extended and flexible, whereas the other one is compact and rigid. The compact conformation is induced by Mg^{2+} -ATP, but not by ATP alone, and is stabilized by 2KG. Thus, in the absence of both effectors, a tight complex of PII and the transporter forms, but Mg^{2+} -ATP and 2KG binding changes the conformation and property of the T-loop and inhibits the complex formation. The binding of Mg^{2+} -ATP changes the conformation of the T-loop and creates a binding site for 2KG at the tyrosine residue, which can be uridylylated. A negatively charged 2KG in this location may have an effect similar to uridylylation.

1.5 N-Acetyl Glutamate Kinase (NAGK)

1.5.1 NAGK in Cyanobacteria

Recently N-acetyl glutamate kinase (NAGK) was found as a receptor protein for PII-like protein in organisms that perform oxygenic photosynthesis, such as cyanobacteria and eukaryotic photosynthetic organisms (Burillo et al. 2004). NAGK belongs in the amino acid kinase family and catalyzes the second step of arginine synthesis via N-acetyl glutamate. Arginine is essential for living organisms, because it is an amino acid and a nitrogen storage compound. Also, arginine is a precursor of other important biological molecules as well. Microorganisms, plants and some animals synthesize arginine from glutamate through the intermediate molecule, ornithine (Figure 1.3). For the first step of arginine biosynthesis cascade, glutamate is N-acetylated to produce N-acetylglutamate (NAG), then phosphorylated by NAGK to produce N-acetylglutamyl-5-phosphate. After two more steps, N-acetylglutamyl-5-phosphate is converted to N-acetyl-L-ornithine,

which is then deacetylated to make ornithine. The removal of the acetyl group of acetyl-ornithine occurs hydrolytically by transacetylation to glutamate in most organisms. Thus, the acetyl group is recycled to yield NAG (Ramon-Maiques et al. 2006).

It is known that arginine synthesis in most organisms is controlled through feed-back inhibition by the final product, arginine (Cunin et al. 1986; Fernandez-Murga et al. 2004; Slocum 2005). For arginine synthesis, the phosphorylation of NAG is the rate limiting step, and arginine binds to and inhibits NAGK to reduce the rate of arginine biosynthesis. Although the NAGK from some organisms is not sensitive to arginine, (e.g., *E. coli* NAGK), NAGK is inhibited by arginine in most organisms, including plants, cyanobacteria, fungi, algae and most eubacteria and archaea.

Importantly, the function of PII binding to NAGK was found to relieve NAGK from arginine-mediated inhibition and to increase NAGK activity. The first evidence for an interaction between PII and NAGK was found in *Synechococcus elongatus*, which is a cyanobacterium. Saturating amounts of PII activated NAGK about tenfold and the concentrations of arginine needed for inhibition are increased significantly (Maheswaran et al. 2004). Furthermore, a PII-null mutant of *Synechococcus* showed reduced NAGK activity (Heinrich et al. 2004) (Burillo et al. 2004). Also, it was demonstrated that one PII trimer interacted with one NAGK hexamer, and that the interaction was inhibited by 2KG in the presence of ATP and Mg^{2+} (Burillo et al. 2004; Heinrich et al. 2004; Maheswaran et al. 2004). In addition, a serine residue in the T-loop of PII is conserved among cyanobacteria and eukaryotic photosynthetic organisms, and has an essential role for PII and NAGK binding. The interaction between PII and NAGK was inhibited by

phosphorylation of this serine residue (Burillo et al. 2004). These results suggest that non-phosphorylated and non-2KG-binding PII can form a complex with NAGK to activate arginine biosynthesis under nitrogen-replete conditions. In this way, photosynthetic organisms can store some of their energy and nitrogen in the form of arginine.

1.5.2 NAGK in Plants

For plants, NAGK was also found to interact with PII. Both proteins are translated in the cytoplasm and transported to the chloroplast. Gel filtration and isothermal titration calorimetry (ITC) experiments showed that one PII trimer interacts with one NAGK hexamer as seen in cyanobacteria (Chen et al. 2006). The activity assay of PII mixed with NAGK showed that PII only activated the enzyme about 30%. However, the activity of *A. thaliana* NAGK by itself is already as high as the activity of bacterial NAGK with PII.

It is known that NAGK in higher plants can be feedback inhibited by arginine (Caldovic and Tuchman 2003). Biochemical studies have also shown that *A. thaliana* NAGK is inhibited by arginine and form complexes with PII. The formation of complexes is enhanced by the presence of arginine, and PII increased NAGK enzyme activity about 3.5 fold under arginine inhibition. Furthermore, the NAGK kinetics shifted from sigmoidal to hyperbolic in the presence of arginine and PII (Figure 1.4). Finally, no other metabolite was found to control the interaction of PII and NAGK, thus the primary

function of PII: NAGK complex formation might be to relieve feedback inhibition by arginine and over-produce arginine (Chen et al. 2006).

1.6 Solved Structures of NAGK

The three-dimensional structure of NAGK from *E. coli* shows that it is a homodimeric complex and clarified substrate binding and catalysis (Ramon-Maiques et al. 2002). However, *E. coli* NAGK is arginine insensitive and the structure did not show any arginine binding and inhibition.

Recently, homo-hexameric three-dimensional structures of *Thermotoga maritima* (*T. maritima*) NAGK with arginine and *Pseudomonas aeruginosa* (*P. aeruginosa*) NAGK without arginine were determined (Figure 1.5). They form homo-hexamers with a central hole of about 30 Å diameter by linking three *E. coli* NAGK like homodimers through the N-terminus mobile kinked α -helix, which is absent from *E. coli* NAGK (Figure 1.5). Arginine is found in each subunit of *T. maritima* NAGK and two arginine molecules are sandwiching the N-terminal dimer interface. Also, this arginine binding site is sandwiched between N-terminal helix, the central β -sheet, C-terminal loop. This site can be found for *P. aeruginosa* NAGK structure, but it is missing from *E. coli* NAGK. From the structural differences of these two hexameric NAGK structures, arginine-complexed NAGK showed more enlarged active centre conformations, which causes lower catalysis activity. On the other hand, NAG might counter arginine inhibition by promoting active centre closure. The PII protein binding model could be made using solved hexagonal structures. PII is a trimer with T-loops, which are crucial for binding to NAGK.

Therefore, PII should bind to NAGK with the T-loop side. The view along the 3-fold axis of NAGK and PII and their surface potentials shows that NAGK and PII bind with their 3-fold axes aligned (Ramon-Maiques et al. 2006).

1.7 Objective of this Study

The goal of this study has been to determine the detailed three-dimensional structures of *A. thaliana* PII protein, NAGK, and their complex by X-ray crystallography. X-ray crystallography is the most effective method for determining three-dimensional protein structures at atomic or near-atomic resolutions, and determining protein structures at high resolution is important for understanding how they work. To achieve this goal, PII and NAGK were expressed, purified and concentrated for crystallization. Then, a number of crystallization screens were attempted, and conditions were optimized. Diffraction data were measured and used to calculate electron density maps. Molecular models were built to interpret these maps, and the models were analyzed to understand the molecular structures of PII and NAGK.

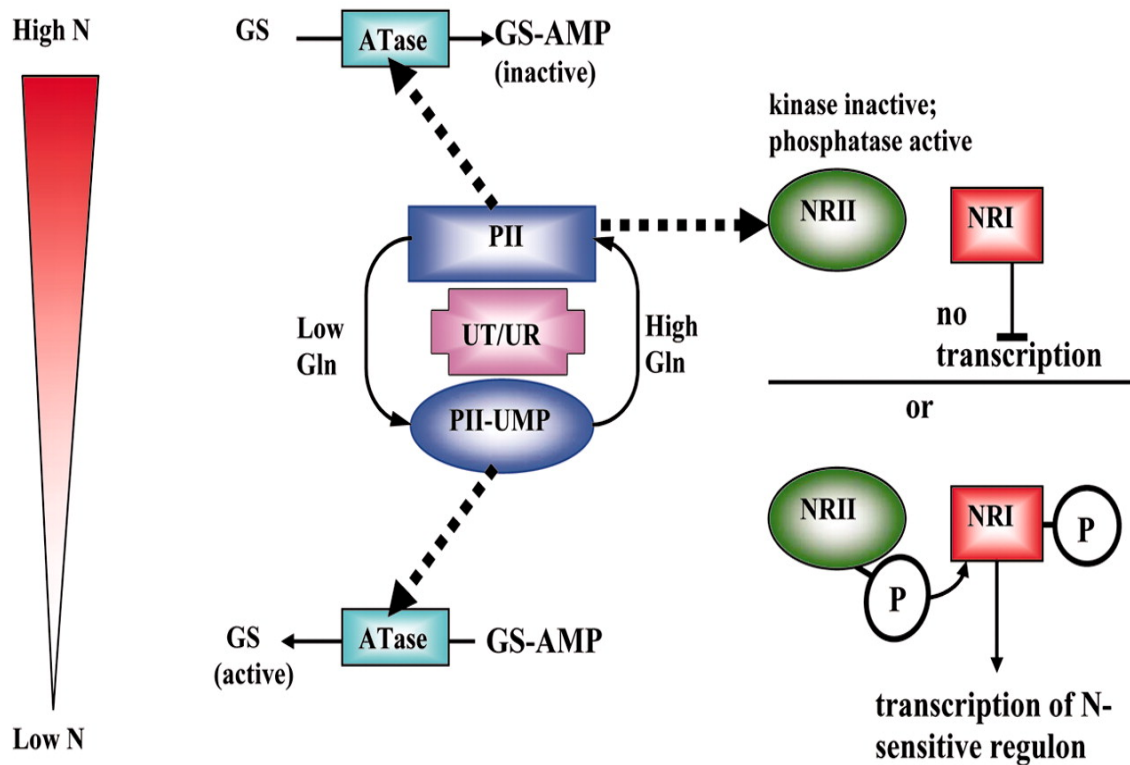


Figure 1.1. Model for the role of PII in *E. coli* (Moorhead and Smith 2003).

When the cellular nitrogen level is high, cellular levels of glutamine (Gln), which signals the nitrogen level, promotes deuridylylation of PII. Then, unmodified PII interacts with ATase, which adenylates and deactivates GS. In parallel, unmodified PII binds NRII to suppress its protein kinase activity, activates its phosphatase activity, and maintains the transcription factor NRI in a dephosphorylated, inactive form. There is no transcription of GS. When the cellular Gln levels are low and both the carbon and energy status are adequate, PII is uridylylated. PII-UMP does not interact with ATase and stimulates the activation of GS. Also, PII does not bind to NRII, and the transcription of GS is active.

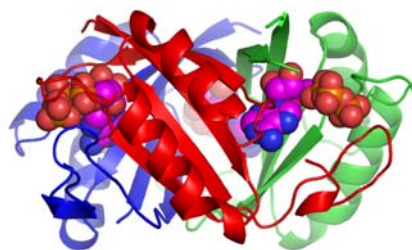
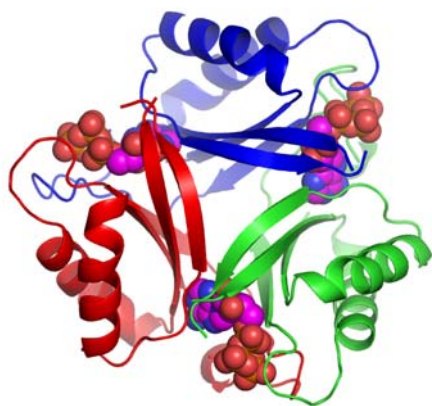
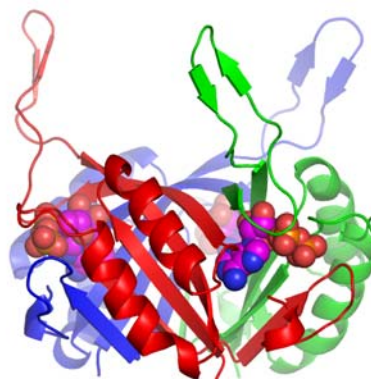
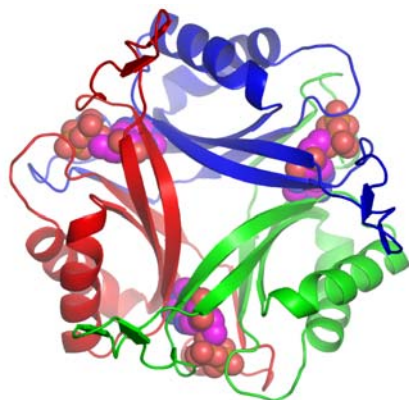
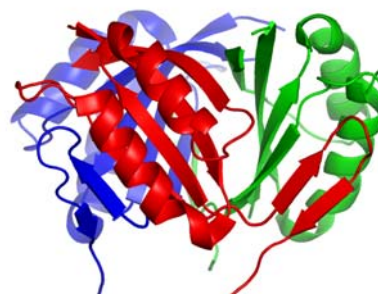
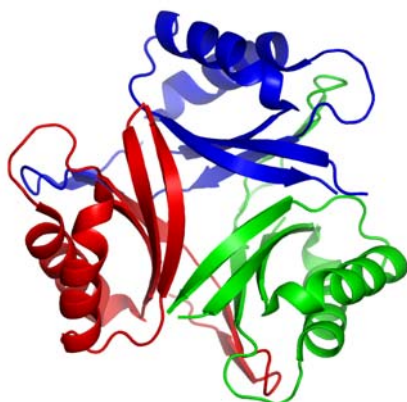
a**b****c**

Figure 1.2. PII structures.

a) *E. coli* PII bound to ATP (pdb file: 2GNK (Xu et al. 1998)); b) *E. coli* GlnK complexed with ammonium transporter (pdb file: 1NS1 (Conroy et al. 2007)). ADP is bound to each protomer; c) PII from the cyanobacterium *Synechocystis* sp. PCC 6803 (pdb file: 1UL3 (Xu et al. 2003)). Each protomer is drawn in ribbon representation with different colours. On the left, the trimer is viewed from the top, down the three-fold rotation axis of the trimer. On the right, the trimer is viewed from the side, perpendicular to the three-fold axis.

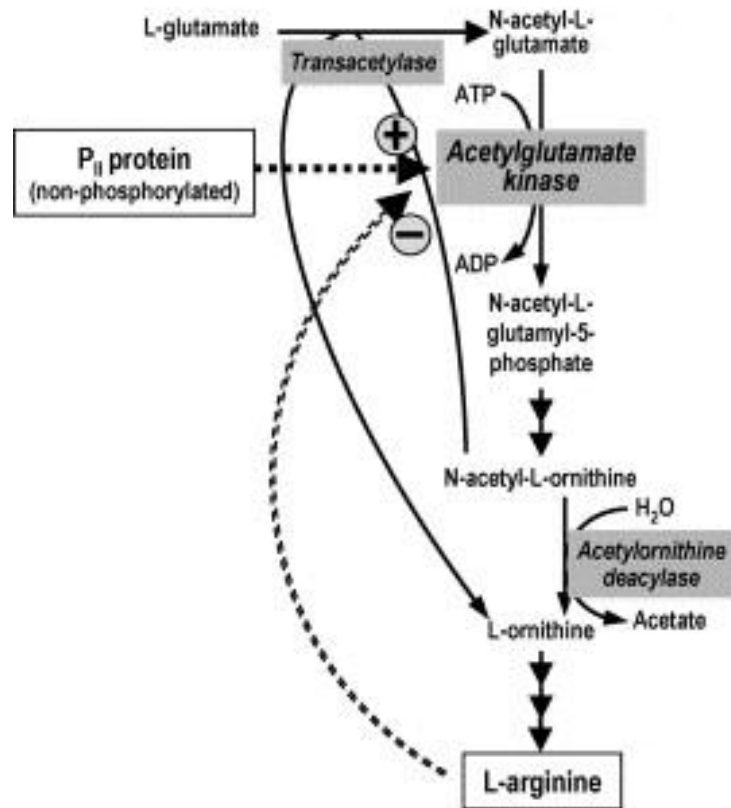


Figure 1.3. Generalized arginine biosynthesis route from glutamate (Ramon-Maiques et al. 2006).

Enzymes are highlighted using grey shading, and the effectors arginine and protein PII are enclosed in rectangular boxes. NAGK is feed-back inhibited by arginine and activated by the PII protein.

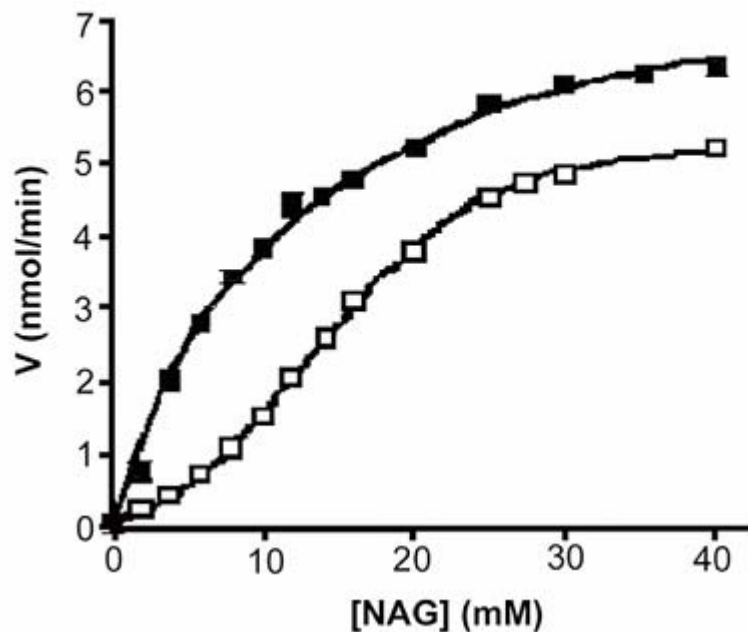


Figure 1.4. Effect of PII on the kinetic profile of NAGK under arginine inhibition (Chen et al. 2006).

PII shifts the kinetic profile of NAGK from sigmoidal to hyperbolic in the presence of the inhibitor arginine. The concentration of arginine used in all assays was 0.32 mM. The non-filled squares show NAGK alone, and the filled squares show the PII: NAGK complex.

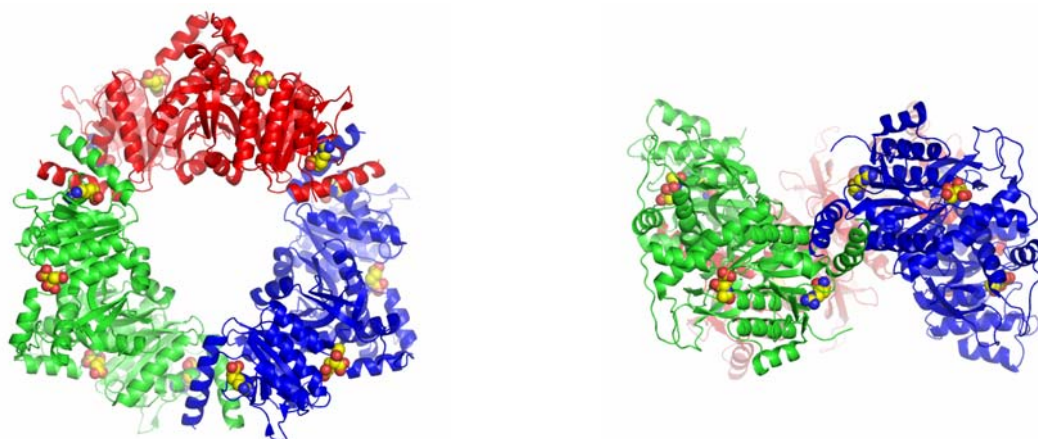
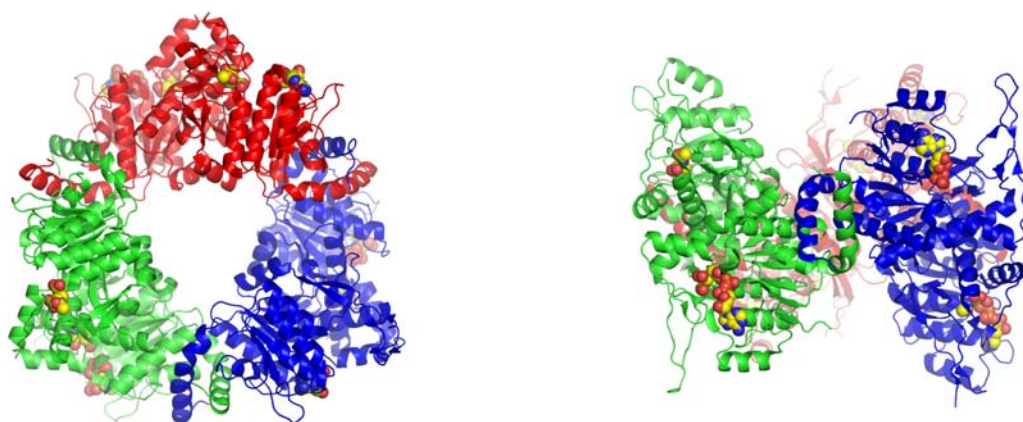
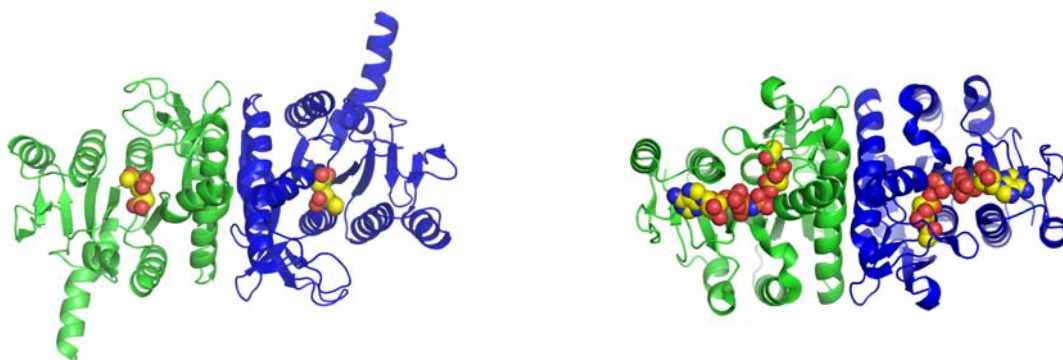
a**b****c**

Figure 1.5. Structures of bacterial NAGK.

a) *T. maritima* NAGK hexamer bound to arginine (pdb file: 2BTY (Ramon-Maiques et al. 2006)); b) *P. aeruginosa* NAGK hexamer bound to ADP and NAG (pdb file: 2BUF (Ramon-Maiques et al. 2006)). For a and b, each homodimer is coloured differently. Also, on the left, the hexamer is viewed from the top, down the three-fold rotation axis of the hexamer. On the right, the hexamer is viewed from the side, perpendicular to the three-fold axis; c) comparison of *E. coli* NAGK dimer (on the right) (pdb file: 1GS5 (Ramon-Maiques et al. 2002)) and *T. maritima* NAGK dimer (on the left). The N-terminal α -helices, which are crucial for hexamer formation, are missing on *E. coli* NAGK.

Chapter Two: Materials and Methods

2.1 Expression of PII

The pET3a vector with cloned PII protein (Chen et al. 2006) was prepared by Byron Berenger and transformed into competent cells of Rosetta gami pLysS cells. These cells were streaked on a Luria-Bertani (LB), 100 mg/L ampicillin, 34 mg/L chloramphenicol agar plate. The plate was incubated overnight at 37°C. A few colonies were taken from the plate and inoculated in a 100 mL LB, 100 mg/L ampicillin, 34 mg/L chloramphenicol starter culture and grown overnight in a Barnstead shaker at 37°C. One mL of the starter culture was taken to make a glycerol stock solution, and 50 mL of the culture was transferred to 1 L terrific broth, 100 mg/L ampicillin, 34 mg/L chloramphenicol media and grown at 37°C until the absorbance at 595 nm reached 0.25 with a path length of 5 mm. Then, isopropyl-beta-D-thiogalactopyranoside (IPTG; Invitrogen) was added to the culture to a final concentration of 200 µM. Induction was carried out overnight at 25°C. The cells were harvested by centrifugation at 5,000 rpm for 10 minute in a Sorvall centrifuge with GS-3 rotor, and then the cell pellets were re-suspended in a buffer solution containing 100 mM NaCl, 25 mM Na-HEPES pH 7.0 and 1 mM Na-EDTA. Suspended cells were stored at -70°C.

2.2 Purification of PII

As the first step for the purification, 1 mM phenylmethyl sulphonyl fluoride (PMSF) and about 1 ng DNase (Sigma) were added to the re-suspended pellets from 1 L of cells. Then they were sonicated for 4 minute using a Branson sonifier at 50% duty cycle. The sample was centrifuged at 12,000 rpm for 30 minute in a Sorvall centrifuge with SS-34

rotor and the supernatant was retained. The sample was then purified by cation exchange column chromatography (Macro-Prep High S, Bio-Rad). The column (4 cm height, 2.5 cm diameter, 20 mL bed volume) was equilibrated by running 25 mM Na-HEPES pH 7.0 with 1 mM Na-EDTA. The protein sample was loaded onto the column after being diluted to a final NaCl concentration of 20 mM to ensure maximum amount of protein binding. Three mL fractions were eluted from the column with a gradient of 25 mM Na-HEPES pH 7.0, 1 mM Na-EDTA and NaCl between 0 – 1 M.

The protein concentration in each fraction eluted was assayed using the BioRad Coomassie Blue Bradford assay (Bradford 1976) with Bovine Serum Albumin (BSA) standard (BioRad). Most of the PII was eluted at 120 – 160 mM NaCl. The purity of each protein fractions were verified by SDS PAGE (Laemmli 1970) stained by Coomassie Blue dye (50% (v/v) methanol, 10% (v/v) acetic acid, 0.25% (w/v) Coomassie Brilliant blue). Selected fractions were poured together for the next purification step.

PII protein was further purified by hydrophobic interaction column chromatography (Phenyl Sepharose, Amersham Biosciences). The column was equilibrated with 1 M ammonium sulfate (AS) with 25 mM Na-HEPES pH 7.0 and 1 mM Na-EDTA. The protein sample was loaded onto the column after adding 4 M AS to a final AS concentration of 1 M. Three mL fractions were eluted from the column with 25 mM Na-HEPES pH 7.0, 1 mM Na-EDTA and AS between 1 - 0 M. The protein concentration in each fraction eluted was assayed using the BioRad Coomassie Blue Bradford assay with Bovine Serum Albumin (BSA) standard (BioRad). Most of the protein was eluted at 0.5

– 0.2 M AS. Then the purity of PII in each fraction was examined by SDS PAGE stained by Coomassie Blue dye (50% (v/v) methanol, 10% (v/v) acetic acid, 0.25% (w/v) Coomassie Brilliant blue). Pure PII fractions were mixed together and dialyzed into a buffer with 30 mM NaCl, 25 mM Na-HEPES and 5% (v/v) glycerol, and then concentrated with a Vivaspin 5 kDa spin concentrator to a final concentration of ~ 7 mg/mL.

2.3 Crystallization of PII

2.3.1 Crystal Growth Screening

The sparse matrix screening on concentrated PII (~ 7 mg/ml) was attempted using the Index HT, Crystal Screen Cryo and SaltRx sparse matrix screens (Hampton Research). Each screen contained 96 different solutions sampling a wide range of conditions generally amenable to protein crystallization. One hundred μL of each crystallization solution was pipetted into the wells of a Corning 96 well CrystalEX plate and 1 μL of the same solution was combined with 1 μL of the protein solution in the top shelves of the plate in a sitting drop setup. The plates were kept at room temperature and monitored every day for crystal growth.

2.3.2 Crystal Optimization

Concentrated PII (~ 7 mg/mL) was crystallized using the hanging drop vapour diffusion method at room temperature by mixing 2 μL of the protein solution with 2 μL crystallization solution and equilibrating over 1 mL of crystallization solution. The drops were set up in Nextal crystal trays and were kept at room temperature. The best crystals

were grown with a crystallization solution containing 1.4 M tri-ammonium citrate pH 7.0 and 10% (v/v) glycerol. For condition optimization, the protein concentration was varied between 4 – 7 mg/mL, and various ligands including ATP and 2KG were added. To optimize crystal growth precipitant concentration, cryo-protectants and detergents in the crystallization solution were varied. The most commonly used cryoprotectant is glycerol. As a detergent, CHAPS, which is a weak zwitterionic detergent, was used. Also, seeding was attempted. Small crystals (~20 – 50 μm in length) of PII or crushed crystals of PII were seeded into new drops using a nylon fibre CryoLoop (Hampton Research). To minimize over-nucleation of the crystals, seeds were transferred after few cycles of dilution into precipitant solutions. After seeding, crystals continued to grow for about ten days, reaching a maximum size of ~200 X 200 X 100 μm .

2.3.3 Post-Crystallization Treatments

Crystals were soaked into different conditions prior to data collection for further cryo-protection and in an attempt to bind ligands to the protein. After the crystal had grown, it was transferred with a nylon fibre CryoLoop to a new drop containing the soaking solution with no protein. PII crystals were soaked into malonate solutions to remove citrate molecules from crystals. Also, soaking can be used for the dehydration of crystals to improve diffraction quality (Heras and Martin 2005). Generally, 30 – 70% of crystal volume is water, and crystals with higher density tend to diffract better. To dehydrate PII crystals, they were transferred serially, for about 1 h, in solutions containing increasing concentrations of citrate. In addition, transferring lids with drops and crystals onto new

precipitant solutions for crystal dehydration were attempted as well. It is a more gentle way to dehydrate, because it is not necessary to touch crystals with the loop.

2.3.4 X-ray Analysis of PII Crystals

An x-ray diffraction analysis was performed on crystals obtained with well solution containing 1.4 M ammonium citrate pH 7.0 and 10% (v/v) glycerol. An x-ray diffraction analysis was also performed on crystals soaked in 2.5 M malonate, 0.1 M Na-HEPES pH 7.0, and 10% (v/v) glycerol. The crystals were scooped up with a nylon fibre CryoLoop and flash-cooled to -170°C with a nitrogen gas stream (Oxford Cryostream). Diffraction data were collected using Cu-K α X-rays (1.54 Å wavelength) generated from a Rigaku RU-H3R X-ray generator and a Mar 345 image plate detector. Full data sets were collected on the home X-ray source by taking 20 minute exposures every 0.5° rotation of the crystal. A total of 400 exposures were taken for the data set. The crystals grown in ammonium citrate were found to belong to space group C2 with unit cell parameters $a = 92.71$, $b = 66.75$, $c = 61.74\text{Å}$, $\alpha = \gamma = 90^{\circ}$ and $\beta = 118.9^{\circ}$. The crystals soaked in malonate belong to space group C2 with unit cell parameters $a = 92.59$, $b = 66.73$, $c = 61.49\text{Å}$, $\alpha = \gamma = 90^{\circ}$ and $\beta = 118.9^{\circ}$. The data were processed, scaled, and merged using the HKL software package (Otwinowski 1997) that consists of DENZO, XDisplayF, SCALEPACK, and programs from CCP4 (version 4.2.2) (Collaborative Computational Project 1994). DENZO was used to index and integrate diffraction data, which could be visualized on XdisplayF. SCALEPACK was used to merge the entire data set and further refine the crystal parameters. Crystallographic statistics are summarized in Table 3.1.

The structure of PII with citrate was determined using the molecular replacement method (Storoni et al. 2004) using the structure of PII from *Synechocystis* sp. PCC 6803 (pdb file: 1UL3) as the search model. This cyanobacterial PII structure has approximately 50% sequence identity to *A. thaliana* PII and is the closest homologue with a known three-dimensional structure. The solvent content of the crystals was calculated to be 35% ($V_m = 1.9 \text{ \AA}^3/\text{Da}$) if a single PII trimer were present in the asymmetric unit. Crystallographic calculations were performed using programs in the CCP4 suite. The program PHASER (Storoni et al. 2004) was used for all molecular replacement calculations. The program Mifit (McRee 2004) was used to manually build PII model into the electron density map, and the model was refined using REFMAC (Winn et al. 2001). Procheck (Morris et al. 1992) was used to evaluate stereochemical parameters in the model. For the structure of PII with malonate, the *A. thaliana* PII structure with citrate was used as the search model.

2.4 Digestion of His-tagged NAGK

Initially, several different crystallization screens were attempted on purified His-tagged NAGK kindly supplied from Y. Chan (Dr. Moorhead lab), but no crystals were found. Therefore, proteolysis with enterokinase and trypsin was attempted to remove the N-terminal his-tag and possibly other flexible regions. His-tagged NAGK was digested with enterokinase and trypsin under different conditions of temperature, protein and enzyme concentrations, concentrations of substrates and inhibitors, as well as pH in order to find optimal digestion conditions. Trypsin was found to be better than enterokinase, but multiple digestion products were still generated, even under optimal digestion conditions.

2.5 Cloning of NAGK

The NAGK gene was amplified using the Polymerase Chain Reaction (PCR) (Saiki et al. 1988) using Vent polymerase and the His-tagged NAGK expression clone in the pRSET A plasmid (Invitrogen) as a template (Chen et al. 2006). First, *E. coli* DH5 α cells with pRSET A plasmid carrying the His-tagged NAGK expression clone were streaked on a LB agar plate with 100 mg/L ampicillin, and incubated overnight at 37°C. A few colonies were taken from the plate, inoculated in a 200 mL LB culture with 100 mg/L ampicillin and grown overnight at 37°C. Then, NAGK template was purified using midi prep kit (Qiagen) and eluted in water. The concentration of the template was measured using PicoGreen dsDNA quantitation reagent (Mullis and Faloona 1987). Primers for the NAGK template were prepared (Table 2.1). The PCR products were cleaned using the Qiagen PCR purification kit (Qiagen). First, the PCR products were digested with NdeI and cleaned using Minielute clean up kit (Qiagen). Then, they were digested with BglII and cleaned again.

Next, JM109 cells with pET3a plasmids were grown in 1 L LB culture with 100 mg/L ampicillin. The pET3a plasmids were purified with the Qiagen maxi prep kit (Qiagen), eluted in water, and the concentration of the plasmid was measured. The plasmids were digested with NdeI and BamHI for ligation. The digested PCR products were ligated into the digested pET3a to produce an expression construct of the full-length NAGK with a predicted mass of ~31kDa and the addition of a single methionine residue to the N-terminus.

2.6 Expression and Purification of NAGK

The pET3a recombinant plasmid encoding the cloned NAGK protein was transformed into competent cells of Rosetta gami pLysS cells. Cells were grown, sonicated and centrifuged by an identical protocol used for the PII protein expression and extraction, except that LB was used instead of terrific broth to grow cells. First, a blue dye column (BioRad) was used to capture most of the NAGK from the clarified cell extract. The column was equilibrated by running 20 mM Na-HEPES pH 7.0, 1 mM Na-EDTA, 2 mM DTT (dithiothreitol) and 10% (v/v) glycerol. The protein sample was loaded onto the column after being diluted to a final NaCl concentration of 30 mM to ensure maximum amount of protein binding. After washing the column with 80 mL of 250 mM NaCl, 20 mM Na-HEPES pH 7.0, 1 mM Na-EDTA, 2 mM DTT and 10% (v/v) glycerol, 8 mL fractions were eluted using 1.2M NaCl, 20 mM Na-HEPES pH 7.0, 1 mM Na-EDTA, 2 mM DTT and 10% (v/v) glycerol. After measuring the protein concentration of eluted fractions and checking for the presence of NAGK in eluted fractions using a NAGK activity assay (Chen et al. 2006), NAGK active fractions were pooled together for the next purification step.

The pooled NAGK was precipitated by the addition of ammonium sulfate (40 – 55% saturation) at 6°C overnight. The next morning, the precipitated protein was collected by centrifugation at 15,000 rpm for 30 min in a Sorvall centrifuge with SS-34 rotor, and then dissolved with 20 mM Tris-Cl pH 8.0, 0.2 mM Na-EDTA, 2 mM DTT and 10% (v/v) glycerol. Then, it was dialyzed overnight into 30 mM NaCl, 20 mM Tris-Cl pH 8.0, 0.2 mM Na-EDTA, 2 mM DTT and 10% (v/v) glycerol.

NAGK was further purified with anion exchange chromatography with a Hitrap QHP column (Amersham Biosciences). The column was equilibrated with 20 mM NaCl, 20 mM Tris-Cl pH 8.0, 0.2 mM Na-EDTA, 2 mM DTT and 10% (v/v) glycerol buffer, and the protein sample was loaded. NAGK was eluted into 1 mL fractions using a linear gradient of 0.02-1 M NaCl, and protein concentrations of NAGK active fractions were measured and purity was checked with SDS-PAGE gels.

Finally, NAGK fractions were pooled together and purified by gel filtration chromatography using a Superdex 200 10/300 GL column (Amersham Biosciences). The column was equilibrated with 100 mM NaCl, 10 mM Tris-Cl pH 8.0, 1 mM Na-EDTA, 2 mM DTT and 5% (v/v) glycerol buffer, which is the protein concentrating buffer, and 1 mL fractions were collected. After examining the purity of NAGK in each fraction collected using SDS-PAGE gels, pure protein was concentrated to about 9 mg/mL using centrifugal concentrators.

2.7 Crystallization of NAGK

2.7.1 Crystal Growth Screening

Using the Hydra-II-Plus-One pipetting robot (Matrix), 20 μ L of each crystallization solution was placed into the bases of a Corning 96 plate and 0.4 μ L of the same solution was combined with 0.4 μ L of the protein solution in the top shelves of the plate in a sitting drop setup.

Screening on concentrated NAGK (~6 mg/mL) was attempted using the Index HT (Hampton Research), PEGS (Qiagen) and CRYOS (Qiagen) sparse matrix screens, each of which contains 96 different conditions. Conditions which showed sign of crystallization were optimized and several substrates or products binding to NAGK (ADP, AMP-PNP, N-acetyl glutamate and arginine) were added for co-crystallization.

NAGK was crystallized in two different conditions for diffraction analysis. For the first NAGK crystal (AMP-NAGK), NAGK with 20 mM magnesium chloride, 10mM AMP-PNP and 10mM NAG was crystallized using reservoir solution containing 22% (w/v) PEG 4000, 0.18 M Na acetate, 0.1 M Tris-Cl pH 8.5, 2 mM DTT and 16% (v/v) glycerol. For another crystal (ADP-NAGK), NAGK with 5 mM ADP and 5 mM NAG was crystallized using reservoir solution containing 24% (w/v) PEG 3350, 0.2 M Li₂SO₄, 0.1 M BisTris-Cl pH 6.5, 2 mM DTT and 12% (v/v) glycerol. For both crystal forms, the hanging drop vapor diffusion method at room temperature by mixing 2 μ L NAGK with an equal volume of reservoir solution was used. Also, both crystals were allowed to grow for about two weeks and dehydrated overnight by transferring lids with drops and crystals onto new precipitant solutions having higher precipitant concentrations.

2.7.2 Crystallization of the PII: NAGK Complex

NAGK (~6 mg/mL) and PII (~6 mg/mL) were mixed with 3:1 and 2:1 mass ratio, and screening was attempted using the Index HT (Hampton research), PEGS (Qiagen) and CRYOS (Qiagen) sparse matrix screens, each of which contains 96 different conditions. Conditions which showed crystals were optimized and several substrates, products,

inhibitors and effectors binding to NAGK and PII (ADP, AMP-PNP, N-acetyl glutamate and arginine) were added for co-crystallization.

Under optimized conditions, NAGK and PII were mixed with 2:1 mass ratio in the presence of 40 mM arginine, 20 mM magnesium chloride, 10 mM ADP and 10 mM NAG as additives. It was crystallized using the hanging drop vapor diffusion method at room temperature by mixing 2 μ L of the PII:NAGK mixture with an equal volume of reservoir solution containing 8.5% (w/v) PEG 8000, 8.5% (w/v) PEG 1000, 0.1 M Na-HEPES pH 7.0, 0.4 M TMAO, 50 mM arginine, 2 mM DTT and 12% (v/v) glycerol. Crystals were allowed to grow for about two weeks and gently dehydrated overnight by transferring lids with drops and crystals onto new precipitant solutions having higher precipitant concentrations.

2.7.3 X-ray Analysis of NAGK and the PII: NAGK Complex Crystals

Prior to x-ray diffraction analysis, the PII: NAGK crystal (0.15 X 0.15 X 0.15 mm³), AMP-NAGK (0.15 X 0.15 X 0.10 mm³), and ADP-NAGK (0.2 X 0.2 X 0.03 mm³) were scooped up with nylon loops (Mitegen) and flash-cooled in a nitrogen gas stream at 100K.

Crystals were screened on the home X-ray source by taking 20 minute – 1 hour exposures at 0° and 90° rotations. For two NAGK crystals not complexed with PII, diffraction data were measured using synchrotron light sources at the Advanced Light Source (ALS) Beamline, under an agreement with the Alberta Synchrotron Institute (ASI). 180 frames of 6.73 s exposures and 112 frames of 1.37 s exposures at 1.0° crystal rotations were collected for AMP-NAGK crystal. 632 frames of 1.0 s exposures at 0.3° crystal rotations

were collected for ADP-NAGK crystal. The diffraction data of the PII: NAGK complex crystal was measured using synchrotron light source at the Canadian Light Source Beamline CMCF-1. 231 frames of 1.0 s exposures and 100 frames of 1.0 s exposures at 0.5° crystal rotations were collected. The PII: NAGK complex crystal was found to belong to space group $P2_13$ with unit cell parameters $a = b = c = 171.13\text{\AA}$, $\alpha = \beta = \gamma = 90^\circ$. AMP-NAGK crystal was found to belong to space group $R3$ with unit cell parameters $a = 99.37$, $b = 99.38$, $c = 179.52\text{\AA}$, $\alpha = \beta = 90^\circ$, $\gamma = 120^\circ$, and ADP-NAGK crystal had space group $P321$ with unit cell parameters $a = b = 177.37$, $c = 58.15\text{\AA}$, $\alpha = \beta = 90^\circ$, $\gamma = 120^\circ$. Data were processed and scaled using DENZO, SCALEPACK (Otwinowski 1997) and programs from CCP4 (version 5.0.2) (Collaborative Computational Project 1994). Crystallographic statistics are summarized in Table 4.1 and 4.2.

The structure of the PII:NAGK complex was determined using the molecular replacement method (Storoni et al. 2004) using the structure of PII from *A. thaliana* (pdb file: 2O66 (Mizuno et al. 2007) (~100% sequence identity)) and the one of NAGK from *P. aeruginosa* (pdb file: 2BUF (Ramon-Maiques et al. 2006) (~45% sequence identity)) as the search models. The solvent content of the crystal was calculated to be 73% ($V_m = 1.9 \text{ \AA}^3/\text{Da}$) if two PII and NAGK monomers were present in the asymmetric unit. Molecular replacement calculations were carried out using PHASER (Storoni et al. 2004). Then, the structure of NAGK subunit in the PII: NAGK complex was used as a model for two NAGK structures. The correct solutions yielded two and three monomers in the asymmetric unit and 55% and 57% of solvents contents for AMP-NAGK and ADP-NAGK crystals. Program Mifit (McRee 2004) was used to manually build models

into the electron density maps, and the models were refined using REFMAC (Winn et al. 2001). Procheck (Morris et al. 1992) was used to evaluate stereochemical parameters in the models.

Table 2.1. Sequences of primers used for NAGK cloning

	Sequence (5'→3')
Primer 1	GGGAATTCCATATGACCGTATCAACACCACCT
Primer 2	GAAGATCTTTATCCAGTAATCATAGTTCCAGC

Chapter Three: Results 1: Structures of PII

3.1 Purification of PII

PII in *A. thaliana* was expressed and purified from *E. coli* strain Rossetta gami plysS minus its transit peptide as the mature form that exists in chloroplasts (Smith et al. 2002; Smith et al. 2004). From a liter of terrific broth culture, approximately 20 mg of PII was obtained after two steps of purification. For crystallization, usually over 95% of purity is required, and PII showed great purity on SDS-PAGE gels (Figure 3.1).

3.2 Crystallization and X-ray Diffraction Analysis of PII

Monoclinic crystals diffracting to 1.9Å resolution were grown from tri-ammonium citrate (Figure 3.2). The crystal structure of *A. thaliana* PII was determined with the molecular replacement technique (Table 3.1). Initially, there were only small crystals, but larger crystals could be obtained after condition optimization. First, the protein concentration was varied between 4 – 7 mg/ml, and various ligands including ATP and 2KG were added. PII binding molecules may change the conformation of PII and make PII crystals better. To optimize the concentration of crystal growth precipitant, the concentration of tri-ammonium citrate was varied. Also, varying concentrations of glycerol was added as a cryo protectant. The crystals were grown optimally with a crystallization solution containing 1.4 M tri-ammonium citrate pH 7.0 and 10% (v/v) glycerol. Seeding crystals into new drops helped with obtaining good crystals and avoiding too many small crystals in the drops. Before the crystals were used for the x-ray diffraction analysis, they were dehydrated overnight by equilibrating crystals against new precipitant solutions having

higher precipitant concentrations. Although, excess concentration of ATP and 2KG were added into the PII solution, tri-ammonium citrate bound to PII instead of ATP and 2KG.

3.3 Interactions with Citrate and Malonate

Although extensive crystallization screens and post-crystallization soaking trials were performed using low-salt conditions in the presence of polymeric precipitants in both the presence and absence of natural effectors ATP and α KG, PII could only be crystallized in the presence of high concentrations of either citrate or malonate (Figure 3.4). Therefore, citrate and malonate bind in a positively charged pocket that has previously been shown to bind to the triphosphate group of ATP (Xu et al. 1998; Xu et al. 2001; Sakai et al. 2005) and sulfate anions (Xu et al. 2003) in PII proteins from bacteria and archaea. Although, it is not known whether citrate and malonate bind to PII at physiological concentrations in the cell, they may act as competitive inhibitors of ATP binding. ATP and α KG were added at concentrations of up to 50 mM to crystallization and soaking trials in an attempt to remove citrate and malonate, but this was unsuccessful. A structural comparison of *Arabidopsis* PII with citrate and *E. coli* PII with ATP revealed that citrate binds to the ATP binding pocket of PII. Citrate binds near the triphosphate binding site of ATP.

3.4 Crystal Structures of PII

3.4.1 Overall Structure of PII

The crystal structure shows that PII is a homotrimer of 15kDa subunits, which is found in the asymmetric unit of the crystal. Each subunit is composed of a double β - α - β motif in

which two α -helices are facing outside and four anti-parallel β -sheets are facing inside of homotrimer (Figure 3.3). Therefore, the core of the PII homotrimer is made of 12 anti-parallel β -sheets.

The long T-loop connecting the β 2 and β 3 strands in each protomer projects from one surface of PII. Similar to *E. coli* PII, the T-loop in the *A. thaliana* PII structure is mostly disordered (residues 49-63, 49-64, and 48-64 in subunits A, B, and C) (Figure 3.3). Disordered T-loop structures have been found in the crystal structures of various archaea and eubacteria (Cheah et al. 1994; Carr et al. 1996; Xu et al. 1998; Xu et al. 2001; Machado Benelli et al. 2002; Xu et al. 2003; Schwarzenbacher et al. 2004; Sakai et al. 2005; Nichols et al. 2006). Although a few crystal structures of *E. coli*, *Synechococcus*, and *Thermotoga* PII show ordered structures of T-loops, these structures are stabilized by crystal-packing interactions and likely do not represent a stable conformation of the T-loop for the free proteins in solutions. Studies by post-translational modifications and mutational analysis have indicated that T-loop has an important function for PII to interact with other downstream proteins in prokaryotes (Arcondeguy et al. 2001; Forchhammer 2004) and probably also in eukaryotes. This has been confirmed by the recent structures of PII proteins bound to effector ion channels (Conroy et al. 2007; Gruswitz et al. 2007) and enzymes (see below).

3.4.2 N-terminal Region of PII

A novel part revealed by the structure of *A. thaliana* PII is the N-terminal region with 13 amino acids, which is highly conserved only in plant PII (Figure 3.5). The N-terminus

projects from the opposite surface of the T-loop (Figure 3.3). This N-terminal region is stabilized by salt bridges with residues near the C-terminal end of the $\alpha 2$ helix and the C-terminus of the same protomer (Figure 3.6). Lys79, which is in the end of $\alpha 2$ and perfectly conserved in all plant PII, forms numerous interactions with highly conserved residues at the N-terminus. The hydrophobic aliphatic portion of Lys79 packs against the large aromatic side chains of Tyr6 and Tyr13, and the positively charged primary amino group forms hydrogen bonds with the negatively charged side chains of Asp5 and Asp9. Furthermore, Lys11 forms a salt bridge with Glu121 at the C-terminus, and both of them are highly conserved in plant PII proteins. Finally, Pro8 is preceded by a *cis*-peptide bond that causes the polypeptide backbone to adopt a sharp turn. Pro8 is perfectly conserved in plant PII but absent in bacterial and archaeal PII. We hypothesize that the highly conserved structure of the N-terminus may form a second protein-protein binding site in addition to the T-loop.

3.4.3 C-terminal Region of PII

The structure of the C-terminal region of PII reveals a number of features that are highly conserved only in plants (Figure 3.5). The C-terminal region is located near the ATP binding site and adopts slightly different structures in different protomers. The structure is well-ordered up to Glu124 in all three protomers, but the remaining 10 residues are disordered in two of the protomers. In the third one, the C-terminus is ordered up to Met 130, though it is stabilized by packing interactions with an adjacent molecule in the crystal lattice. The C-terminus runs into the adenosine binding site of ATP. It might suggest that in the absence of ATP, the C-terminus segment occupies the ATP-binding

site, and it may take a different conformation when ATP is bound. Because this C-terminal segment is only found in plant PII, these structural observations suggest that ATP-dependent conformational changes in the C-terminal segment may be involved with ATP-dependent interactions with PII binding proteins. This prediction is strikingly confirmed by the structure of the PII: NAGK complex.

3.4.4 Other Conserved Residues

There are a number of residues highly conserved only in plants, although most of the residues highly conserved in all eukaryotic and prokaryotic PII proteins are buried residues which form the hydrophobic core and intersubunit contacts of the trimer (Cheah et al. 1994; Xu et al. 1998). For instance, Trp22, Arg37 and Asp65 are highly conserved only in plants. Interestingly, they are located on the surface of the PII trimer near the T-loop. Therefore, they might be involved in intermolecular interactions with other proteins. The recent structure of the PII protein bound to NAGK showed the importance and functions of these plant specific residues (see below).

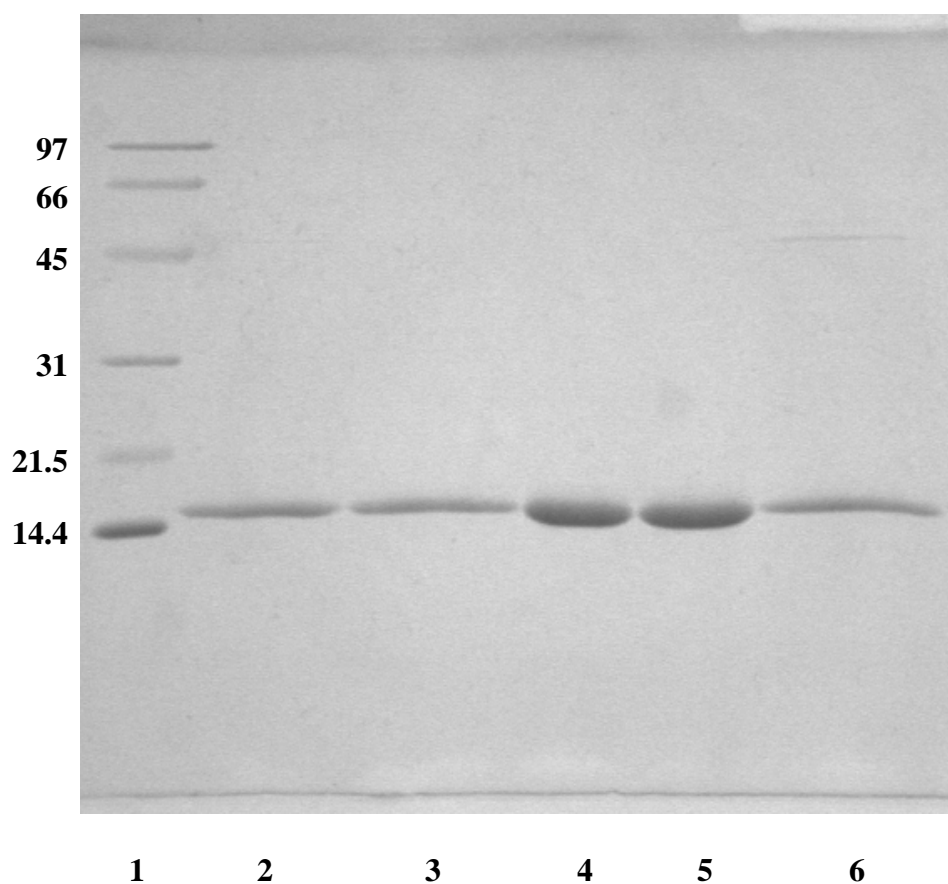


Figure 3.1. SDS-PAGE analysis of purified PII.

PII was visualized by Coomassie blue stained 20% SDS-PAGE. Lane 1 contains molecular weight marker proteins: Phosphorylase b, 97kDa: serum albumin, 66kDa: ovalbumin, 45kDa: carbonic anhydrase, 31kDa: trypsin inhibitor, 21.5kDa: lysozyme, 14.4kDa. Lanes 2 to 6 show the eluted fractions from hydrophobic interaction chromatography.

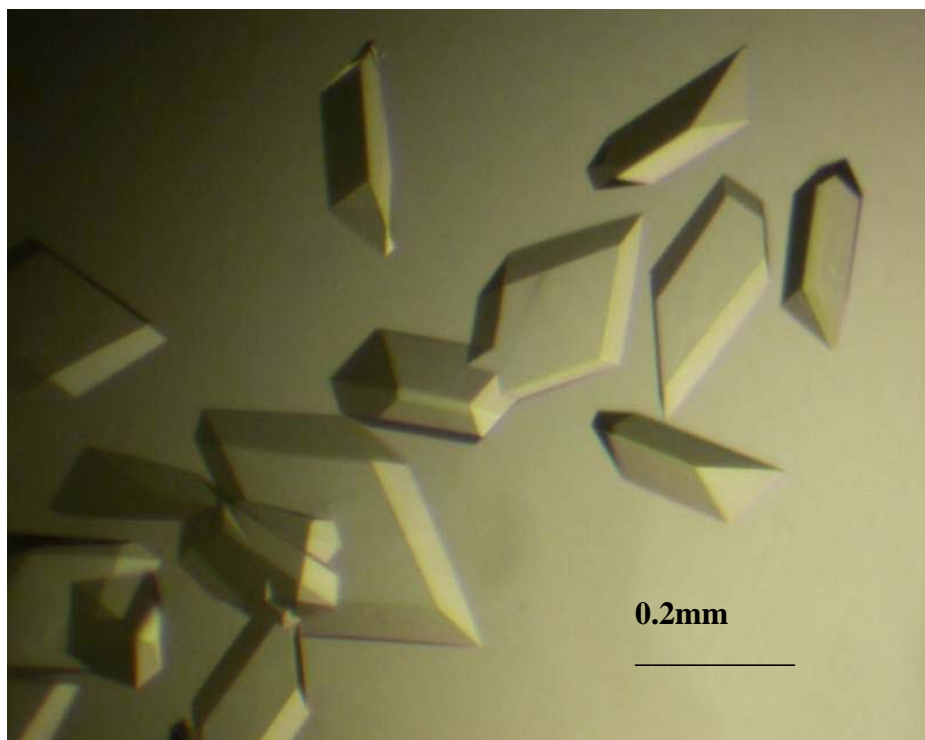


Figure 3.2. PII crystals grown in citrate.

Crystals of PII grown by seeding in crystallization solution containing 1.4 M Ammonium citrate pH 7.0 and 10% (v/v) glycerol.

Table 3.1. X-ray diffraction and refinement statistics for *A. thaliana* PII crystal

	Citrate complex	Malonate complex
Space group	C2	C2
Unit cell lengths (Å)	92.71, 66.75, 61.74	92.59, 66.73, 61.49
Unit cell angles (°)	90, 118.9, 90	90, 118.4, 90
Data Collection		
Wavelength (Å)	1.54	1.54
Resolution (Å)	20-1.9	20-2.5
Total reflections ¹	86074 (6815)	52167 (4596)
Unique reflections ¹	25717 (2469)	11464 (1139)
Completeness (%) ¹	99.2 (95.3)	99.7 (98.2)
Redundancy ¹	3.3 (2.8)	4.6 (4.0)
I/σ ¹	24.0 (5.0)	14.2 (2.4)
R _{sym} ^{1,2}	0.051 (0.244)	0.104 (0.517)
Refinement Statistics		
R _{work} ^{1,3}	0.191 (0.224)	0.201 (0.249)
R _{free} ^{1,4}	0.225 (0.284)	0.266 (0.408)
Number of Atoms		
protein	2509	2477
ligand	39	21
Solvent and ions	153	30
R.M.S. Deviations from Ideal Geometry		
Bond lengths (Å)	0.007	0.008
Bond angles (°)	1.03	1.04
Average Temperature Factors (Å²)		
Wilson plot	18.5	41.9
protein	24.6	42.9
ligand	37.0	58.5
water	32.9	46.6
Ramachandran plot (% residues)		
Most favoured	97.8	95.9
Additional allowed	2.2	4.1
Generously allowed	0.0	0.0
Disallowed	0.0	0.0

¹Values from the outermost resolution shell (Citrate: 1.97 – 1.90; Malonate: 2.59 – 2.50) are given in parentheses

² $R_{\text{sym}} = \sum_h \sum_i (|I_i(h) - \langle I(h) \rangle|) / \sum_h \sum_i I_i(h)$, where $I_i(h)$ is the i^{th} integrated intensity of a given reflection and $\langle I(h) \rangle$ is the weighted mean of all measurements of $I(h)$.

³ $R_{\text{work}} = \sum_h ||F(h)_o| - |F(h)_c|| / \sum_h |F(h)_o|$ for the 95% of reflection data used in refinement.

⁴ $R_{\text{free}} = \sum_h ||F(h)_o| - |F(h)_c|| / \sum_h |F(h)_o|$ for the 5% of reflection data excluded from refinement.

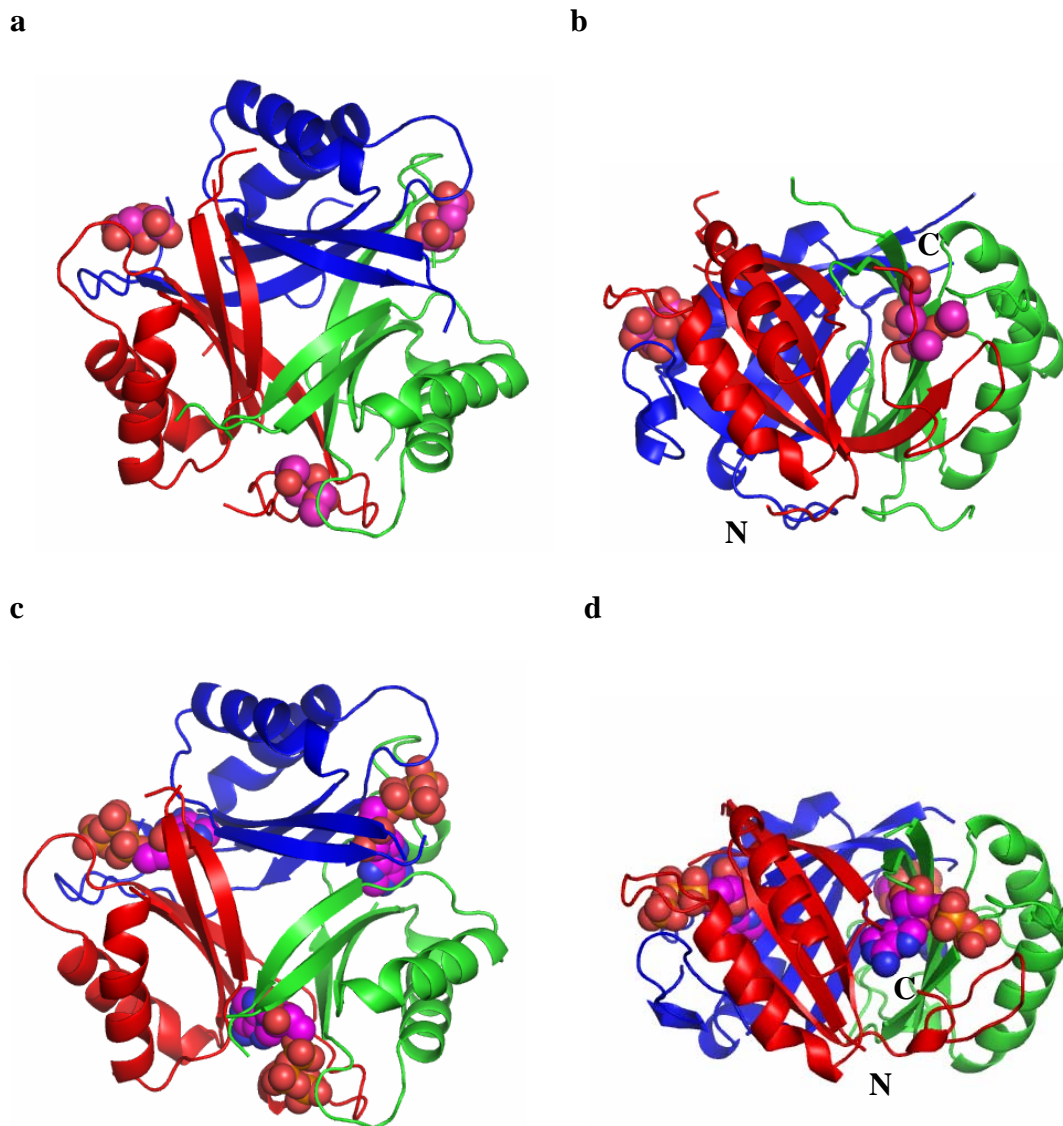


Figure 3.3. Conformational differences between *A. thaliana* PII structure and *E. coli* PII structure with ATP.

a) Structure of *A. thaliana* PII with citrate. Each monomer binds to one citrate molecule. T-loop is not shown, since it is disordered; b) side view of *A. thaliana* PII structure. The N terminus and C terminus of red PII monomer are shown; c) *E. coli* GlnK bound to ATP (Xu et al. 1998); d) Side view of GlnK structure.

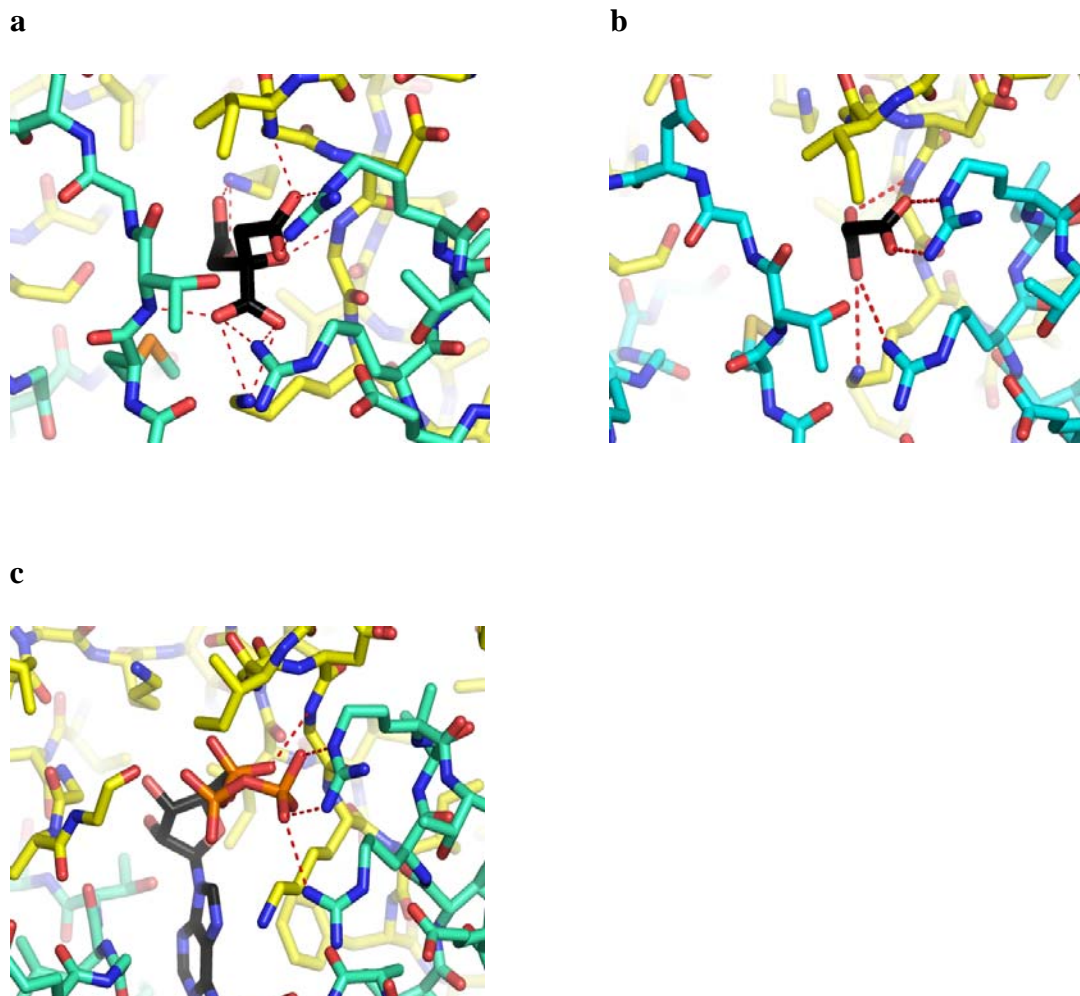


Figure 3.4. ATP binding sites of PII protein.

a) ATP binding site of *A. thaliana* PII with citrate; b) ATP binding site of *A. thaliana* PII with malonate; c) ATP binding site of *Thermus thermophilus* PII (pdb file: 1V3S (Sakai et al. 2005)) with ATP bound.

Figure 3.5. Sequence alignments of PII.

Sequence alignments of PII from plants (*Arabidopsis thaliana*, *Ricinus communis*, *Medicago sativa*, *Lycopersicon esculentum*, *Oryza sativa*, and *Pinus pinaster*), red algae (*Porphyra purpurea*), cyanobacteria (*Synechococcus* sp. PCC 7942 and *Synechocystis* sp. PCC 6803), archaeobacteria (*Thermus thermophilus*), and bacteria (*Herbaspirillum seropedicae*, *Escherichia coli* GlnB (2PII) and GlnK (1GNK)). PDB identifiers have been added to identify some of the three-dimensional structures that are currently available. Residues highly conserved only in plants at the N- and C-termini as well as internal residues that directly interact with the N-terminus are coloured red. Conserved residues important for complex formation with NAGK are coloured green. Highly conserved residues involved with the binding of ATP are coloured blue. Boxed residues are highly conserved plant-specific residues that differ from those found in archaea, bacteria, cyanobacteria, and red algae.

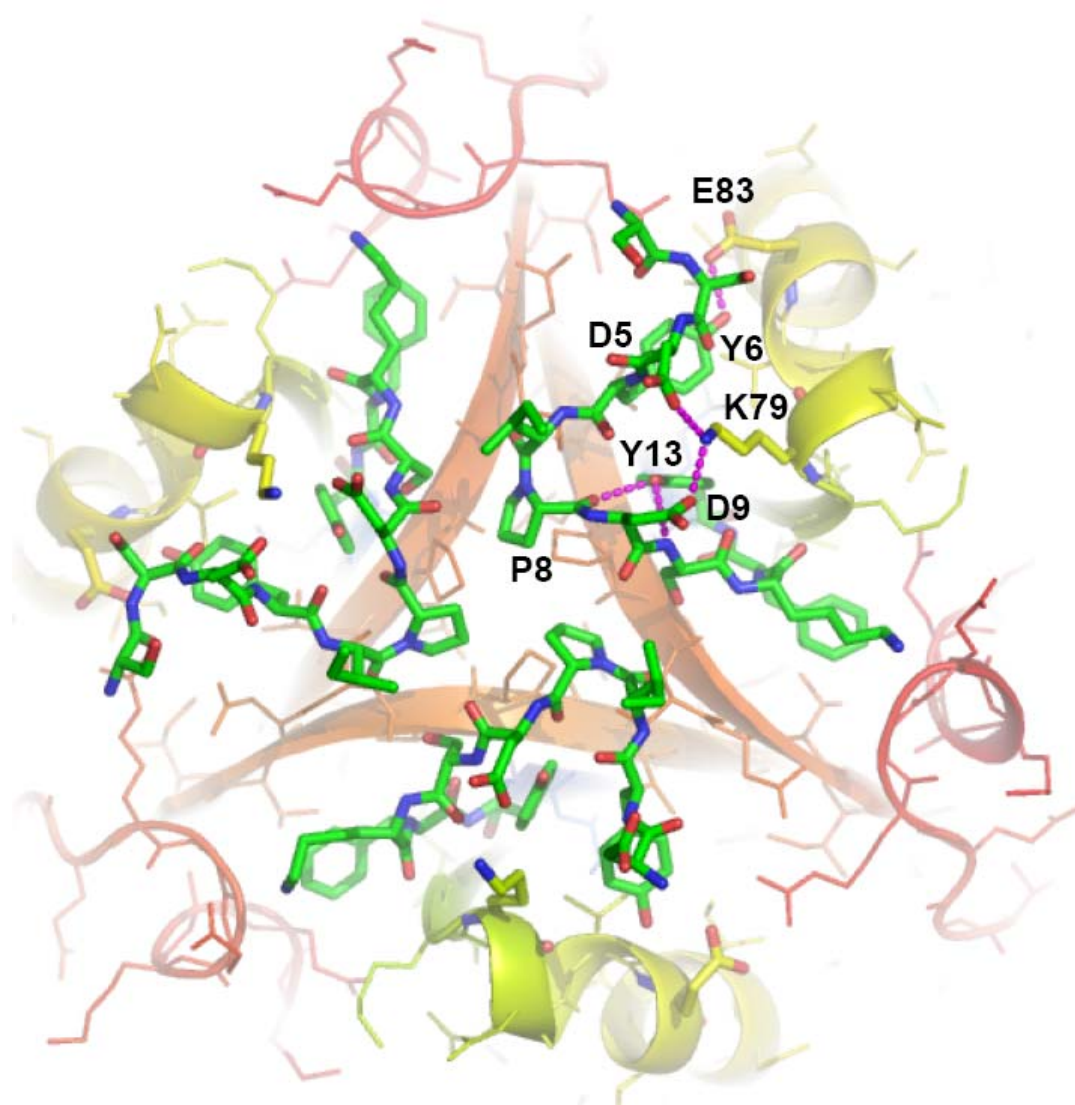


Figure 3.6. View of the N-terminal region of *A. thaliana* PII.

Hydrogen bonds are drawn as dashed red lines. Nitrogen atoms are coloured blue, and oxygen atoms are coloured red.

Chapter Four: Result 2: Structures of the PII: NAGK complex and NAGK

4.1 Digestion of His-tagged NAGK

Initially, crystallization trials were performed on His-tagged NAGK kindly provided by Dr. Moorhead laboratory, but promising crystals could not be obtained. Generally, it is known that tags may interfere with crystal packing, so I initially attempted to remove the His-tag by proteolysis. Although an engineered enterokinase cleavage site was expected to provide a means to remove the His-tag, enterokinase also cut NAGK at other sites. Digestions always showed a few bands on SDS-PAGE gels. Different conditions, such as temperature, concentration of enzyme and protein, pH were tried, but digestion conditions yielding a single band could not be obtained. Also, the fact that NAGK forms hexamers made the purification very hard after digestion. Some monomers might be digested more, though others are not. Trypsin was also used in an attempt to remove the His-tag. Although, trypsin was better than enterokinase, other parts in NAGK were digested as well.

4.2 Cloning, Expression and Purification of NAGK

Cloning of non-tagged NAGK was performed to obtain a more homogeneous sample for crystallization. Cloning of the mature form of NAGK was successful and NAGK with a mass of ~31 kDa was synthesized. Non-tagged NAGK was expressed with LB media and purified. Because the calculated pI of NAGK using PROWL (<http://prowl.rockefeller.edu/>) is about 6.4, cation exchange chromatography was used as an initial purification step at pH 6.0. Although NAGK bound to the column and good purity could be obtained, some of the protein did not bind to the column. The pI of

NAGK is below 7.0, so anion exchange column can be another choice. However, it can not be used as a first step, because the extract contains nucleic acids that are strongly negatively charged and bind to the column very strongly. For a good first purification step, a blue dye column at pH 7.0 was chosen, because most of the NAGK in the extract bound to the column. Dye columns are generally used for proteins which bind to nucleotide cofactors, such as ATP and NAD⁺/NADH (Scopes 1987). However, the dye column is also negatively charged and has hydrophobic properties. NAGK may have bound to the column because of negative charge and hydrophobicity, since NAGK was not eluted by the addition of ATP to the column. NAGK was eluted using a NaCl gradient, though it was eluted very broadly. The next step used was ammonium sulfate precipitation, because NAGK was in high salt already and this is an effective method for storing proteins. After this step, the precipitate was dissolved and dialyzed into low salt buffer at pH 8.0 for anion exchange chromatography. This step worked very well to remove contaminant proteins. Finally, the gel filtration column was used. This step worked very well, because NAGK forms a hexamer and is much bigger than many other contaminant proteins (Figure 4.1). Approximately 2 mg of NAGK was obtained from 1 L of LB media.

4.3 Crystallization and X-ray Diffraction Analysis of the PII: NAGK Complex

First, sparse matrix crystal screens were attempted on a mixture of purified NAGK and PII without any tags and extra residues. These screens yielded several different crystal forms. Most of the crystals obtained initially were needle-like, but more promisingly, a cubic shaped crystal with a smooth surface was found (Figure 4.2). Most interestingly,

different ratios of PII and NAGK showed differences in crystal appearance. Although most of these cubic crystals had large sizes and very smooth surfaces, they did not diffract well enough for structural analysis. Many trials of condition optimization were attempted, but high resolution diffraction data could not be measured.

After performing many crystallization screens, a second crystallization condition was found with 8.5% (w/v) PEG 8000, 8.5% (w/v) PEG 1000 and 15% (v/v) glycerol. These crystals were reproduced in hanging drops and many series of optimization trials were performed. First, different ratios of PII and NAGK were used in an attempt to obtain better crystals. The mass ratio of 2 PII protomers to 1 NAGK protomer, using protein concentration measurements from the BioRad Coomassie Blue Bradford assay (Bradford 1976), showed the best crystals. Also, different binding molecules were added into the protein solution, because the binding molecules might change the conformation of proteins in the crystals and allow the proteins crystallize better. The addition of arginine, ADP, NAG and $MgCl_2$ into the protein solution prior to the crystallization trials gave better crystals. Furthermore, trimethylamine oxide (TMAO) was added into the crystallization solution. TMAO is known as a protein structure stabilizing agent, and also it is a cryoprotectant agent (Jiang et al. 2006). The best crystal was obtained with a crystallization solution containing 8.5% (w/v) PEG 8000, 8.5% (w/v) PEG 1000, 0.1 M Na-HEPES pH 7.0, 0.4 M TMAO, 50 mM arginine, 2 mM DTT and 12% (v/v) glycerol. Finally, a large complex crystal giving high resolution structural data was grown (Figure 4.2). Before the crystal was used for the x-ray diffraction analysis, it was dehydrated overnight by equilibrating crystals against new precipitant solutions having higher

precipitant concentrations. The structure was determined with the molecular replacement technique to 2.5Å resolution (Table 4.1). Ramachandran plots were generated by Procheck (Morris et al. 1992), and stereochemical parameters in the model were evaluated (Figure 4.3).

4.4 Crystal Structure of the PII: NAGK Complex

4.4.1 Complex Formation between PII and NAGK.

The asymmetric unit of the crystal (space group P2₁3) contains two protomers of NAGK and two protomers of PII. A crystallographic three-fold rotational symmetry axis coincides with the molecular three-fold rotational axis of the complex to generate the dodecameric complex that forms in solution. The solved complex structure showed that two PII trimers bind to one NAGK hexamer, thus closing the central hole of the hexamer (Figure 4.4). The overall dimensions of the complex are ~115 X 105 X 105 Å, with the longest dimension spanning along the three-fold rotation axis reaching from the N-terminal segments of one PII trimer to the N-terminal segments of the second PII trimer.

Each PII protomer contacts a single, separate NAGK protomer with the T-loop (Figure 4.5), which was disordered in previously determined PII structures (Mizuno et al. 2007). The T-loop is well-ordered and forms numerous contacts with NAGK in the complex. The side chains of Arg56 and Ser60 in PII form hydrogen bonds with the main chain carbonyl and amide groups from residues Val159 and Val162 in NAGK. In addition, electrostatic interactions are formed by the side chains of Arg56 and Glu61 in PII with the oppositely charged side chains of Glu201 and Arg145 in NAGK. The main chain

amide groups of Glu61 and Gly59 in PII also form hydrogen bonds with the carbonyl groups of Ala160 and Gln265 in NAGK. Furthermore, the side chain of Trp22 of PII forms a hydrogen bond with the main chain carbonyl group of Ala264 of NAGK, as well as van der Waals contacts with Gln265 and Gly266. All of these residues in PII except Trp22 are in the T-loop. They are binding to the ends of two central helices in NAGK that are adjacent to the ATP and NAG substrate binding sites. Thus, the binding of PII may activate NAGK by bringing the ATP and NAG binding sites together.

The pattern of sequence conservation in residues at the PII: NAGK interface indicates that the mode of binding between PII and NAGK is highly conserved in cyanobacteria and plants (Figure 4.6). Arginine-sensitive bacterial NAGK also share many of these conserved residues. However, Arg145 and Gln265 are not conserved for bacterial NAGK, but are perfectly conserved for plants and cyanobacteria. *T. maritima* and *P. aeruginosa* NAGK have glutamate and lysine for Arg145, and have glycine for Gln265. Also, Arg56 for PII is conserved in plants and cyanobacteria, but not in bacteria. Trp22 for PII is conserved only in plants, and cyanobacteria and bacteria have phenylalanine instead. Thus, the binding of PII to NAGK might be stronger for plants.

4.4.2 Overall Structure of *A. thaliana* NAGK.

The NAGK hexameric structure adopts a ring-like shape that consists of dimers arranged about a three-fold rotation axis, as previously seen in the bacterial NAGK hexamers from *T. maritima* and *P. aeruginosa* (Figure 1.4). The general organization of protomers is also similar to the bacterial NAGK (Ramon-Maiques et al. 2006).

NAGK is constructed with two domains separated by a hinge (residues 211–212). The N-terminal domain binds NAG and the C-terminal domain binds ATP. Each protomer interacts with adjacent protomers through two distinct interfaces (A and B) lying along two-fold rotation axes (Figure 4.7). Interface A is formed primarily by packing interactions between the edges of the central 8-stranded β -sheet, an adjacent loop and two flanking α -helices. Interface B is formed between the N-terminal helices of adjacent protomers. First approximately fifteen residues preceding the N-terminal alpha helix are disordered and not conserved (Figure 4.6). Interface A is found in all bacterial NAGK, but interface B and the N-terminal helix seem to be found only in organisms where arginine acts an allosteric inhibitor. For example, *E. coli* NAGK, which forms a dimer, is not allosterically inhibited by arginine and does not have interface B and the N-terminal helix (Ramon-Maiques et al. 2002). The N- and C-termini, as well as the allosteric inhibitor arginine are located in close proximity. The N and C-termini are connected with mostly hydrophobic contacts. Also, as seen previously in the NAGK hexamers from *T. maritima* and *P. aeruginosa*, arginine binds near the C-terminal end of the N-terminal helix and C-terminus.

4.4.3 Structural Differences between NAGK protomers in the PII: NAGK Complex.

There is an interesting difference between the structures of the two NAGK protomers in the asymmetric unit of the complex. One of the NAGK protomers is in a more closed conformation and the other protomer is in a more open conformation (Figure 4.8). Superimposing of these NAGK protomers showed no significant differences at the PII binding sites, and both NAGK bind PII equally with the same residues. The distance

between Gly251 α C and Gly96 α C is 4.2Å for closed, but it is 7.0Å for open. Therefore, the distance between ADP and NAG is closer in the closed form of NAGK. The distance between the β -phosphate and the closest carboxylate oxygen atom in NAG is 5.5Å for the closed form, but it is 7.3Å for open form.

Also, there are some differences with ADP and NAG binding residues between the open and closed forms of NAGK. Both open and closed forms bind to NAG and ADP similarly, but the closed NAGK protomer can bind NAG and ADP more tightly. The closed NAGK protomer is binding to NAG with the side chains of Asn192, Asn194 and Arg98 (Figure 4.9). The main chain amide groups of Gly76, Arg98 and Ala 195 also form hydrogen bonds with NAG. However, there are no interactions between NAG and the side chain of Asn194 or between NAG and the main chain amide groups of Gly76 and Arg98 for the open form. As a result, the closed NAGK protomer forms more interactions with NAG.

ADP also binds to the closed protomer with more interactions (Figure 4.10). The closed protomer binds to ADP with the side chains of Lys255 and the main chain amide groups of Ala45 and Gly44. In addition, it binds with the main chain carbonyl groups of Lys247 and Leu221 by forming hydrogen bonds, and the adenosine base group of ADP has a van der Waals contact with Met252. Furthermore, α - and β -phosphate groups have interactions with Mg²⁺ ion, which keeps ADP tightly bound to NAGK. The phosphate groups interact with Asp196 and the carbonyl group of Gly251 through Mg²⁺ ion. However for the opened NAGK protomer, Gly44 and Ala45 are too far from the β -

phosphate group to have hydrogen bonds. In addition, no electron density is seen for Mg^{2+} next to the phosphate groups. Thus, the binding of ADP appears to be weaker in the open conformation as well.

The residues binding to ADP and NAG are highly conserved among plants, cyanobacteria and bacteria (Figure 4.6). NAGK may need to adopt open and closed conformations to promote the binding of substrates and release of products, as well as to promote catalysis. It is likely that the closed NAGK conformation, which has the shorter distance between ADP and NAG, should be closer to the transition state conformation required for catalysis than the open form. Perhaps the open form is needed for the exchange of substrates and products.

Comparisons of the *A. thaliana* NAGK structures in the PII: NAGK complex with the arginine bound *T. maritima* NAGK structure shows that both the open and closed *A. thaliana* NAGK protomers are more closed than the respective open and closed bacterial proteins (Figure 4.11). Therefore, PII binding might have brought the two NAGK domains closer together to make NAGK more active.

4.4.4 Arginine Binding Site of the PII: NAGK Complex

The arginine binding site for plant NAGK was found in the PII: NAGK complex structure. Arginine is sandwiched between the N-terminal helix, the central β -sheet, C-terminal loop, and the helix of residues 280-285 (Figure 4.12). Arginine binding residues are highly conserved in all of the bacterial, archaeal, cyanobacterial and plant NAGK

which are sensitive to arginine (Figure 4.6). However, there are a few differences between plant and bacterial NAGK. For example, arginine is not binding to the N-terminal helix for plant NAGK. Arginine molecule of *T. maritima* NAGK binds to Tyr15 (Ramon-Maiques et al. 2006). This Tyr15 is conserved for bacteria and cyanobacteria, but it is phenylalanine for plants (Figure 4.6). As a result, the tyrosine-mediated N-terminal movement by arginine proposed for bacterial NAGK does not likely happen for plant NAGK.

Because we have not yet determined an arginine-bound structure of plant NAGK in the absence of PII, it is difficult to explain precisely how arginine inhibits plant NAGK. However, if the NAGK structures in the PII: NAGK complex and bacterial TmNAGK are compared, there are interesting differences. For example, Arg84 of the arginine-inhibited form of *T. maritima* NAGK, which is equivalent to *A. thaliana* Arg98, does not bind to NAG, whereas *A. thaliana* NAGK shows that Arg98 interacts with the carboxylate of NAG. As a result, arginine binding to plant NAGK might move Arg98 away from NAG and lower the binding affinity. Lowering the binding affinity of NAG may then result in the inhibition of NAGK. Since the arginine binding sites of two adjacent protomers are also connected through N-terminal helices from adjacent protomers, the residues in the N-terminal helices close to arginine binding sites may transmit signals through these interactions.

4.4.5 Structure of PII in the PII: NAGK Complex

The structures of the two PII trimers in the complex appear to be very similar to the structures of free PII previously solved with citrate and malonate (pdb file: 2O66 and 2O67 (Mizuno et al. 2007)) (Figure 4.13). The main difference between the structures of free and complexed PII is the conformation of the T-loop (residues 49-66), which is disordered without complex formation. The T-loops of all three copies in the asymmetric unit of non-complexed PII crystals are all disordered and appear to be highly flexible. However, the T-loop becomes well-ordered and forms numerous contacts with NAGK in the complex.

One of the most interesting new interactions seen in the PII: NAGK complex, but not in uncomplexed PII, involves Arg37 of PII. Arg37 is conserved only in plants, and forms an extensive network of hydrogen bonds with Asn64, Ala49 and Gly51 on the next PII protomer (Figure 4.14). These residues are also perfectly conserved only in plants and sit at the edge of the T-loop (Figure 3.5). Thus, Arg37 likely stabilizes the conformation of the T-loop required for binding to NAGK. In the structures of uncomplexed PII, Asn64, Ala49 and Gly51 were all disordered.

The C-terminal segment of PII (residues 125-134) also adopts a different conformation in the PII: NAGK complex. The C-terminus is located very close to the T-loop and ATP binding site. In uncomplexed PII, the C-terminus was mostly disordered except one protomer, which was stabilized by crystal contacts. In the complex, the C-terminus has a more stable and likely very different structure, because it is pushed away by the T-loop

(Figure 4.15) and the T-loop has a fixed structure. In addition, there is a hydrogen bond between Thr127 and Gly51 on the next protomer (Figure 4.14). It might be another factor stabilizing the C-terminal structure.

Although few PII structures complexed with ADP and ATP have been solved, the structure of the PII: NAGK complex is the first plant PII structure with bound ATP (Figure 4.16). ATP was not added into the crystallization solution of the PII: NAGK complex crystal, but ATP produced by *E. coli* likely bound to PII when PII was expressed. ATP in the complex binds to PII at the same place where the citrate molecule was found in the free PII with citrate. Superimposing of complexed PII with NAGK and the free PII with citrate shows that the triphosphate moiety binds at the same position of citrate (Figure 4.17). Furthermore, the superposition of ATP binding sites of PII protomers from *A. thaliana*, *Thermus thermophilus* (*T. thermophilus*) (pdb file: 1V3S (Sakai et al. 2005)), *E. coli* (pdb file: 2GNK (Xu et al. 1998)), *M. jannaschii* (pdb file: 2J9E (Yildiz et al. 2007)) and *E. coli* GlnK bound to ADP in the ammonium transporter complex (pdb file: 2NS1 (Gruswitz et al. 2007)) shows that the general organization of residues surrounding the adenosine base of ATP are quite similar (Figure 4.17).

There are only a few structures of PII proteins with ordered T-loop structures, likely because the T-loops are flexible. To compare the shapes of the T-loops, *A. thaliana* PII with NAGK was superimposed with *E. coli* GlnK with the transmembrane ammonium transporter (pdb file: 2NS1 (Gruswitz et al. 2007)), *Synechococcus* sp. PCC 7942 PII (pdb file: 1QY7 (Xu et al. 2003)) and *M. jannaschii* PII with bound Mg^{2+} -ATP and 2KG

(pdb file: 2J9E (Yildiz et al. 2007)). They have very different conformations (Figure 4.18). The T-loops of *Synechococcus* sp. PCC 7942 PII are stabilized by crystal packing and stretching perpendicularly to the three fold axis of trimer. The T-loops of *E. coli* GlnK with the transmembrane ammonium transporter are stretching parallel to the three fold axis of the trimer to act as a plug stopping the flow of ammonia when bound to the transporter. However, the T-loops of the PII: NAGK complex adopt a very different conformation. The T-loops of the PII: NAGK complex are bent approximately perpendicular to the three fold rotation axis. Perhaps, T-loops are highly flexible and may change conformations for different interacting proteins. The T-loop structure of *M. jannaschii* PII with bound Mg^{2+} -ATP and 2KG is similar to the structure of the PII in the PII: NAGK complex (Figure 4.19). The T-loops of *M. jannaschii* PII with bound Mg^{2+} -ATP and 2KG are bent and bind to the 2KG molecule at the top of the loop.

4.4.6 Function of ATP Binding on PII

ATP is well known as a signaling molecule of the cellular energy levels. Therefore, ATP binding should have important structural and functional influences on PII. The PII: NAGK complex structure is a great example showing the molecular mechanism through which ATP binding modulates the regulation of an effector enzyme. As mentioned previously, ATP binding site is located very close to the C-terminal segment and the T-loop. As a result, ATP might have an important function to change the structures of the C-terminus and the T-loop.

From the structure of the PII: NAGK complex, the binding of ATP to PII favors a conformation of the T-loop that interacts with NAGK (Figure 4.14). ATP has numerous interactions with residues at the base of T-loop that appear to stabilize the conformation of T-loop seen in the complex. The triphosphate group of ATP directly coordinates the Mg^{2+} ion that binds to the main chain carbonyl oxygen of Gly48 at the base of the T-loop. Since the metal ion is critical for bridging the negatively charged phosphate group to the carbonyl oxygen, Mg^{2+} binding appears to be essential for stabilizing a conformation of the T-loop that favours interactions with NAGK. The ATP binding residues including Gly48 in *A. thaliana* are conserved in PII from bacteria, archaea and eukaryotes (Figure 4.6). Previous mutagenesis studies in *E. coli* showed that the replacement of the equivalent Mg^{2+} binding residue, Gly37, with Ala can disrupt PII interactions with bacterial receptors, as well as 2KG and ATP modulators (Jiang et al. 1997).

ATP binding to PII has important effects on the structure of the C-terminal segment (residues 125-134), which is only found in plants, where the sequence is highly conserved. As mentioned previously, the C-terminal segment in PII complexed with NAGK and in free PII bound to citrate have very different conformations (Figure 4.15). In the PII: NAGK complex, the adenosine base of ATP lies in a hydrophobic pocket occupied by Met126 in the absence of bound adenosine nucleotides. Displacement of Met126 from the ATP-binding pocket in turn allows the movement of the C-terminal segment away from the position occupied by the T-loop in the conformation required for interacting with NAGK. Met126 is perfectly conserved in plants. Therefore, the coupled

changes in the conformations of the C-terminal segment and the T-loop by ATP might be essential components of an ATP-dependent switch found only in plants.

4.4.7 Comparison of Structural Data with the Experimental Data.

The binding ratio in the complex crystal structure is 1 PII monomer: 1 NAGK monomer. However, isothermal titration calorimetry (ITC) and gel filtration chromatography indicated that the ratio is 1 PII monomer: 2 NAGK monomers (Chen et al. 2006). Only one PII trimer binds to one NAGK hexamer. One of the possible reasons of the difference is the method used to measure the PII and NAGK concentrations. The Bradford assay relies on the increase in absorption of Coomassie Blue G250 following binding to protein. Because different proteins bind different amounts of dye, only an approximate value for the absolute concentration of a specific protein can be obtained by this method (Bradford 1976). Another possibility is that the crystal of the complex structure was formed in the presence of arginine, but arginine was absent during the gel filtration and ITC experiments. Since arginine appears to help the binding of PII to NAGK, the number of PII binding might have been higher if arginine was present. The main function of plant PII: NAGK complex formation is the relief from the arginine inhibition.

Unfortunately, we have not been able to determine a structure of free NAGK bound to arginine from *A. thaliana*. Thus, it is difficult to determine how arginine inhibits NAGK. However, the NAGK structures without arginine, which should be in the active forms, and the one complexed with PII have highly similar conformations. This is consistent

with the prediction that PII can change the inactivated form of NAGK to the activated form.

4.4.8 Activity Change by 2-ketoglutarate (2KG) Binding to PII.

In the presence of ATP and 2KG, the activity of the PII: NAGK complex increases (Chen et al. 2006). However, the PII: NAGK structure did not have 2KG. 2KG binds to PII and signals carbon status in the chloroplast only when ATP binds to PII. 2KG likely has the ability to interact with ATP and the T-loop and affect the PII binding to NAGK. There is only one PII structure with 2KG (Yildiz et al. 2007) (2J9E). This PII structure is from *M. jannaschii*, and it was shown that ATP binding changes the conformation of the T-loop and let 2KG bind to the T-loop. One 2KG molecule binds to a single protomer and sits on the T-loop (Figure 4.19). The superposition of *M. jannaschii* PII with 2KG and PII in the PII: NAGK complex showed the very similar overall T-loop structures. Also, the detailed conformations of the 2KG binding sites are similar. Tyr51, which is perfectly conserved in bacteria and cyanobacteria, in *M. jannaschii* PII binds to 2KG with a hydrophobic contact. Phe62, which is perfectly conserved in plants, in *A. thaliana* PII has a hydrophobic property as well and is located at this position (Figure 4.19).

On the PII (GlnK): transmembrane ammonia channel (AmtB) complex, the 2KG binding sites were investigated using the DOCK6 program (Gruswitz et al. 2007). For the GlnK: AmtB complex, 2KG promotes the dissociation of GlnK from the channel. Therefore, 2KG is an important molecule for regulating the ammonia transport system. Two potential 2KG binding sites were located at the base of T-loops, and one of them is in

close proximity to the ADP binding site. This site was previously proposed based on the free *E. coli* PII structure as well (pdb file: 2GNK (Xu et al. 1998)). It has also been proposed that a counter ion such as Mg^{2+} may be necessary for the stronger binding of 2KG.

Superposition of the possible 2KG binding sites of the GlnK: AmtB and the PII: NAGK complex shows that the GlnK: AmtB complex has a large enough space to hold 2KG, but the PII: NAGK complex does not (Figure 4.20). This is because the T-loop of the GlnK: AmtB complex is straight, but the one of PII: NAGK is bent with a small loop around residues 49-53 that run into the possible 2KG binding site. The C-terminus also runs into the possible 2KG binding site.

4.5 Crystallization and X-ray Diffraction Analysis of NAGK

Crystals of NAGK without any tags and extra residues were obtained. Interestingly, the shapes of crystals differ depending on substrates added (Figure 4.21). This might suggest that the binding of different substrates may cause conformational changes in NAGK. Although crystallization screens of NAGK yielded many different types of crystals, most crystal forms yielded very poor diffraction patterns that were unsuccessful for structural analysis.

After performing many crystallization screens and condition optimization attempts, two crystals with good diffraction have been obtained (Figure 4.22). The crystals of NAGK were grown in two different conditions, and both of the structures were determined with

the molecular replacement technique using the refined structure of NAGK from the PII: NAGK complex.

The first NAGK crystallization condition was found in a screening condition with 25% (w/v) PEG 4000, 0.18 M Na acetate, and these crystals reproduced in hanging drops as well. This crystal form was obtained with $MgCl_2$, AMP-PNP and NAG. A modification in the crystallization conditions was first made by changing pH. Various buffers with different pH (6.5- 8.5) were attempted, and a buffer with pH 8.5 gave the best crystals. Also, glycerol was added as a cryo-protectant, and the concentrations of PEG 4000 and Na acetate were optimized. The best crystal was obtained with a crystallization solution containing 22% (w/v) PEG 4000, 0.18 M Na acetate, 0.1 M Tris-Cl pH 8.5, 2 mM DTT and 16% (v/v) glycerol (Figure 4.22). After the overnight crystal dehydration, the crystal structure of NAGK complexed with AMP-PNP was determined to 2.3Å resolution.

Another NAGK crystallization condition was found in a screening condition with 25% (w/v) PEG 3350, 0.2 M Li_2SO_4 . The crystal was found in this condition with ADP and NAG. These crystals reproduced in hanging drops. First, the pH of the crystallization solution was changed by adding a buffer. Buffers with various pH (6.5- 8.5) were attempted, and pH 6.5 showed the best crystals. Glycerol was also added as a cryo-protectant. The concentrations of PEG 3350 and Li_2SO_4 were optimized. The best crystal was obtained using reservoir solution containing 24% (w/v) PEG 3350, 0.2 M Li_2SO_4 , 0.1 M BisTris-Cl pH 6.5, 2 mM DTT and 12% (v/v) glycerol (Figure 4.22). Crystals were dehydrated overnight by equilibrating crystals against new precipitant

solutions having higher precipitant concentrations. The crystal structure of NAGK complexed with ADP was determined to 3.0Å resolution.

4.6 Crystal Structures of NAGK

NAGK with AMP-PNP has two 31kDa subunits, and NAGK with ADP has three subunits in the asymmetric unit of the crystal. Each subunit in the asymmetric unit of each crystal is virtually identical after superimposing, but the subunits from the AMP-PNP complex show a more opened conformation than the subunits from the ADP complex. The biologically relevant hexamers from both NAGK structures show ring-like shapes similar to those seen in the PII: NAGK complex and NAGK from *T. maritima* and *P. aeruginosa* (Figure 4.23). The overall fold of each monomer is also similar to *E. coli* NAGK (Ramon-Maiques et al. 2006).

The structure of NAGK protomer bound to AMP-PNP is open and similar to the structure of the open NAGK protomer in the PII: NAGK complex. On the other hand, NAGK protomer bound to ADP has a more closed conformation and is similar to the structure of the closed NAGK protomer in the PII: NAGK complex. Therefore, the free NAGK also has different transition state conformations, which were shown in the PII: NAGK complex structure.

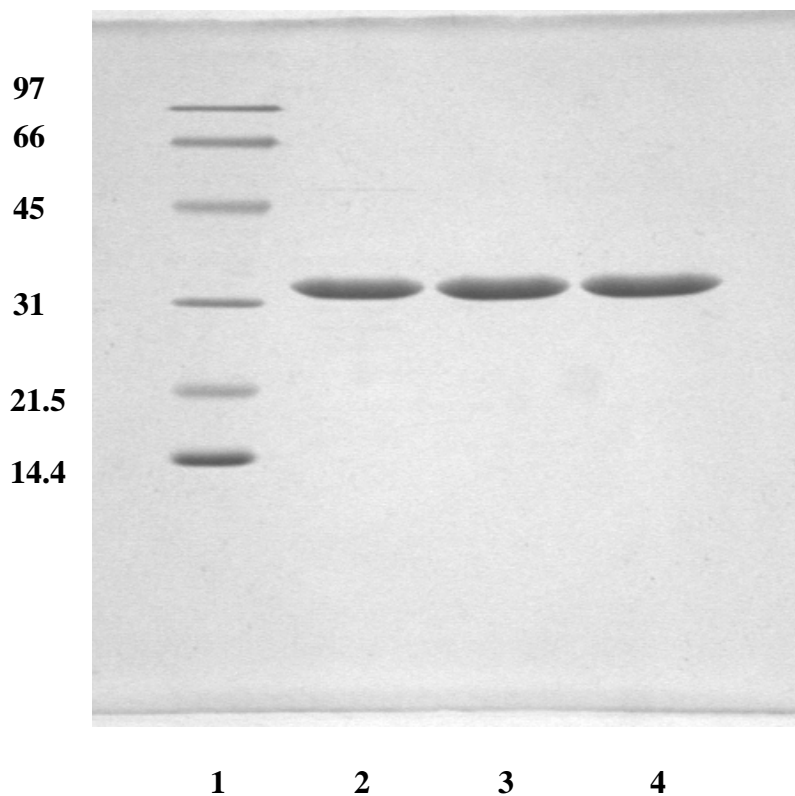


Figure 4.1. SDS-PAGE analysis of purified NAGK.

NAGK was visualized by Coomassie blue stained 20% SDS-PAGE. Lane 1 shows molecular weight marker proteins and they are exactly same to the one used in Figure 3.1. Lanes 2 to 4 show the fractions eluted. None of the fractions show any strong contaminating bands.

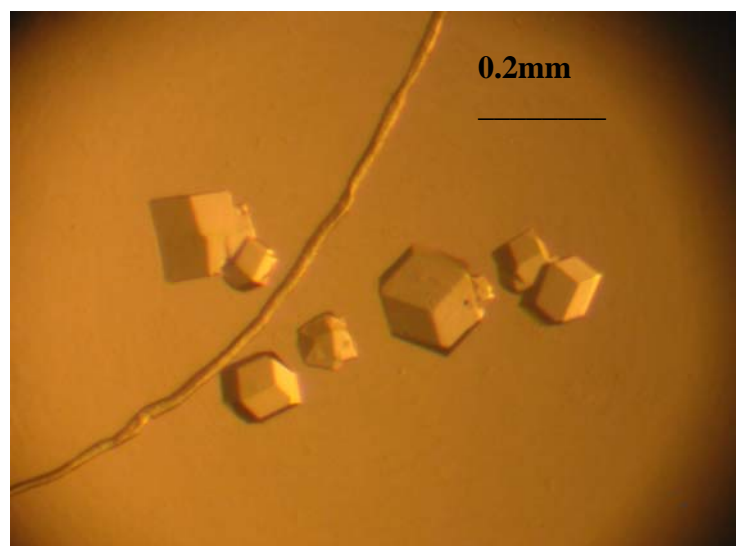
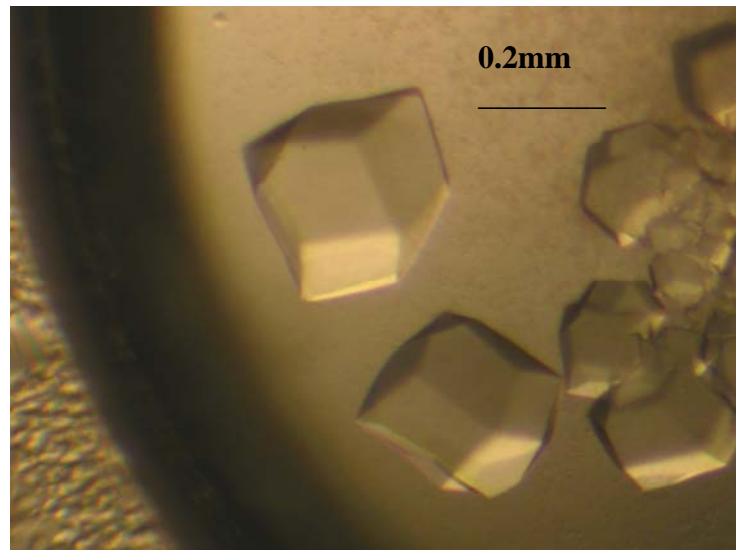
a**b**

Figure 4.2. Crystals of the PII: NAGK complex.

a) Initial cubic crystals of the PII: NAGK complex; b) final cubic crystals of the PII: NAGK complex, which gave a 2.5Å resolution structure.

Table 4.1. X-ray diffraction and refinement statistics for *A. thaliana* PII: NAGK complex crystal.

	The PII: NAGK complex
Space group	P213
Unit cell lengths (Å)	171.13, 171.13, 171.13
Unit cell angles (°)	90, 90, 90
Data Collection	
Wavelength (Å)	1.3361
Resolution (Å)	40-2.5
Total reflections ¹	1016215 (84178)
Unique reflections ¹	57349 (5692)
Completeness (%) ¹	100 (100)
Redundancy ¹	17.7 (15.5)
I/σ ¹	38 (3.2)
R _{sym} ^{1,2}	0.127 (0.950)
Refinement Statistics	
R _{work} ^{1,3}	0.201 (0.262)
R _{free} ^{1,4}	0.229 (0.349)
Number of Atoms	
protein	6095
ligand	167
Solvent and ions	64
R.M.S. Deviations from Ideal Geometry	
Bond lengths (Å)	0.008
Bond angles (°)	1.272

Average Temperature	
Factors (Å²)	
Wilson plot	61.9
protein	67.8
ligand	60.3
water	55.0
Ramachandran plot	
(% residues)	
Most favoured	93.3
Additional allowed	6.4
Generously allowed	0.1
Disallowed	0.1

¹Values from the outermost resolution shell (2.59 – 2.50) are given in parentheses

² $R_{\text{sym}} = \frac{\sum_h \sum_i (|I_i(h) - \langle I(h) \rangle|)}{\sum_h \sum_i I_i(h)}$, where $I_i(h)$ is the i^{th} integrated intensity of a given reflection and $\langle I(h) \rangle$ is the weighted mean of all measurements of $I(h)$.

³ $R_{\text{work}} = \frac{\sum_h ||F(h)_o| - |F(h)_c||}{\sum_h |F(h)_o|}$ for the 95% of reflection data used in refinement.

⁴ $R_{\text{free}} = \frac{\sum_h ||F(h)_o| - |F(h)_c||}{\sum_h |F(h)_o|}$ for the 5% of reflection data excluded from refinement.

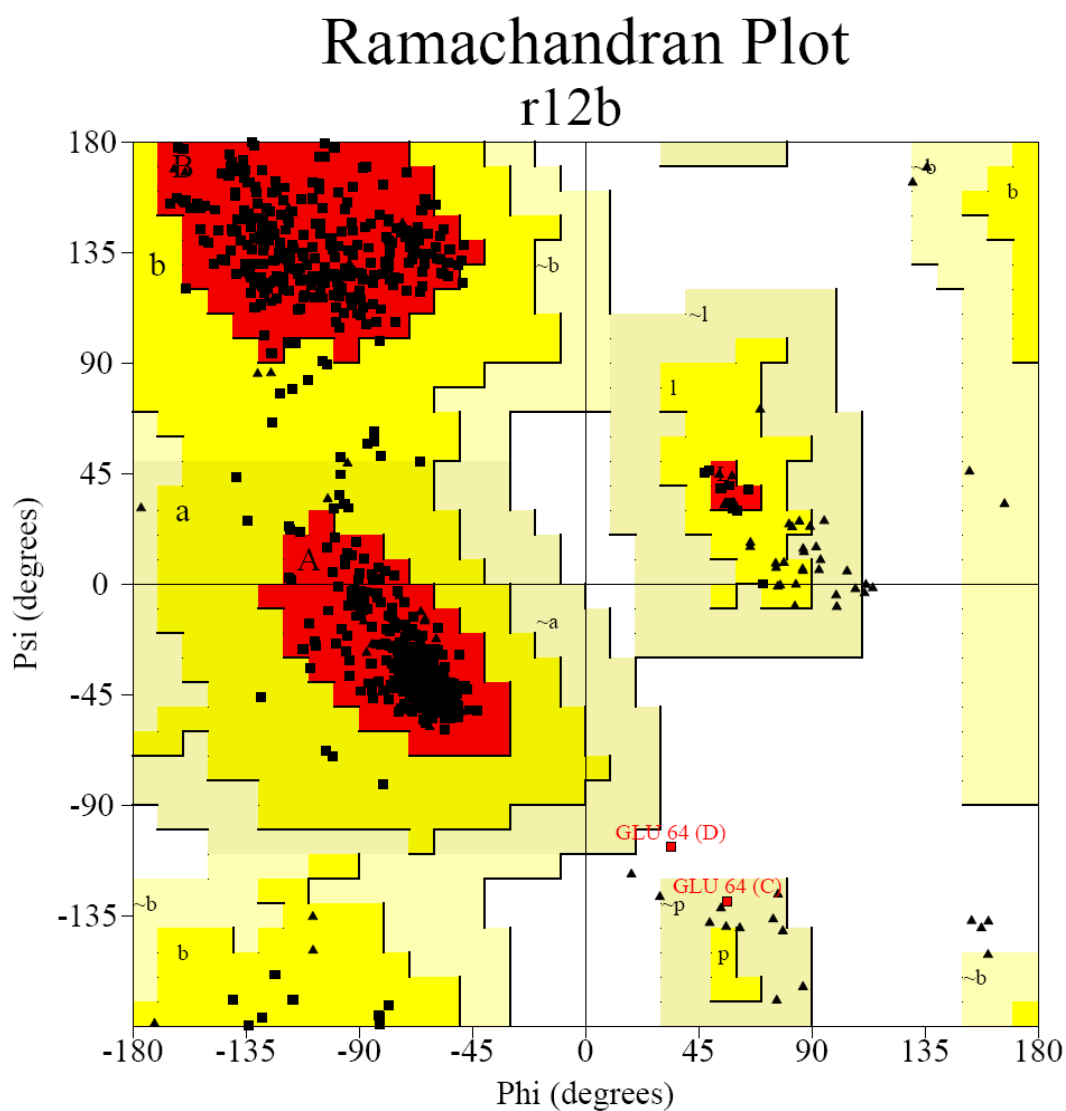
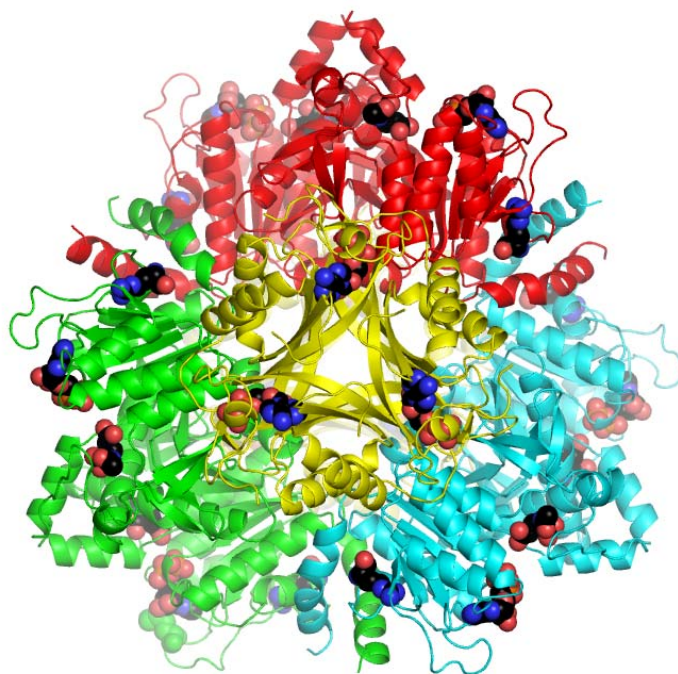
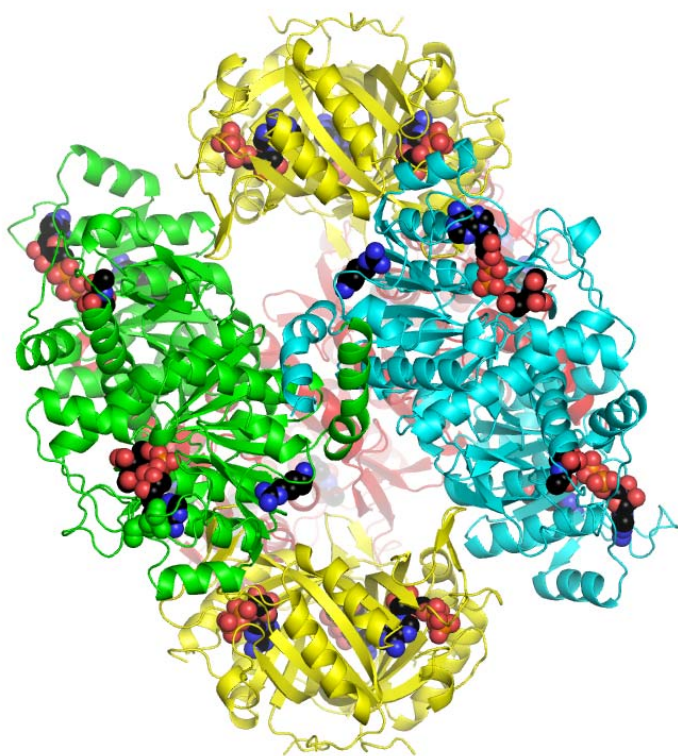


Figure 4.3. Ramachandran plot of the PII: NAGK crystal structure.

The glycine residues are shown as triangles, and the remaining residues are shown as squares. The residues coloured in red are generously allowed or disallowed residues.

a**b**

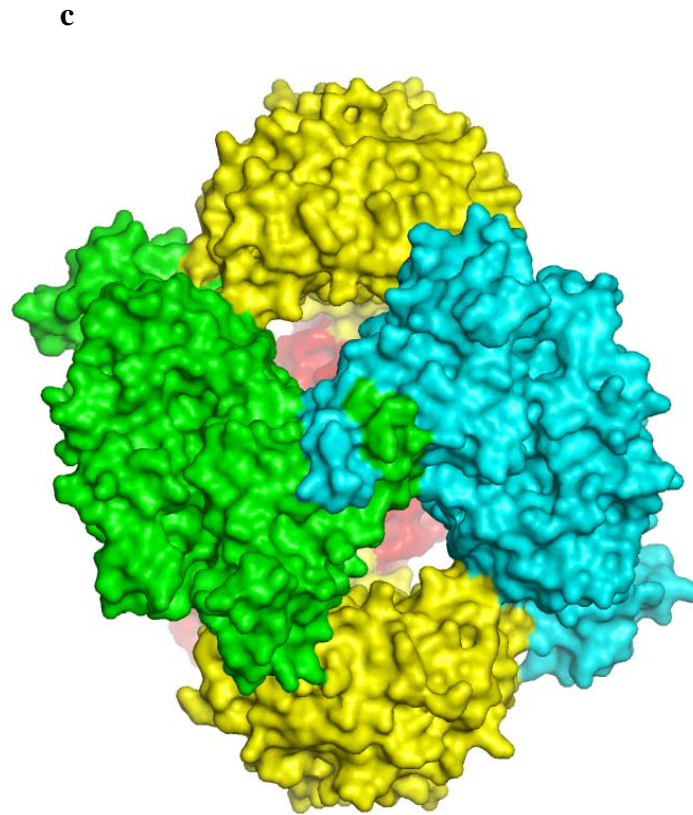


Figure 4.4. Structures of *A. thaliana* PII: NAGK complex.

a) The PII: NAGK complex is viewed along to the 3-fold axis; b) the complex is viewed perpendicularly to the 3-fold axis. Each homodimer is coloured differently. PII is coloured in yellow; c) the space fill model of the PII: NAGK complex.

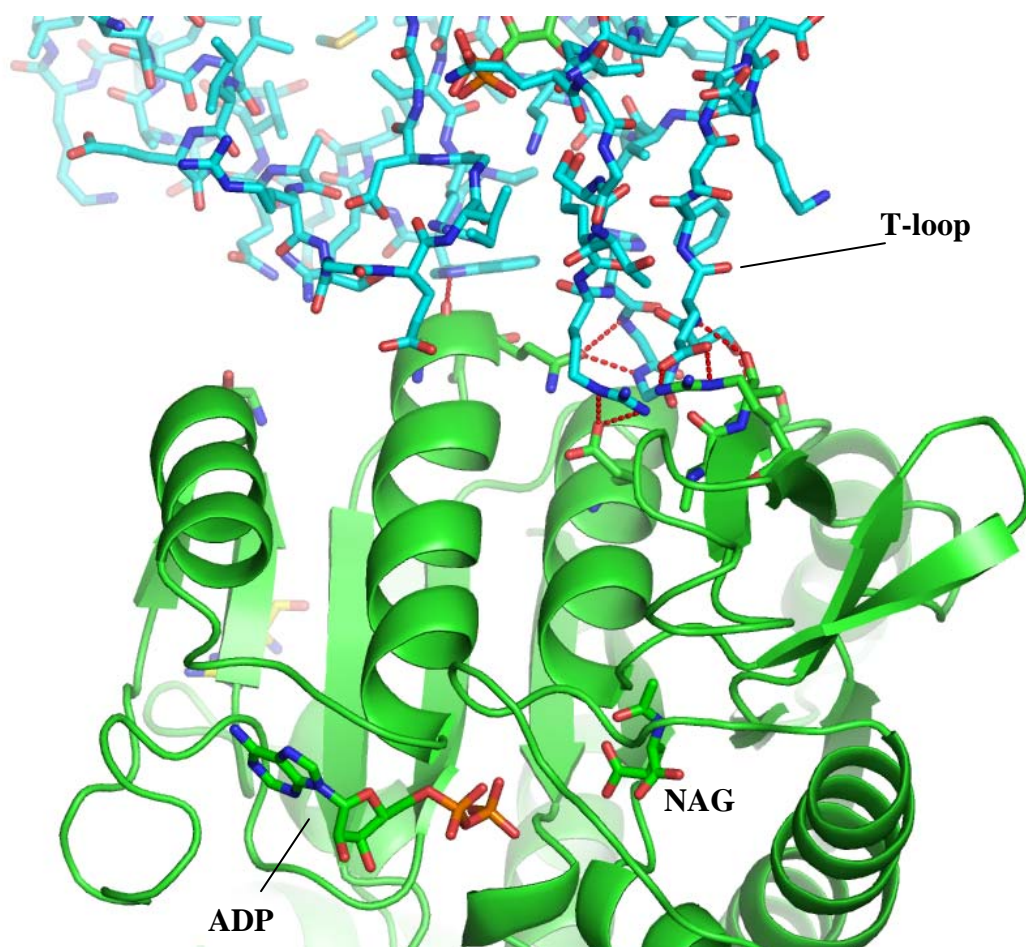
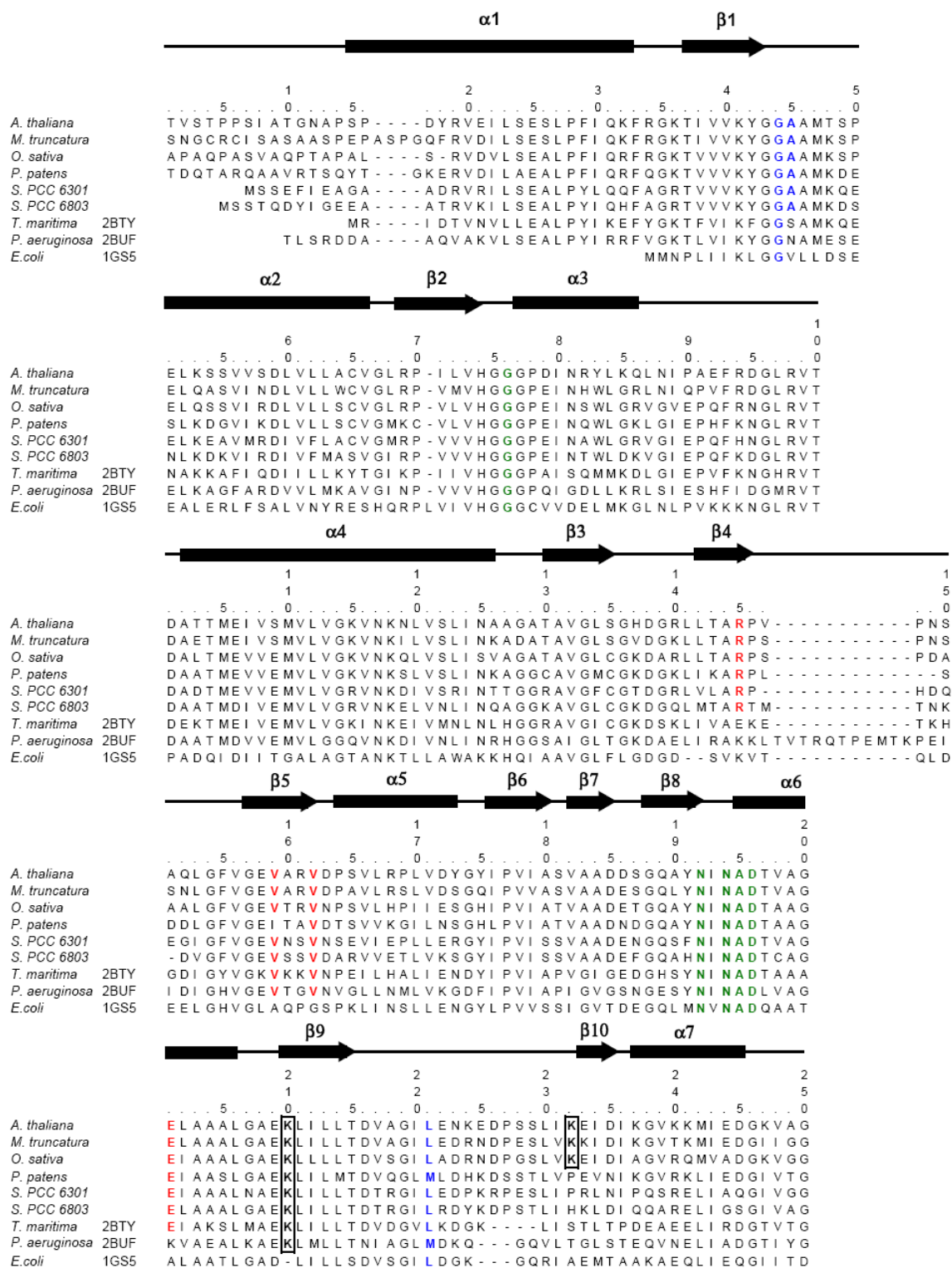


Figure 4.5. PII binding site of the PII: NAGK complex.

The red dotted lines show hydrogen bonds and electrostatic interactions formed between PII and NAGK. Most of the bindings are made by the T-loop.



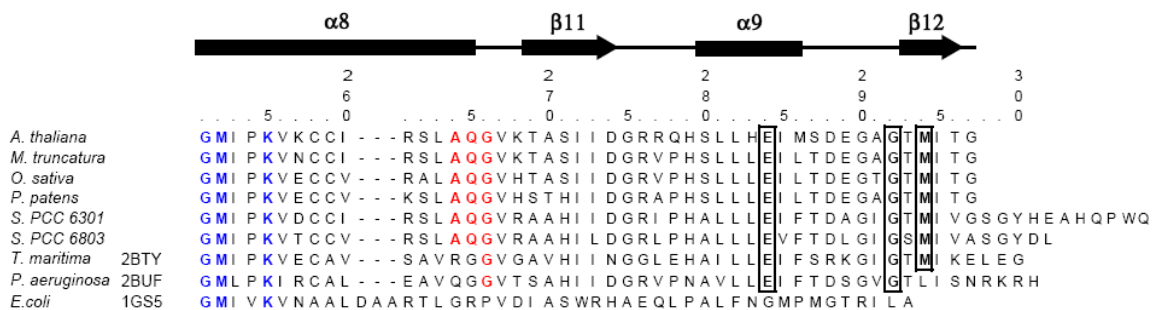


Figure 4.6. Sequence alignments of NAGK.

Sequence alignments of NAGK from plants (*Arabidopsis thaliana*, *Medicago truncatula*, *Oryza sativa*, and *Physcomitrella patens*), cyanobacteria (*Synechococcus elongatus* PCC 6301 and *Synechocystis* sp. PCC 6803), and bacteria (*Thermotoga maritima* (2BTY), *Pseudomonas aeruginosa* (2BUF), and *Escherichia coli* (1GS5)). PDB identifiers have been added to identify some of the three-dimensional structures that are currently available. Residues conserved for complex formation with PII are coloured red. Conserved residues for NAG binding are coloured green. Conserved residues involved with the binding of ATP are coloured blue. Boxed residues are conserved residues for arginine binding.

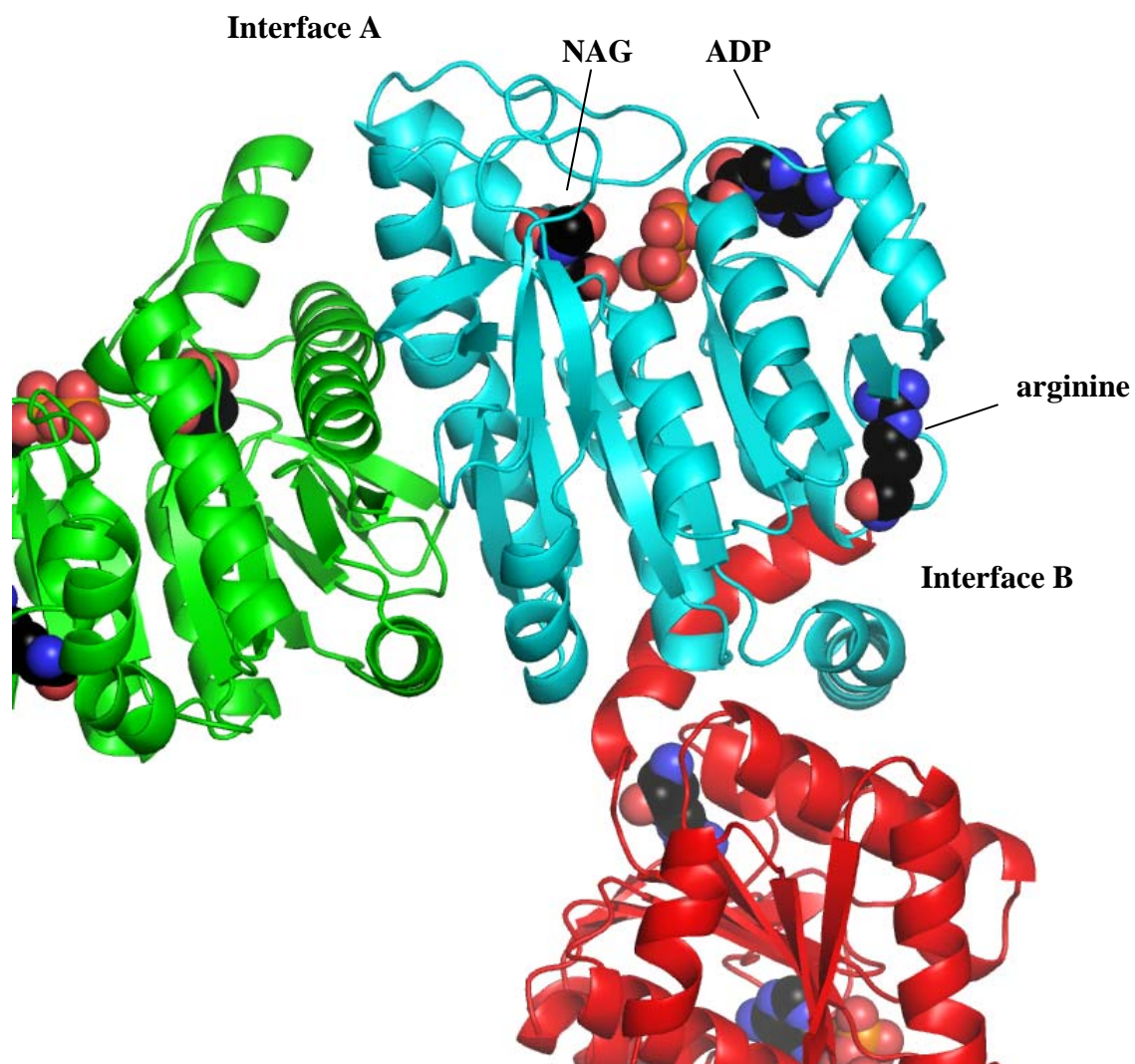


Figure 4.7. Interaction of NAGK protomers.

Two distinct interfaces, A and B, for the protomer coloured in blue are shown. Interface A is formed primarily by packing interactions between the edges of the central β -sheets, an adjacent loop and two flanking α -helices. Interface B is formed between the N-terminal helices of adjacent protomers.

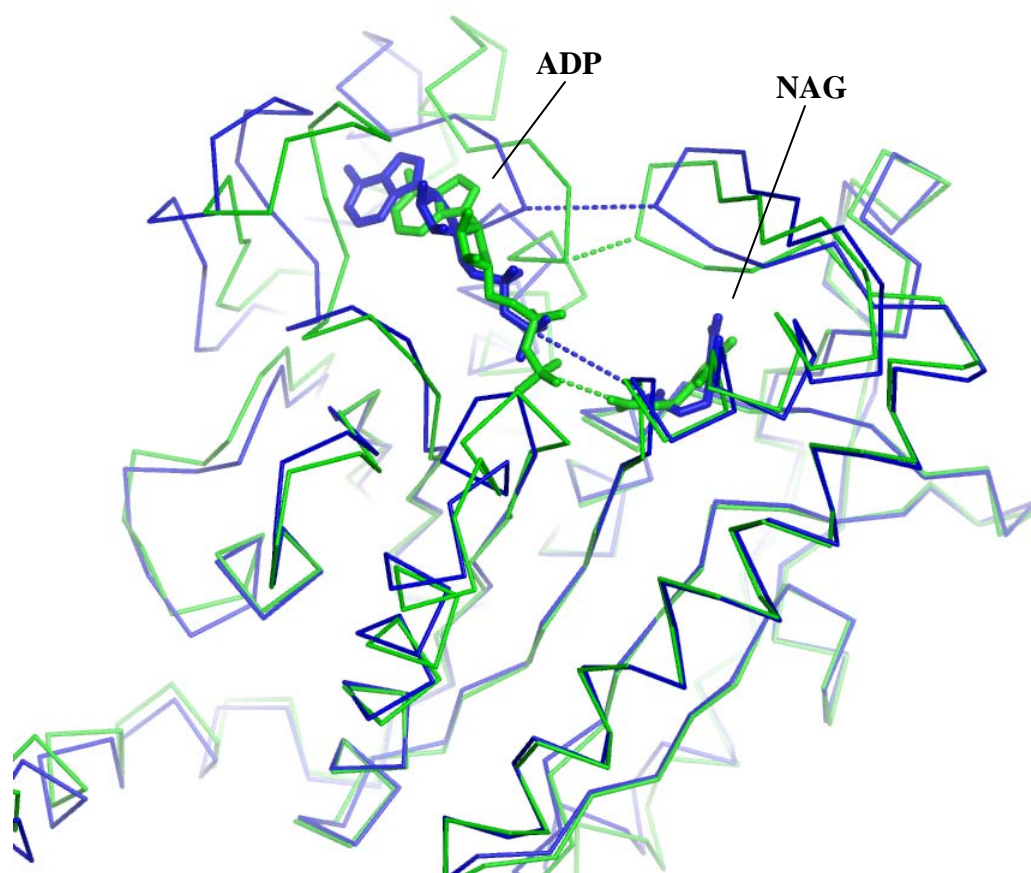


Figure 4.8. Conformational differences between two NAGK protomers in the PII:NAGK complex.

The open form is coloured in blue, and the closed form is coloured in green. The closed form of NAGK has a shorter distance between ADP and NAG.

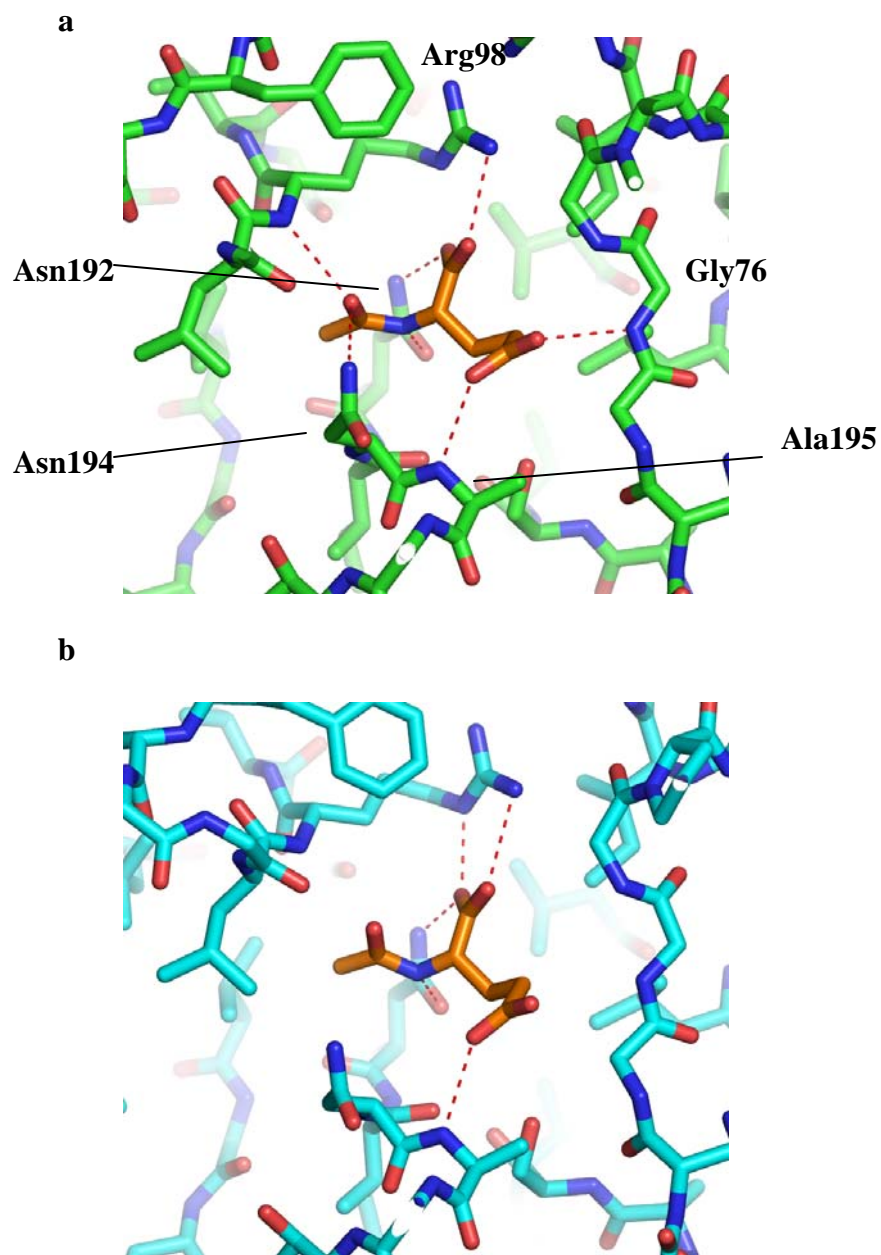


Figure 4.9. NAG binding sites of NAGK in the PII: NAGK complex.

a) NAG binding site in the closed NAGK protomer; b) NAG binding site in the open NAGK protomer. The number of the hydrogen bonds formed is smaller than the closed protomer.

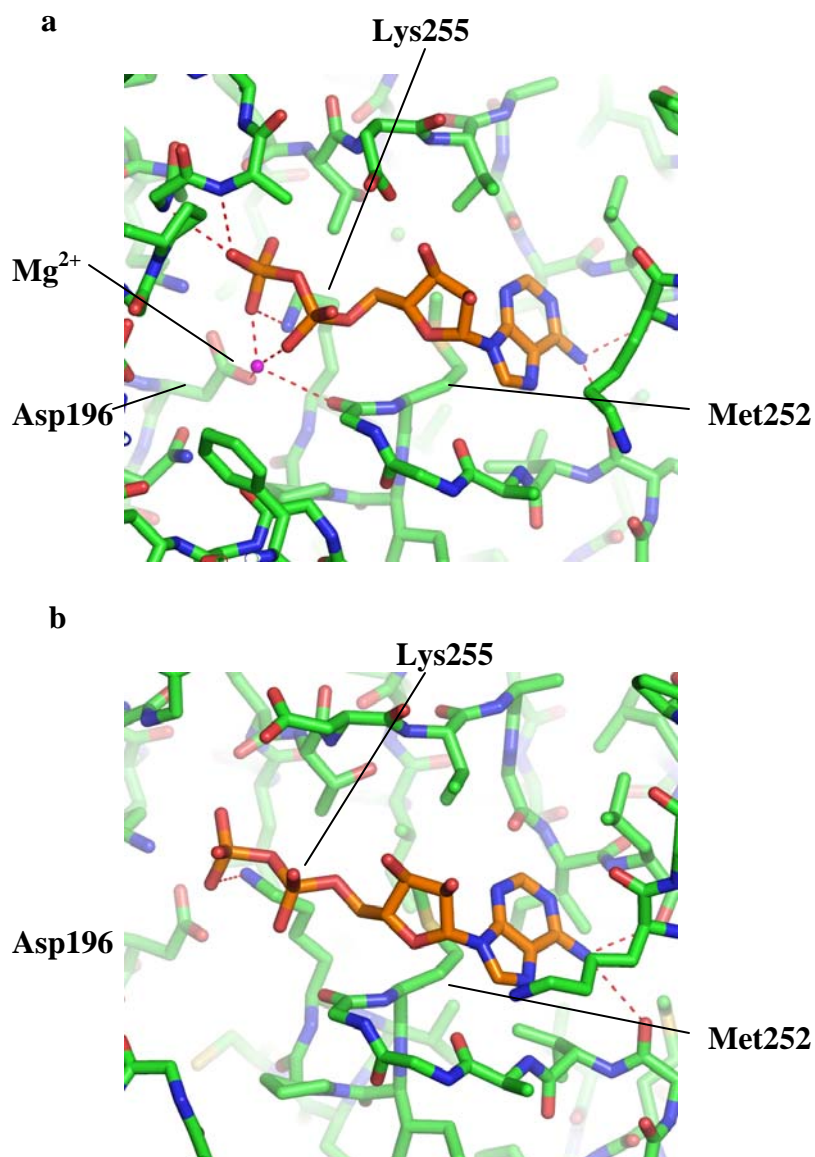


Figure 4.10. ADP binding sites of NAGK in the PII: NAGK complex.

a) ADP binding site in the closed NAGK protomer. The phosphate groups are making interactions with Asp196 and the carbonyl group of Gly251. Also, Mg²⁺ interacts with the phosphate groups; b) ADP binding site in the open NAGK protomer. The number of the hydrogen bonds formed is smaller than the closed protomer.

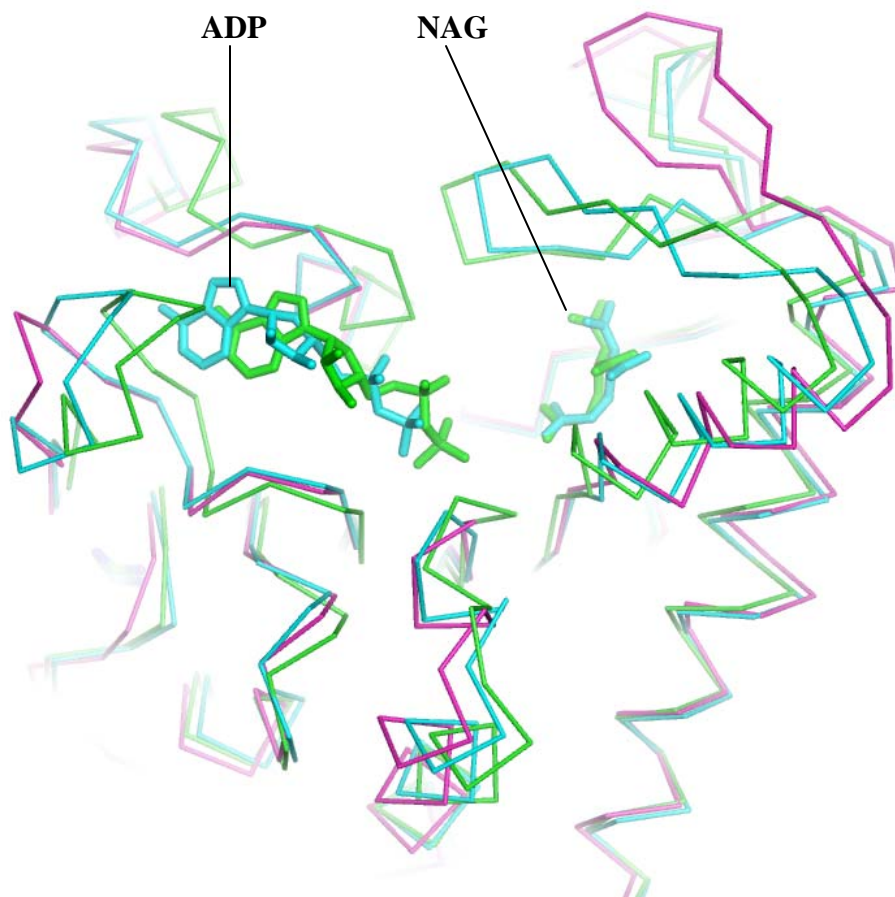


Figure 4.11. Conformational differences between two NAGK protomers in the PII: NAGK complex and bacterial *T. maritima* NAGK bound to arginine molecule.

Movement of the active centre is illustrated by the superposition of the NAGK monomers from the open (blue) and closed (green) NAGK in the PII: NAGK complex and *T. maritima* NAGK bound to arginine (magenta). The bound ADP and NAG in the PII: NAGK complex are shown as well. Especially, the NAG binding loop of *T. maritima* NAGK protomer has more open conformation. PII binding might trigger the active site closure against the arginine mediated active site opening.

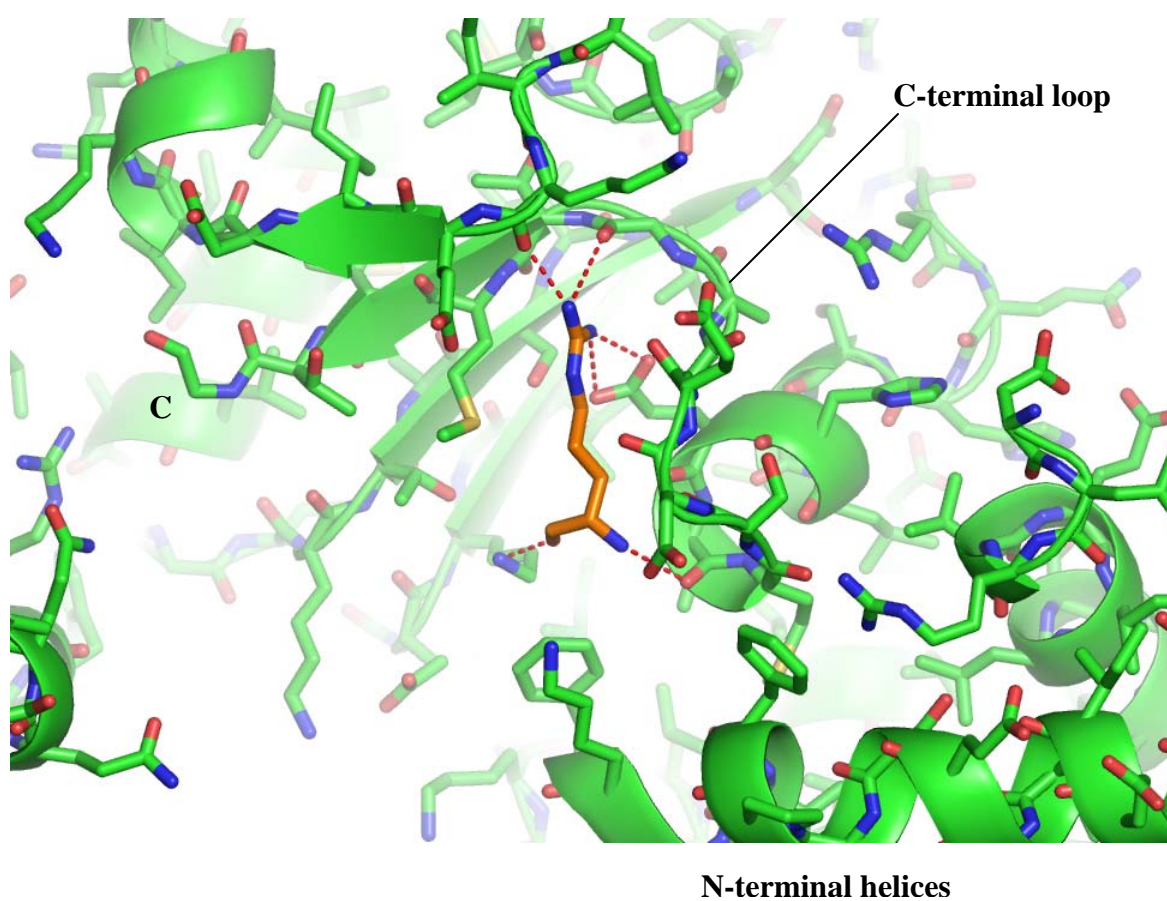


Figure 4.12. Arginine binding site of the closed NAGK protomer in the PII: NAGK complex.

The red dotted lines show hydrogen bonds and electrostatic interactions formed between arginine molecule and NAGK.

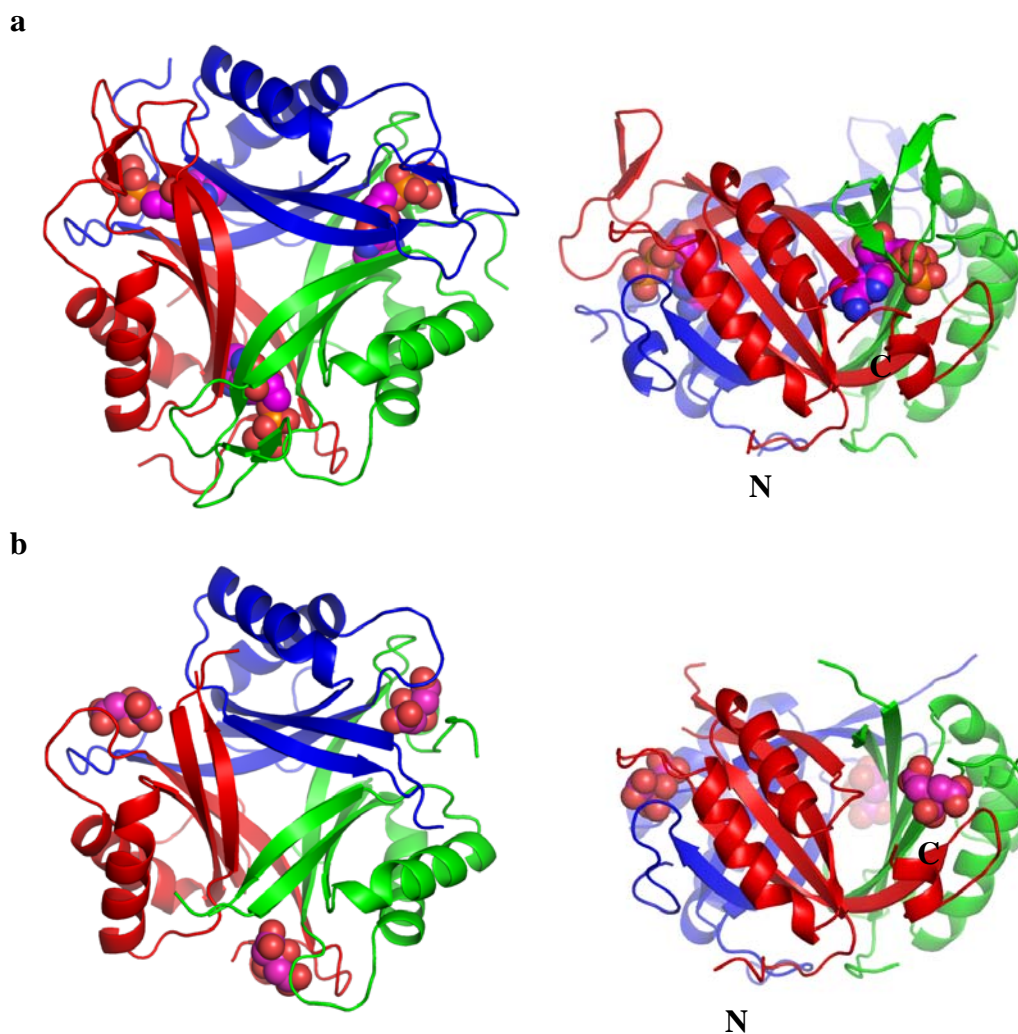


Figure 4.13. Conformational differences between *A. thaliana* PII without NAGK and *A. thaliana* PII complexed with NAGK.

a) Solved structure of PII complexed with NAGK. Each protomer binds to one ATP molecule. T-loop is shown; b) structure of PII without NAGK bound. T-loop is not shown, because it is disordered. Each protomer binds to one citrate molecule. On the left, they are viewed along to the 3-fold axis. On the right, they are viewed perpendicularly to the 3-fold axis. N terminus and C terminus of red PII monomer are shown.

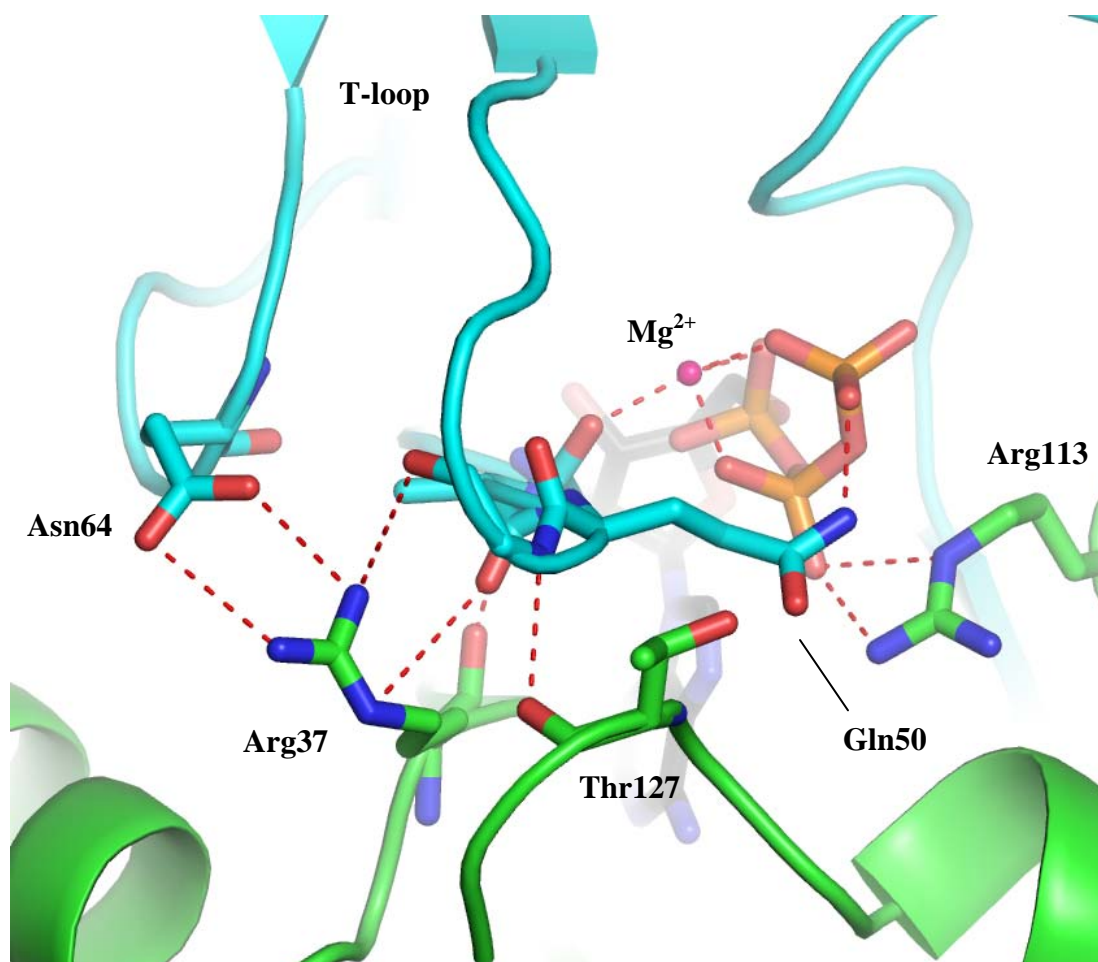


Figure 4.14. Interactions around the edge of the T-loop.

There are numerous interactions around the edge of the T-loop. Arg37, which is conserved only for plants, binds to Asn64, Ala49 and Gly51 on the next PII protomer (blue) and stabilizes the structure of the T-loop. There is a contact between Thr127 in the C-terminus and Gly51 of the T-loop in the next protomer. It may stabilize the C-terminal structure. ATP phosphate group binds with Gln50 in the T-loop and Arg113 in the C-terminus. Introduction of γ -phosphate group of ATP may push them away and cause conformational changes in the T-loop and C-terminus.

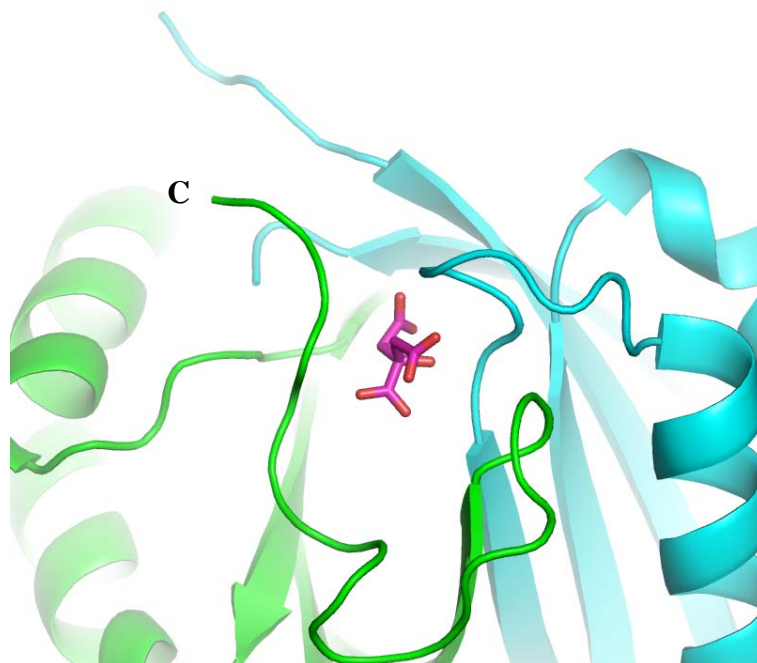
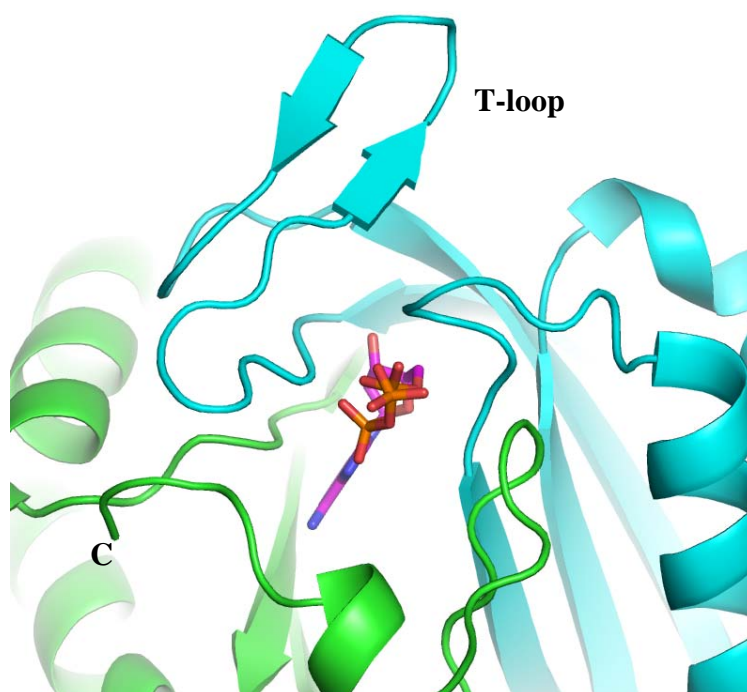
a**b**

Figure 4.15. Conformational differences around ATP binding site between *A. thaliana* PII complexed and non-complexed with NAGK.

a) ATP binding site of PII without NAGK bound. Two protomers are coloured differently. T-loop is disordered. Citrate molecule is binding to the ATP binding site, which is sandwiched by two PII protomers; b) ATP binding site of PII complexed with NAGK. T-loop is shown, since it is stabilized by the PII: NAGK complex formation. ADP is binding to the ATP binding site. The C-terminus is pushed away by the T-loop.

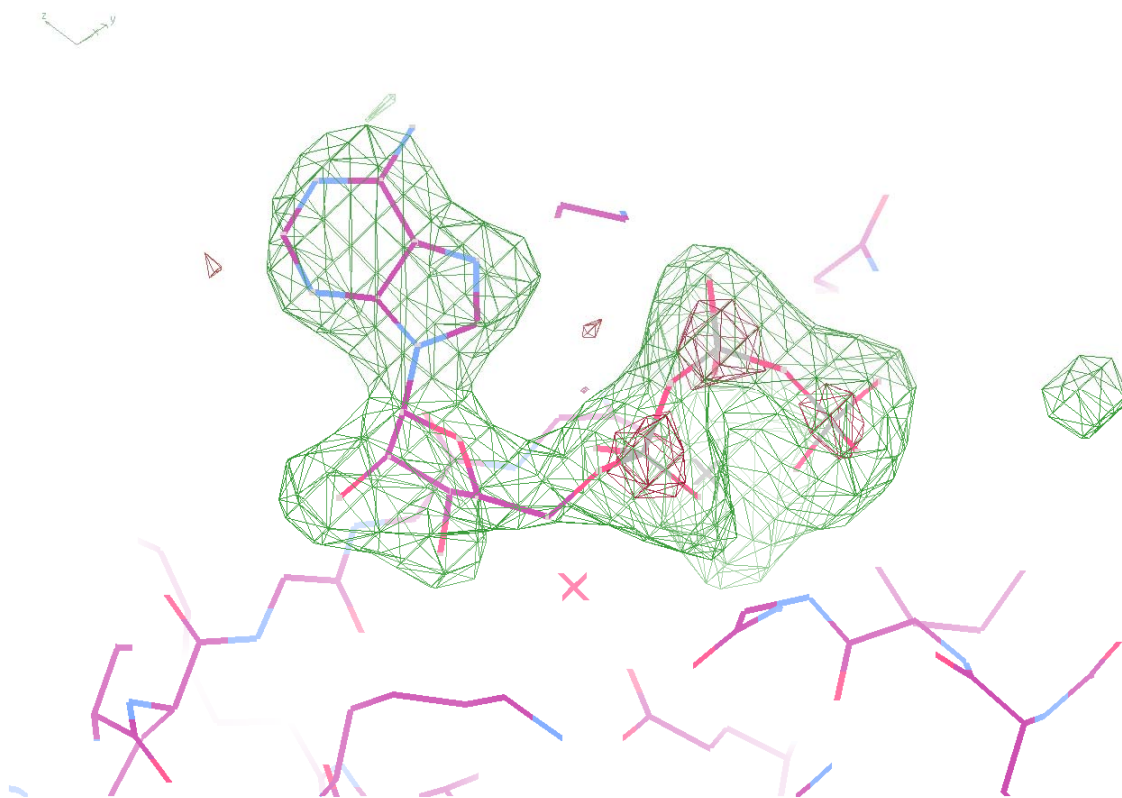
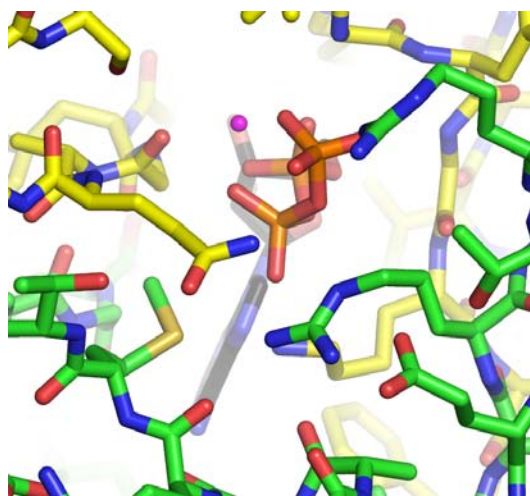
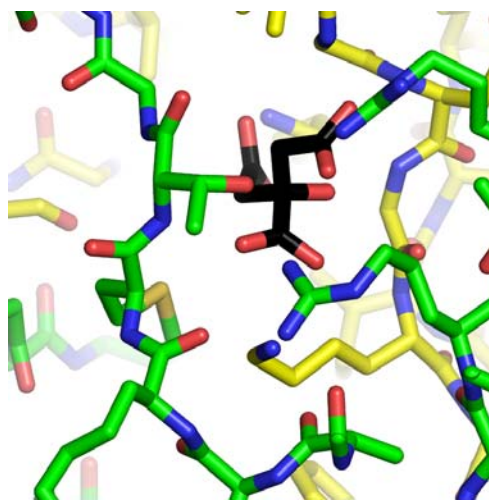
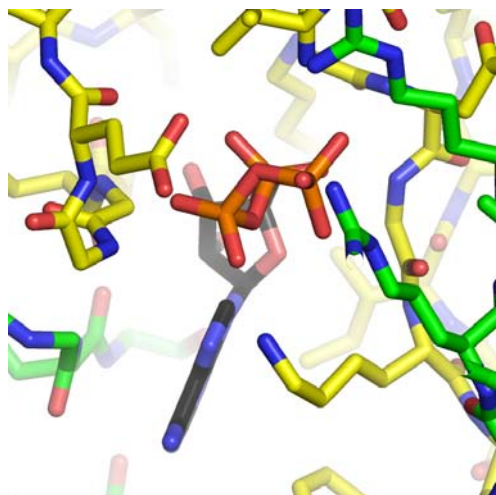
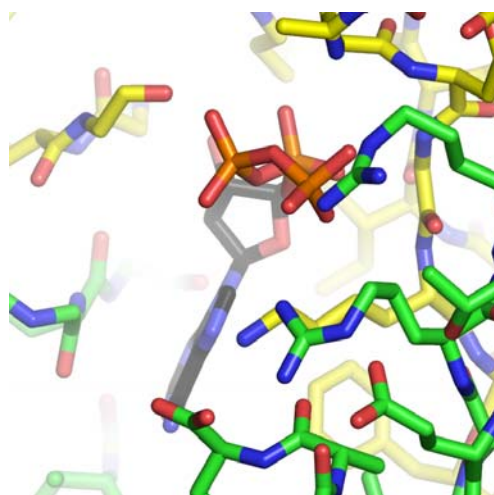


Figure 4.16. Difference electron density map at the ATP binding site in *A. thaliana* PII.

Electron density over 4 standard deviation is coloured in green, and the one over 14 standard deviation is coloured in red. The three red electron densities indicate the location of the tri-phosphate group in ATP.

a**b****c****d**

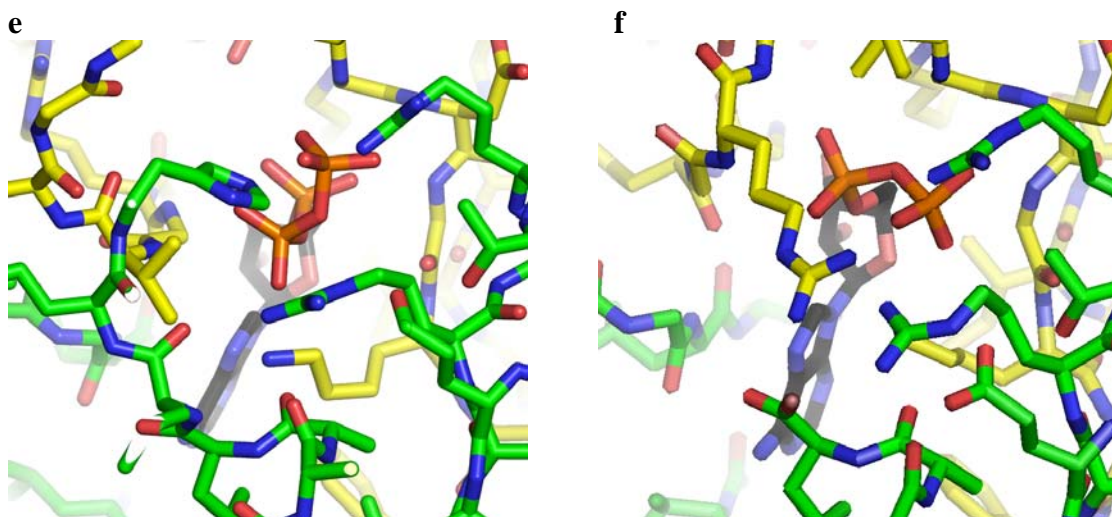


Figure 4.17. ATP binding sites of PII

a) ATP binding site of *A. thaliana* PII structure with ATP bound in the PII: NAGK complex; b) the free PII structure with citrate bound; c) ATP binding to *Thermus thermophilus* PII (pdb file: 1V3S (Sakai et al. 2005)); d) *E. coli* PII with ATP (pdb file: 2GNK (Xu et al. 1998)); e) *M. jannaschii* PII with ATP (pdb file: 2J9E (Yildiz et al. 2007)); f) *E. coli* GlnK with ADP in the ammonium transporter complex (pdb file: 2NS1 (Gruswitz et al. 2007))

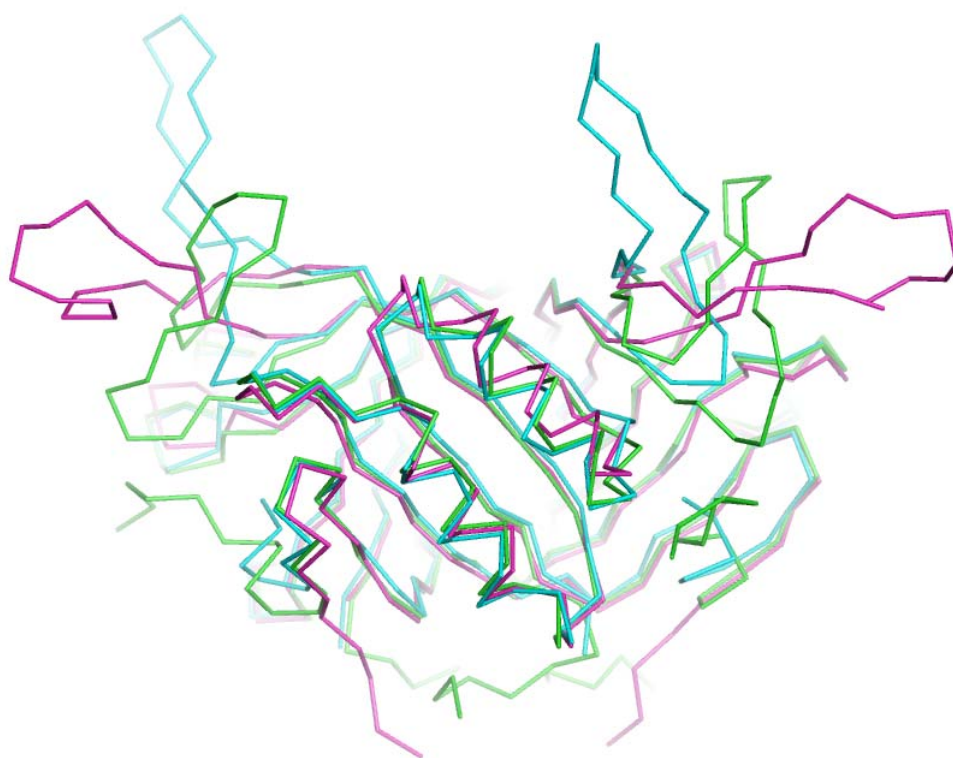


Figure 4.18. Structural differences of the T-loops.

The *E. coli* GlnK with the transmembrane ammonium transporter (pdb file: 2NS1 (Gruswitz et al. 2007)) is coloured in blue. The *Synechococcus* sp. PCC 7942 PII (pdb file: 1QY7 (Xu et al. 2003)) is coloured in purple. The *A. thaliana* PII complexed with NAGK is coloured in green. Although main structures of PII are similar, all of three PII have very different T-loop conformations.

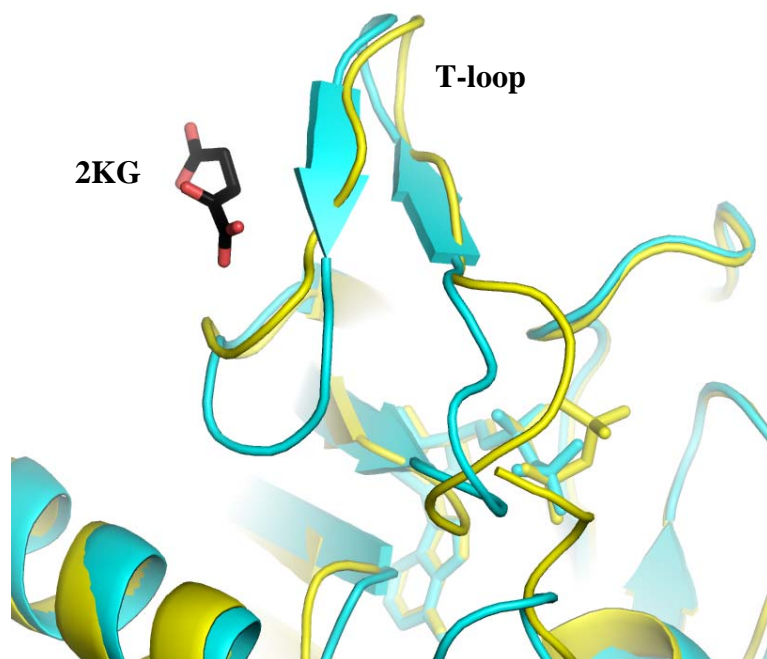
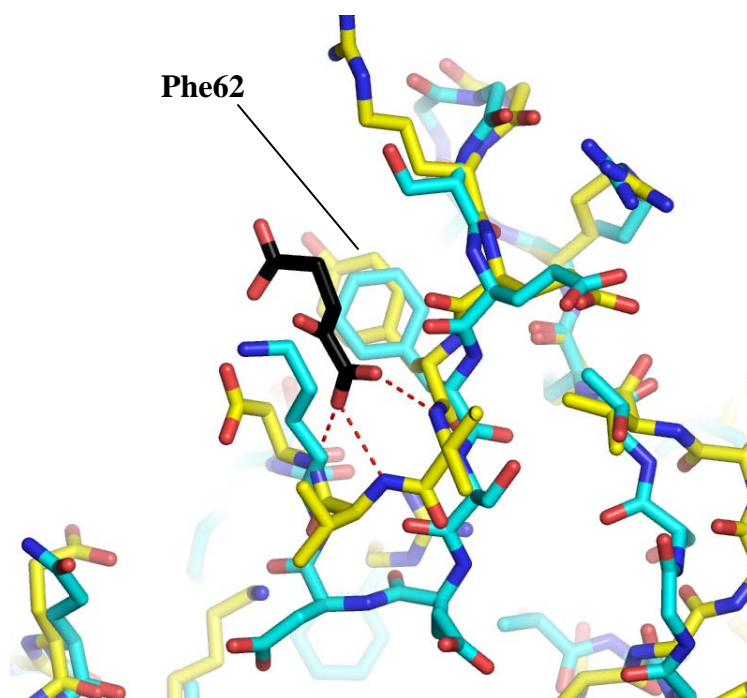
a**b**

Figure 4.19. Superposition of the possible 2KG binding sites on the T-loops of the *M. jannaschii* PII and the PII: NAGK complex.

a) Ribbon diagrams of T-loops of PII in the PII: NAGK complex and *M. jannaschii* PII with bound Mg^{2+} -ATP and 2KG. PII in the PII: NAGK complex is coloured in blue. *M. jannaschii* PII with bound Mg^{2+} -ATP and 2KG is coloured in yellow. 2KG is coloured in black. The general organizations of T-loops are very similar; b) detailed view of 2KG binding site. The red dashed lines shows the bonds formed between 2KG and *M. jannaschii* PII (yellow). Tyr51 in *M. jannaschii* PII binds to 2KG with a hydrophobic contact. Phe62 of *A. thaliana* PII has a hydrophobic property as well and is located at this position.

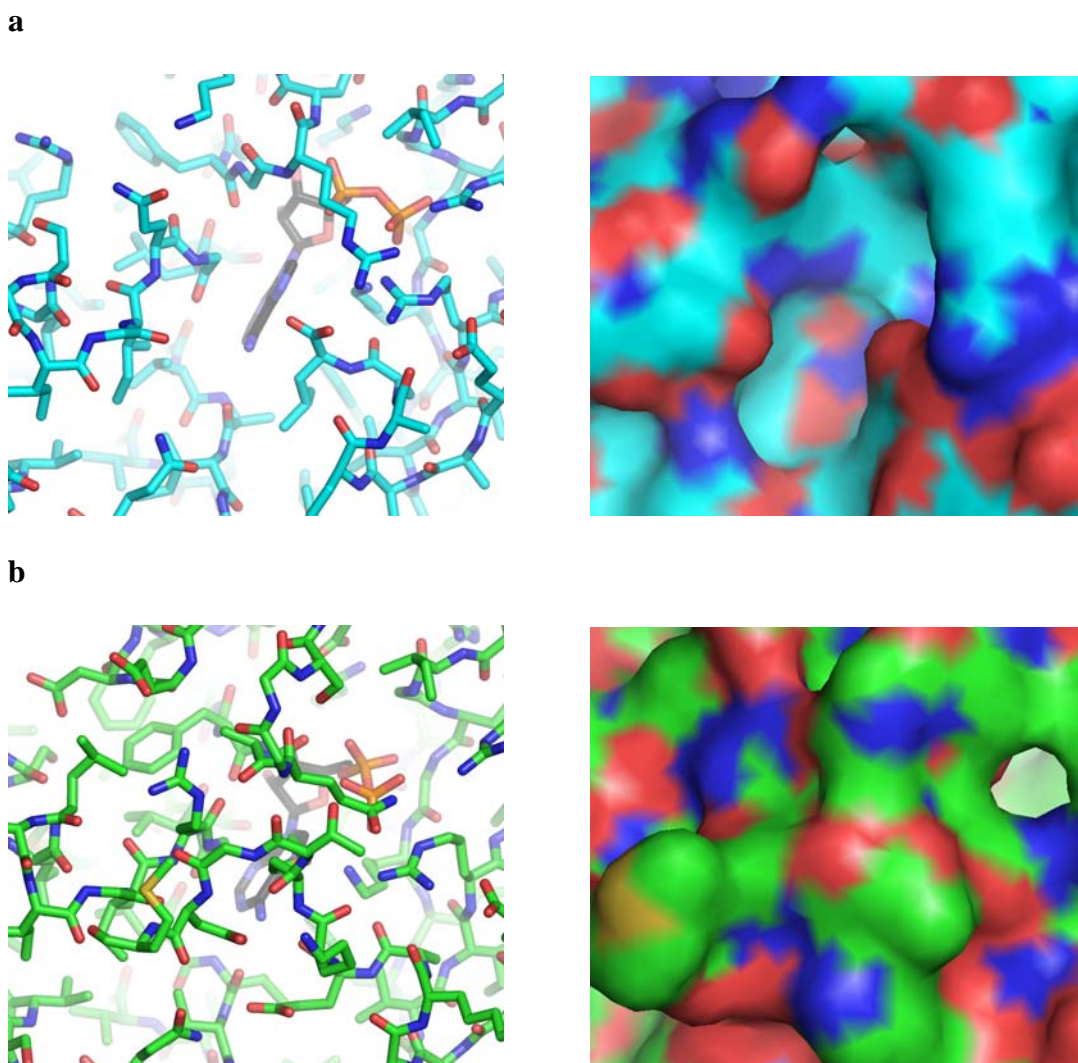


Figure 4.20. Superposition of the possible 2KG binding sites of the GlnK: AmtB complex and the PII: NAGK complexes.

a) The possible 2KG binding site beside the ATP binding site of the GlnK: AmtB complex. A detailed stick representation is on the left, and the space filled model is shown on the right; b) the possible 2KG binding site beside the ATP binding site of the PII: NAGK complex. The empty space seen in the GlnK: AmtB complex is covered with a small loop around residues 49-53 and the C-terminal segment.

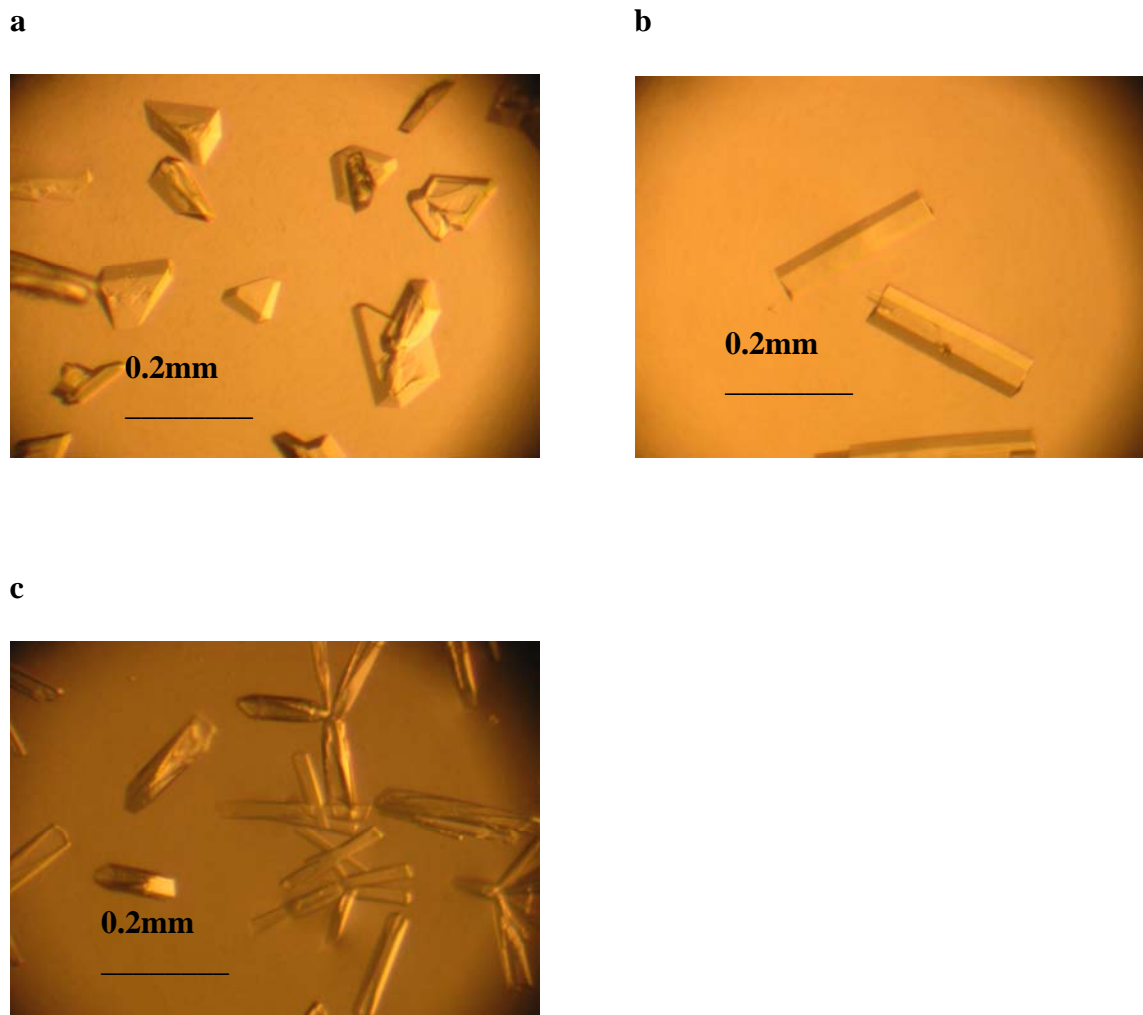


Figure 4.21. Crystals grown in the PEG3350 conditions with different substrates.

a) Crystals of NAGK grown without any substrates; b) crystals of NAGK with 5mM NAG and ADP; c) crystals of NAGK with 5mM NAG, ADP and Arginine.

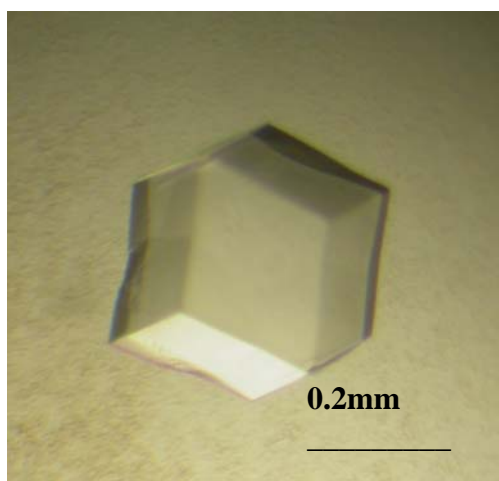
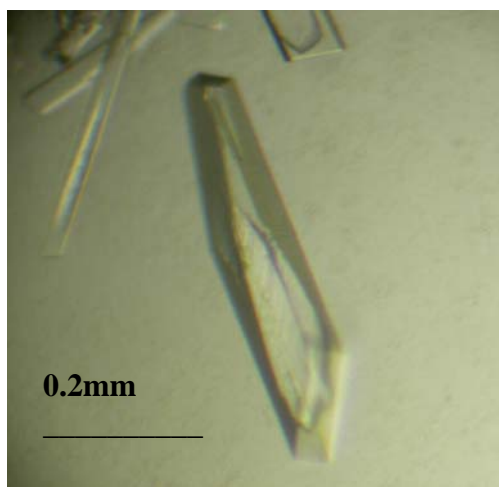
a**b**

Figure 4.22. Crystals of NAGK.

a) The NAGK crystal grown in PEG 4000 condition with AMP-PNP; b) the NAGK crystal grown in PEG 3350 condition with ADP.

Table 4.2. X-ray diffraction and refinement statistics for *A. thaliana* NAGK crystals

	AMP-PNP complex	ADP complex
Space group	R3	P321
Unit cell lengths (Å)	99.37, 99.38, 179.07	177.37, 177.37, 58.15
Unit cell angles (°)	90, 90, 120	90, 90, 120
Data Collection		
Wavelength (Å)	1.116	1.116
Resolution (Å)	40-2.3	40-3.0
Total reflections ¹	192882 (18784)	133609 (11718)
Unique reflections ¹	29300 (2846)	20264 (1953)
Completeness (%) ¹	99.4 (96.6)	95.2 (92.8)
Redundancy ¹	6.6 (3.6)	6.6 (6.0)
I/σ ¹	38.4 (3.0)	17.4 (2.6)
R _{sym} ^{1,2}	0.062 (0.259)	0.094 (0.684)
Refinement Statistics		
R _{work} ^{1,3}	0.214 (0.241)	0.217 (0.345)
R _{free} ^{1,4}	0.245 (0.326)	0.288 (0.409)
Number of Atoms		
protein	4165	6279
ligand	76	102
Solvent and ions	1	0
R.M.S. Deviations from Ideal Geometry		
Bond lengths (Å)	0.007	0.008
Bond angles (°)	1.181	1.250
Average Temperature Factors (Å²)		
Wilson plot	58.4	88.8
protein	74.5	86.1
ligand	99.2	105.0
water	72.5	—
Ramachandran plot (% residues)		
Most favoured	93.7	86.2
Additional allowed	6.1	13.1
Generously allowed	0.2	0.4
Disallowed	0	0.3

¹Values from the outermost resolution shell (AMP-PNP complex: 2.38 – 2.30; ADP complex: 3.11 – 3.00) are given in parentheses

² $R_{\text{sym}} = \sum_h \sum_i (|I_i(\mathbf{h}) - \langle I(\mathbf{h}) \rangle|) / \sum_h \sum_i I_i(\mathbf{h})$, where $I_i(\mathbf{h})$ is the i^{th} integrated intensity of a given reflection and $\langle I(\mathbf{h}) \rangle$ is the weighted mean of all measurements of $I(\mathbf{h})$.

³ $R_{\text{work}} = \sum_h ||F(\mathbf{h})_o| - |F(\mathbf{h})_c|| / \sum_h |F(\mathbf{h})_o|$ for the 95% of reflection data used in refinement.

⁴ $R_{\text{free}} = \sum_h ||F(\mathbf{h})_o| - |F(\mathbf{h})_c|| / \sum_h |F(\mathbf{h})_o|$ for the 5% of reflection data excluded from refinement.

a

b

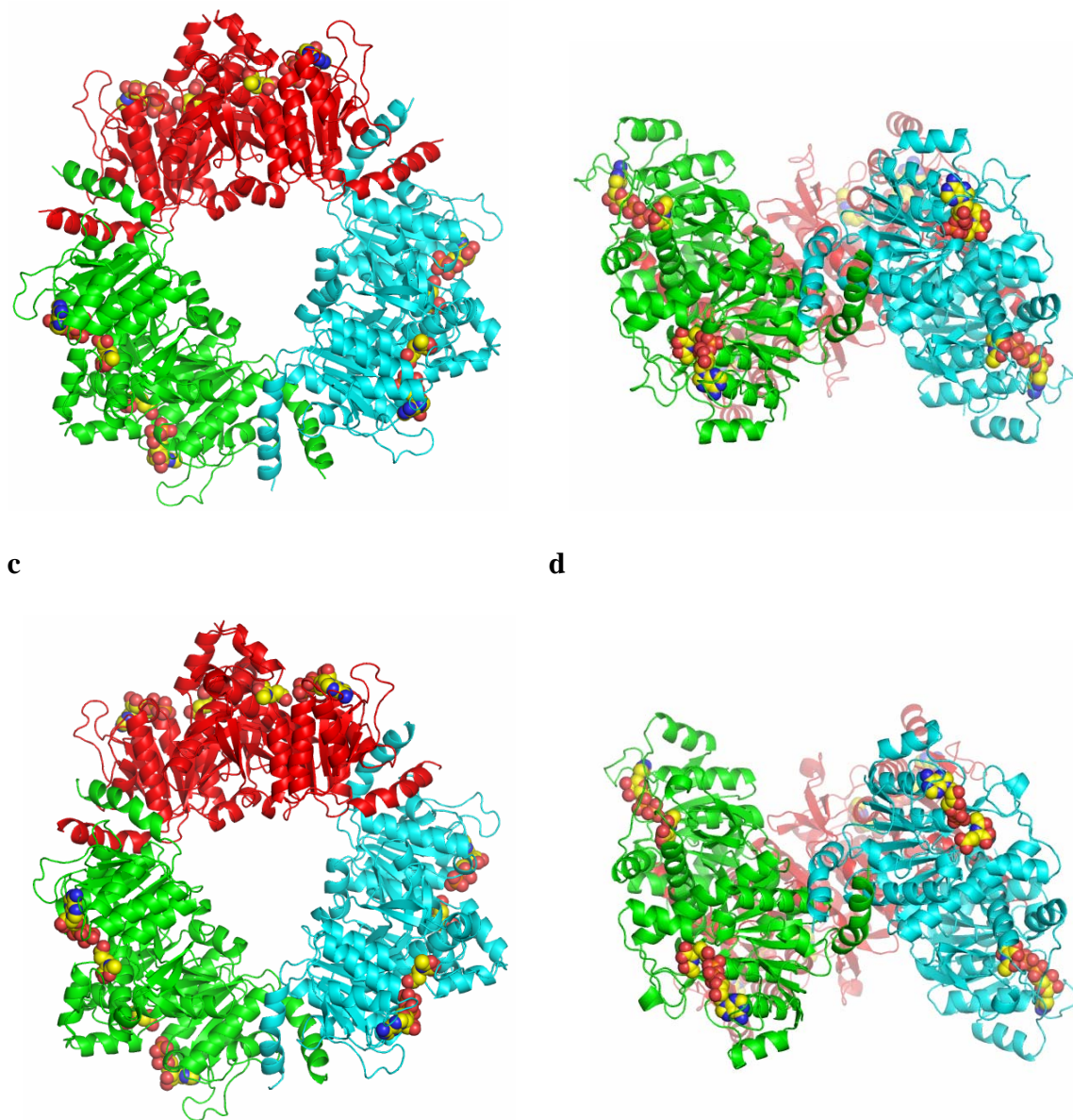


Figure 4.23. Structures of *A. thaliana* NAGK hexamers.

NAGK with ADP (a and b) and NAGK with AMP-PNP (c and d) are viewed along (b and d) or perpendicularly (a and c) to the 3-fold axis. Each homodimer is coloured differently.

Chapter Five: Discussion

5.1 Structure of PII from *A. thaliana*

The high resolution *A. thaliana* PII structure reveals many interesting features that are highly conserved in the sequences of a wide range of plant PII proteins. On the other hand, the *A. thaliana* PII structure showed novel structural differences between PII proteins from plants and PII proteins from bacteria, archaea, and red algae. The most outstanding differences seen in plant PII proteins are several highly conserved solvent exposed residues near the T-loops and unique N and C-terminal structures. The differences on the T-loops by themselves are not clearly seen, because they were disordered in free PII. Because T-loops are very flexible and important for protein: protein interactions, the best way to solve the T-loop structures is by solving the structure of PII: protein complexes. The C-terminus and solvent exposed residues near the T-loops are located on the same side of the PII trimer, and they are close to the ATP and proposed 2KG binding sites. Thus, these residues might change conformations by interacting with ATP and 2KG and be involved in the ATP and 2KG dependent intermolecular interactions.

The plant specific N-terminal region is located on the opposite side of the T-loop and C-terminus. Therefore this region may not be involved with the binding of ATP and 2KG. Instead, the N-terminus may be interacting or binding to other proteins, or may be sensitive to metabolites other than ATP and 2KG. On the other hand, the N-terminus has tight binding to other segments of the PII trimer. These segments are the $\alpha 2$ helix of the same protomer and the C-terminal $\beta 4$ strand of the adjacent protomer, which interact with

the ATP-binding site and T-loop. Therefore, the signals caused by ATP and 2KG binding can be transmitted to the N-terminus indirectly through them.

The function of plant specific portions of PII protein is not understood yet. The solved structure of *A. thaliana* PII shows the orientations and interactions of residues in the plant specific portions in high resolution and can be used to plan experiments to test their functions. For example, several highly conserved solvent exposed residues near the T-loops can be replaced with other amino acids without affecting the overall structure of PII.

The structural basis of interactions between PII proteins and PII binding enzymes like NAGK has not been understood well yet. The solved *A. thaliana* PII structure gives ideas for intermolecular interactions. Recently, homohexameric structures of bacterial NAGK from *P. aeruginosa* and *T. maritima* have been determined (Ramon-Maiques et al. 2006). In these structures, homodimers are arranged about a three-fold rotational axis. Based on the high similarity of residues for intersubunits contacts to form hexamers and the gel filtration experiments results, plant NAGK also form homohexamers. The molecular dimensions and symmetry of the PII trimer suggest that the three-fold rotational axes of NAGK and PII may align during complex formation.

5.2 Structure of the PII: NAGK Complex from *A. thaliana*

The 2.5Å resolution of *A. thaliana* PII: NAGK complex structure reveals the mechanism of the complex formation for the activation of NAGK in opposition to the feedback inhibition by arginine. There has not been any PII: NAGK complex structures

determined to date, thus this is the first structure of the PII: NAGK complex. For *E. coli*, the complex structure of PII and ammonia channel was determined, but the function of the complex formation is stopping the flow of ammonia by inserting the T-loop of PII into the channel, and it does not trigger any conformational changes of ammonia channel. Although the PII: NAGK complex formation is made by the T-loop as well, it has a completely different mechanism. The PII binding to NAGK causes the conformational change and increases the activity against the inhibition by arginine. Furthermore, the plant PII: NAGK structure shows functions of residues that are conserved only in plants as well.

5.2.1 PII Binding on NAGK

PII binds to NAGK using the T-loop, which was disordered on the free PII structure with citrate or malonate. Each PII protomer binds to each NAGK protomer individually and makes a tight binding with numerous interactions. The T-loop binds and bridges the two domains of NAGK and brings them closer. One domain has the ATP binding site, and the other has the NAG binding site. The complex structure shows both the open and closed conformations of NAGK as different catalytic transitionstate conformations. If the distance between the two domains is too large, the activity of NAGK should be dramatically decreased. *T. maritima* NAGK bound to arginine has a larger opening of two domains than the open NAGK protomer in the PII: NAGK complex has. Also, the open NAGK protomer in the PII: NAGK complex has lower binding affinity for ADP and NAG. PII has a function to bring two domains together, hold substrates tighter, and increase the catalytic activity of NAGK. Therefore, NAGK activity is precisely

controlled in the cell by arginine and PII binding. For arginine sensitive NAGK, most of the residues binding to PII are highly conserved. Also, the PII residues involved in the complex formation are highly conserved as well. Thus, PII proteins other than plant PII may bind NAGK in the similar manner.

5.2.2 Structure of PII

The overall structures of PII in the complex are very similar to the previously determined free PII with citrate. However, the structure of the T-loop revealed a lot of important interactions for PII function. The T-loop has a rigid and stable structure in the complex. The T-loop is stabilized with interactions, which are not seen in the free PII structure. Arg37 is an important residue to make interactions with Asn64, Ala49 and Gly51 and stabilize the base of the T-loop. The structure of Arg37, which is highly conserved only among plant PII proteins, was seen in the free PII structure, but the function was not understood. Also, all of Asn64, Ala49 and Gly51 are highly conserved only in plants and are disordered in the free PII structure, because they are in the T-loop. Therefore, the complex formation successfully revealed the functions of these plant specific residues.

Also, the C-terminal segment of PII, which are only found in plants, is very different between the PII in the complex and the free PII. They are mostly disordered in the free PII structure, but they have stable conformations in the complex. Thr127 stabilizes the structure by forming hydrogen bonds with the amide group of Gly51. Therefore, the C-terminus may have an important function under the complex formation. However, the C-terminal function has not been revealed yet.

The structure of the N-terminal segment did not show any difference between the complexed PII and the free PII. The N-terminus is not directly involved in the T-loop mediated protein: protein interactions, because the N-terminus is located on the opposite side of the T-loop and the C-terminus. The highly conserved plant specific N-terminal region may form independent protein: protein interaction interface.

The T-loop, C-terminal segment and ATP binding site are all located close together. Thus, ATP and Mg^{2+} binding to the ATP binding site may have important influences on the conformations of the T-loop and the C-terminus, and also for the PII: NAGK complex formation.

5.2.3 Function of 2KG for PII

2KG is known to bind to all of the PII proteins from different species including plants, and signals carbon status in the chloroplast only when ATP binds to PII. In bacteria and cyanobacterial systems, the function of 2KG binding was shown to be similar to the covalent modification of the T-loops. 2KG binding causes the dissociation of the GlnK: ammonia channel complex in *E. coli*, and the uridylylation of the T-loop has the same effect. Also, 2KG interferes the complex formation of cyanobacterial PII and NAGK, and the phosphorylation of the T-loop dissociates the complex formation. Therefore, the T-loop mediated complex formations of PII are controlled both by the covalent modifications, uridylylation and phosphorylation, and also the binding of 2KG in bacteria and cyanobacteria. Although there are proposed 2KG binding sites in PII, the 2KG binding site locations are not yet confirmed.

One of the possible 2KG binding sites is located on the T-loop. 2KG on the T-loop may bind close to the tyrosine residue, which is uridylylated or phosphorylated. Thus, the negatively charged 2KG in this location may have the same effect of uridylylation and phosphorylation. Superposition of *A. thaliana* PII T-loop and *M. jannaschii* PII with bound Mg^{2+} -ATP and 2KG shows that the conformation is similar around the possible 2KG binding site. Thus, further experiments, such as mutation studies, can be done to test if it is the 2KG binding site. The most important residue for 2KG binding from *M. jannaschii* PII structure is Tyr51, and the equivalent residue in *A. thaliana* is Phe62. The Phe62 in *A. thaliana*, which has a hydrophobic property, could be replaced with alanine or other amino acids lacking the hydrophobicity without affecting the overall structure of PII.

Another possible 2KG binding site is located beside the ATP binding site and the T-loop of PII. 2KG and ATP bound to PII at this location may cause conformational change of the T-loop and interfere with the complex formation. The PII structure in the PII: NAGK complex does not have enough space for 2KG binding. First, part of the T-loop, residues 49-53, runs into the 2KG pocket. Also, the C-terminal segment covers this site. Thus, the introduction of 2KG into this covered space can cause the conformational changes of the T-loop and the C-terminus. However, it is questionable whether 2KG can open up the cover for binding. 2KG may bind easier before PII and NAGK form the complex, since the possible 2KG binding site is not covered with the T-loop and the C-terminus without the complex formation.

Though it is well known that 2KG binds to plant PII with ATP, plant PII does not seem to control the complex formation in the same ways that bacteria and cyanobacteria do. First of all, plant PII is not covalently modified. Thus, the complex dissociation can not be controlled by the covalent modification. Also, plant PII bound to 2KG did not show the dissociation of the PII: NAGK complex, since PII bound to 2KG showed the increase in the NAGK activity. 2KG may have a completely different function on PII, but it is not clear. The primary function of PII binding to NAGK is to relieve feedback inhibition by arginine in plants.

5.3 Research in the future

In my research project, structures of *A. thaliana* PII, NAGK, and the PII: NAGK complex were determined. These structures reveal substantial information about PII protein mediated nitrogen and carbon metabolism in plants. However, a lot of other studies could be done to increase our understanding of the PII function.

First of all, the detailed crystal structure of NAGK with arginine without forming a complex with PII should give a great insight about the arginine inhibition of NAGK. So far, the crystallization screens gave a few different types of NAGK crystals with arginine. These crystals showed different appearances and grew under different conditions compared with the NAGK crystals without arginine added. However, these crystals did not diffract very well despite the fact that numerous condition optimization trials were performed. The comparison between the structures of NAGK with arginine and the PII:

NAGK complex will reveal the detailed function of PII on the relief of NAGK inhibition by arginine.

Secondly, mutations studies can be done on residues important for the PII: NAGK complex formation. The binding studies and activity assays on mutated PII and NAGK will verify the crystal structure of the PII: NAGK complex. Also, it is helpful to understand which residues are important to increase NAGK activities against arginine inhibition when NAGK forms a complex with PII.

Thirdly, fluorescence studies can be done for the PII: NAGK complex formation. The useful residue for this study is the conserved Trp22 in PII, since there is only one tryptophan residue in PII and NAGK does not have any tryptophan residues. Also, from the structure of the PII: NAGK complex, Trp22 binds to NAGK. Thus, the free Trp22, which is not bound to NAGK, might absorb fluorescence differently with the Trp22 in the complex. It should be a great way to analyze the binding kinetics of PII and NAGK.

References

- Arcondeguy, T., R. Jack and M. Merrick (2001). "P(II) signal transduction proteins, pivotal players in microbial nitrogen control." *Microbiol Mol Biol Rev* 65(1): 80-105.
- Bradford, M. M. (1976). "A rapid and sensitive method for the quantitation of microgram quantities of protein utilizing the principle of protein-dye binding." *Anal Biochem* 72: 248-54.
- Burillo, S., I. Luque, I. Fuentes and A. Contreras (2004). "Interactions between the nitrogen signal transduction protein PII and N-acetyl glutamate kinase in organisms that perform oxygenic photosynthesis." *J Bacteriol* 186(11): 3346-54.
- Caldovic, L. and M. Tuchman (2003). "N-acetylglutamate and its changing role through evolution." *Biochem J* 372(Pt 2): 279-90.
- Carr, P. D., E. Cheah, P. M. Suffolk, S. G. Vasudevan, N. E. Dixon and D. L. Ollis (1996). "X-ray structure of the signal transduction protein from *Escherichia coli* at 1.9 Å." *Acta Crystallogr D Biol Crystallogr* 52(Pt 1): 93-104.
- Cheah, E., P. D. Carr, P. M. Suffolk, S. G. Vasudevan, N. E. Dixon and D. L. Ollis (1994). "Structure of the *Escherichia coli* signal transducing protein PII." *Structure* 2(10): 981-90.
- Chen, Y. M., T. S. Ferrar, E. Lohmeier-Vogel, N. Morrice, Y. Mizuno, B. Berenger, K. K. Ng, D. G. Muench and G. B. Moorhead (2006). "The PII signal transduction protein of *Arabidopsis thaliana* forms an arginine-regulated complex with plastid N-acetyl glutamate kinase." *J Biol Chem* 281(9): 5726-33.
- Collaborative Computational Project, N. (1994). "The CCP4 suite: programs for protein crystallography." *Acta Crystallogr D Biol Crystallogr* 50(Pt 5): 760-3.
- Conroy, M. J., A. Durand, D. Lupo, X. D. Li, P. A. Bullough, F. K. Winkler and M. Merrick (2007). "The crystal structure of the *Escherichia coli* AmtB-GlnK complex reveals how GlnK regulates the ammonia channel." *Proc Natl Acad Sci U S A* 104(4): 1213-8.
- Cunin, R., N. Glansdorff, A. Pierard and V. Stalon (1986). "Biosynthesis and metabolism of arginine in bacteria." *Microbiol Rev* 50(3): 314-52.
- Durand, A. and M. Merrick (2006). "In vitro analysis of the *Escherichia coli* AmtB-GlnK complex reveals a stoichiometric interaction and sensitivity to ATP and 2-oxoglutarate." *J Biol Chem* 281(40): 29558-67.

- Edwards, K. J., P. M. Suffolk, P. D. Carr, M. Megman, E. Cheah and D. L. Ollis (1996). "Crystallization and preliminary X-ray diffraction studies of new crystal forms of *Escherichia coli* P(II) complexed with various ligands." *Acta Crystallogr D Biol Crystallogr* 52(Pt 4): 738-42.
- Ehlers, C., K. Weidenbach, K. Veit, K. Forchhammer and R. A. Schmitz (2005). "Unique mechanistic features of post-translational regulation of glutamine synthetase activity in *Methanosarcina mazei* strain Go1 in response to nitrogen availability." *Mol Microbiol* 55(6): 1841-54.
- Eisenberg, D., H. S. Gill, G. M. Pfluegl and S. H. Rotstein (2000). "Structure-function relationships of glutamine synthetases." *Biochim Biophys Acta* 1477(1-2): 122-45.
- Fernandez-Murga, M. L., F. Gil-Ortiz, J. L. Llacer and V. Rubio (2004). "Arginine biosynthesis in *Thermotoga maritima*: characterization of the arginine-sensitive N-acetyl-L-glutamate kinase." *J Bacteriol* 186(18): 6142-9.
- Ferrario-Mery, S., M. Bouvet, O. Leleu, G. Savino, M. Hodges and C. Meyer (2005). "Physiological characterisation of *Arabidopsis* mutants affected in the expression of the putative regulatory protein PII." *Planta* 223(1): 28-39.
- Forchhammer, K. (2004). "Global carbon/nitrogen control by PII signal transduction in cyanobacteria: from signals to targets." *FEMS Microbiol Rev* 28(3): 319-33.
- Forchhammer, K. and A. Hedler (1997). "Phosphoprotein PII from cyanobacteria--analysis of functional conservation with the PII signal-transduction protein from *Escherichia coli*." *Eur J Biochem* 244(3): 869-75.
- Forchhammer, K. and N. Tandeau de Marsac (1994). "The PII protein in the cyanobacterium *Synechococcus* sp. strain PCC 7942 is modified by serine phosphorylation and signals the cellular N-status." *J Bacteriol* 176(1): 84-91.
- Gruswitz, F., J. O'Connell, 3rd and R. M. Stroud (2007). "Inhibitory complex of the transmembrane ammonia channel, AmtB, and the cytosolic regulatory protein, GlnK, at 1.96 Å." *Proc Natl Acad Sci U S A* 104(1): 42-7.
- Heinrich, A., M. Maheswaran, U. Ruppert and K. Forchhammer (2004). "The *Synechococcus elongatus* P signal transduction protein controls arginine synthesis by complex formation with N-acetyl-L-glutamate kinase." *Mol Microbiol* 52(5): 1303-14.
- Heras, B. and J. L. Martin (2005). "Post-crystallization treatments for improving diffraction quality of protein crystals." *Acta Crystallogr D Biol Crystallogr* 61(Pt 9): 1173-80.

Hisbergues, M., R. Jeanjean, F. Joset, N. Tandeau de Marsac and S. Bedu (1999). "Protein PII regulates both inorganic carbon and nitrate uptake and is modified by a redox signal in *Synechocystis* PCC 6803." *FEBS Lett* 463(3): 216-20.

Hsieh, M. H., H. M. Lam, F. J. van de Loo and G. Coruzzi (1998). "A PII-like protein in *Arabidopsis*: putative role in nitrogen sensing." *Proc Natl Acad Sci U S A* 95(23): 13965-70.

Javelle, A., E. Severi, J. Thornton and M. Merrick (2004). "Ammonium sensing in *Escherichia coli*. Role of the ammonium transporter AmtB and AmtB-GlnK complex formation." *J Biol Chem* 279(10): 8530-8.

Jiang, J., E. M. Lafer and R. Sousa (2006). "Crystallization of a functionally intact Hsc70 chaperone." *Acta Crystallogr Sect F Struct Biol Cryst Commun* 62(Pt 1): 39-43.

Jiang, P., P. Zucker, M. R. Atkinson, E. S. Kamberov, W. Tirasophon, P. Chandran, B. R. Schefke and A. J. Ninfa (1997). "Structure/function analysis of the PII signal transduction protein of *Escherichia coli*: genetic separation of interactions with protein receptors." *J Bacteriol* 179(13): 4342-53.

Kamberov, E. S., M. R. Atkinson, J. Feng, P. Chandran and A. J. Ninfa (1994). "Sensory components controlling bacterial nitrogen assimilation." *Cell Mol Biol Res* 40(3): 175-91.

Kamberov, E. S., M. R. Atkinson and A. J. Ninfa (1995). "The *Escherichia coli* PII signal transduction protein is activated upon binding 2-ketoglutarate and ATP." *J Biol Chem* 270(30): 17797-807.

Laemmli, U. K. (1970). "Cleavage of structural proteins during the assembly of the head of bacteriophage T4." *Nature* 227(5259): 680-5.

Lee, H. M., E. Flores, A. Herrero, J. Houmard and N. Tandeau de Marsac (1998). "A role for the signal transduction protein PII in the control of nitrate/nitrite uptake in a cyanobacterium." *FEBS Lett* 427(2): 291-5.

Li, W. K. W. (1994). "Primary production of prochlorophytes, cyanobacteria, and eucaryotic ultraphytoplankton: measurements from flow cytometric sorting." *Limnol. Oceanogr.* 39: 169-175.

Machado Benelli, E., M. Buck, I. Polikarpov, E. Maltempi de Souza, L. M. Cruz and F. O. Pedrosa (2002). "Herbaspirillum seropedicae signal transduction protein PII is structurally similar to the enteric GlnK." *Eur J Biochem* 269(13): 3296-303.

Magasanik, B. (1993). "The regulation of nitrogen utilization in enteric bacteria." *J Cell Biochem* 51(1): 34-40.

- Maheswaran, M., C. Urbanke and K. Forchhammer (2004). "Complex formation and catalytic activation by the PII signaling protein of N-acetyl-L-glutamate kinase from *Synechococcus elongatus* strain PCC 7942." *J Biol Chem* 279(53): 55202-10.
- McRee, D. E. (2004). "Differential evolution for protein crystallographic optimizations." *Acta Crystallogr D Biol Crystallogr* 60(Pt 12 Pt 1): 2276-9.
- Merrick, M., A. Javelle, A. Durand, E. Severi, J. Thornton, N. D. Avent, M. J. Conroy and P. A. Bullough (2006). "The *Escherichia coli* AmtB protein as a model system for understanding ammonium transport by Amt and Rh proteins." *Transfus Clin Biol* 13(1-2): 97-102.
- Mizuno, Y., B. Berenger, G. B. Moorhead and K. K. Ng (2007). "Crystal structure of *Arabidopsis* PII reveals novel structural elements unique to plants." *Biochemistry* 46(6): 1477-83.
- Moorhead, G. B. and C. S. Smith (2003). "Interpreting the plastid carbon, nitrogen, and energy status. A role for PII?" *Plant Physiol* 133(2): 492-8.
- Morris, A. L., M. W. MacArthur, E. G. Hutchinson and J. M. Thornton (1992). "Stereochemical quality of protein structure coordinates." *Proteins* 12(4): 345-64.
- Mullis, K. B. and F. A. Faloona (1987). "Specific synthesis of DNA in vitro via a polymerase-catalyzed chain reaction." *Methods Enzymol* 155: 335-50.
- Muro-Pastor, M. I., J. C. Reyes and F. J. Florencio (2001). "Cyanobacteria perceive nitrogen status by sensing intracellular 2-oxoglutarate levels." *J Biol Chem* 276(41): 38320-8.
- Nichols, C. E., S. Sainsbury, N. S. Berrow, D. Alderton, N. J. Saunders, D. K. Stammers and R. J. Owens (2006). "Structure of the PII signal transduction protein of *Neisseria meningitidis* at 1.85 Å resolution." *Acta Crystallograph Sect F Struct Biol Cryst Commun* 62(Pt 6): 494-7.
- Ninfa, A. J. and P. Jiang (2005). "PII signal transduction proteins: sensors of alpha-ketoglutarate that regulate nitrogen metabolism." *Curr Opin Microbiol* 8(2): 168-73.
- Otwinowski, Z. M., W. (1997). *Methods Enzymology* 276: 307-326.
- Ramon-Maiques, S., M. L. Fernandez-Murga, F. Gil-Ortiz, A. Vagin, I. Fita and V. Rubio (2006). "Structural bases of feed-back control of arginine biosynthesis, revealed by the structures of two hexameric N-acetylglutamate kinases, from *Thermotoga maritima* and *Pseudomonas aeruginosa*." *J Mol Biol* 356(3): 695-713.

Ramon-Maiques, S., A. Marina, F. Gil-Ortiz, I. Fita and V. Rubio (2002). "Structure of acetylglutamate kinase, a key enzyme for arginine biosynthesis and a prototype for the amino acid kinase enzyme family, during catalysis." *Structure* 10(3): 329-42.

Saiki, R. K., D. H. Gelfand, S. Stoffel, S. J. Scharf, R. Higuchi, G. T. Horn, K. B. Mullis and H. A. Erlich (1988). "Primer-directed enzymatic amplification of DNA with a thermostable DNA polymerase." *Science* 239(4839): 487-91.

Sakai, H., H. Wang, C. Takemoto-Hori, T. Kaminishi, H. Yamaguchi, Y. Kamewari, T. Terada, S. Kuramitsu, M. Shirouzu and S. Yokoyama (2005). "Crystal structures of the signal transducing protein GlnK from *Thermus thermophilus* HB8." *J Struct Biol* 149(1): 99-110.

Schwarzenbacher, R., F. von Delft, P. Abdubek, E. Ambing, T. Biorac, L. S. Brinen, J. M. Canaves, J. Cambell, H. J. Chiu, X. Dai, A. M. Deacon, M. DiDonato, M. A. Elsliger, S. Eshagi, R. Floyd, A. Godzik, C. Grittini, S. K. Grzechnik, E. Hampton, L. Jaroszewski, C. Karlak, H. E. Klock, E. Koesema, J. S. Kovarik, A. Kreuzsch, P. Kuhn, S. A. Lesley, I. Levin, D. McMullan, T. M. McPhillips, et al. (2004). "Crystal structure of a putative PII-like signaling protein (TM0021) from *Thermotoga maritima* at 2.5 Å resolution." *Proteins* 54(4): 810-3.

Scopes, R. K. (1987). "Dye-ligands and multifunctional adsorbents: an empirical approach to affinity chromatography." *Anal Biochem* 165(2): 235-46.

Slocum, R. D. (2005). "Genes, enzymes and regulation of arginine biosynthesis in plants." *Plant Physiol Biochem* 43(8): 729-45.

Smith, C. S., N. A. Morrice and G. B. Moorhead (2004). "Lack of evidence for phosphorylation of *Arabidopsis thaliana* PII: implications for plastid carbon and nitrogen signaling." *Biochim Biophys Acta* 1699(1-2): 145-54.

Smith, C. S., A. M. Weljie and G. B. Moorhead (2003). "Molecular properties of the putative nitrogen sensor PII from *Arabidopsis thaliana*." *Plant J* 33(2): 353-60.

Smith, C. S., S. T. Zaplachinski, D. G. Muench and G. B. Moorhead (2002). "Expression and purification of the chloroplast putative nitrogen sensor, PII, of *Arabidopsis thaliana*." *Protein Expr Purif* 25(2): 342-7.

Son, H. S. and S. G. Rhee (1987). "Cascade control of *Escherichia coli* glutamine synthetase. Purification and properties of PII protein and nucleotide sequence of its structural gene." *J Biol Chem* 262(18): 8690-5.

Stadtman, E. R. (2001). "The story of glutamine synthetase regulation." *J Biol Chem* 276(48): 44357-64.

Storoni, L. C., A. J. McCoy and R. J. Read (2004). "Likelihood-enhanced fast rotation functions." *Acta Crystallogr D Biol Crystallogr* 60(Pt 3): 432-8.

Thomas, G., G. Coutts and M. Merrick (2000). "The *glnKamtB* operon. A conserved gene pair in prokaryotes." *Trends Genet* 16(1): 11-4.

Winn, M. D., M. N. Isupov and G. N. Murshudov (2001). "Use of TLS parameters to model anisotropic displacements in macromolecular refinement." *Acta Crystallogr D Biol Crystallogr* 57(Pt 1): 122-33.

Xu, Y., P. D. Carr, P. Clancy, M. Garcia-Dominguez, K. Forchhammer, F. Florencio, S. G. Vasudevan, N. Tandeau de Marsac and D. L. Ollis (2003). "The structures of the PII proteins from the cyanobacteria *Synechococcus* sp. PCC 7942 and *Synechocystis* sp. PCC 6803." *Acta Crystallogr D Biol Crystallogr* 59(Pt 12): 2183-90.

Xu, Y., P. D. Carr, T. Huber, S. G. Vasudevan and D. L. Ollis (2001). "The structure of the PII-ATP complex." *Eur J Biochem* 268(7): 2028-37.

Xu, Y., E. Cheah, P. D. Carr, W. C. van Heeswijk, H. V. Westerhoff, S. G. Vasudevan and D. L. Ollis (1998). "GlnK, a PII-homologue: structure reveals ATP binding site and indicates how the T-loops may be involved in molecular recognition." *J Mol Biol* 282(1): 149-65.

Yildiz, O., C. Kalthoff, S. Raunser and W. Kuhlbrandt (2007). "Structure of GlnK1 with bound effectors indicates regulatory mechanism for ammonia uptake." *Embo J* 26(2): 589-99.